Cloning, Expression, Purification and Cytochrome *c* Interaction Studies of Human Apaf-1 and Bcl-x_L

A Thesis
Submitted for the Degree of

DOCTOR OF PHILOSOPHY

by

P. NAGESWARA RAO

SCHOOL OF CHEMISTRY
UNIVERSITY OF HYDERABAD
HYDERABAD 500 046
INDIA
June 2009

TABLE OF CONTENTS

School of Chemistry
University of Hyderabad
Central University P. O.
Hyderabad 500 046
India

STATEMENT

I hereby declare that the work embodied in this dissertation is the result of the investigation carried out by me in the School of Chemistry, University of Hyderabad, Hyderabad, under the supervision of **Prof. Abani K. Bhuyan.**

P. NAGESWARA RAO
(03CHPH22)

June, 2009

STATEMENT VERIFIED
(Prof. ABANI K. BHUYAN)
PROJECT SUPERVISOR

School of Chemistry
University of Hyderabad
Central University P.O.
Hyderabad 500 046
India

CERTIFICATE

Certified that the work embodied in this thesis entitled **"Cloning, Expression, Purification and Cytochrome *c* Interaction studies of Human Apaf-1 and Bcl-x_L"** has been carried out by Mr. P. Nageswara Rao under my supervision, and the work has not been submitted elsewhere for a Degree.

Prof. ABANI K. BHUYAN
(THESIS SUPERVISOR)

Dean
School of Chemistry

ACKNOWLEDGEMENTS

First and foremost I offer my sincerest gratitude to my supervisor, ***Prof. Abani K. Bhuyan****, who has supported me throughout my thesis with his patience and knowledge whilst allowing me to work in my own way. I am grateful to my mentor for generously taking me into his laboratory, even though I came from Life Science background, and for introducing me to inter-disciplinary field of Biology and Chemistry. I thank him for all his help, support and encouragement in my professional as well as personal life.*

I wish to express my gratitude to former Deans of our School, Prof. Jemmis, Prof. M. Periasamy and present Dean Prof. D. Basavaiah for providing very good infrastructure and research environment.

I thank my Doctoral Committee members Prof. K.C. Kumara Swamy, Dr. Lalitha Guruprasad and Prof. M.V. Rajasekharan and all other faculty members of School of Chemistry for their support.

My special thanks to Prof. Reddanna and Prof. Aparna Dutta Gupta, Dept. of Animal Sciences, for generously allowing me to use their facilities and for their constant support & encouragement throughout my career in this university. I thank the former and present Heads of Dept. of Animal Sciences for allowing me to use GelDoc and Sonicator.

I was extraordinarily fortunate in working with a very good company people in my laboratory. Rajesh, Prakash, Yadaiah, Krishna, Harish, Umakar, Sony, Shilpa,Yasin, sashi. Jyothsna and Parasu, thank you all for making my life happy and memorable all these days in the lab.

I am very pleasure to thank my friends, colleagues and classmates, Roy, Damu, Manohar, Praveen, Ramakrishna, Ravi, Anil, Anil.k, Pushpa, Aarthi, Nishanth, Chaitanya, Srinivas, Suneel, Bhuvan, Hari, Kavitha, Rams, Anji, Pavan, Selvan and Sathish. I thank all my School and College teachers and my School friends, Surendar, Suresh, Reddy, Badram and Apparao for their support.

I gratefully acknowledge Dr. Gopinath, Dept. of Plant Sciences for assisting me in generating S4 mutants, Mr. Rajeswar for helping with AFM and Dr. G.V. Reddy for his advice and support.

I would also acknowledge all the non –teaching staff, School of Chemistry and CIL staff, Mr. Murthy and Mr. Suresh for their help. Research fellowships and financial support from UGC, CSIR, DST, DBT and Govt. India, are gratefully acknowledged.

I thank P. Narasaiah, Dr. Nagaraju, Shyam baava, Samba, Kittu, Yadagiri, Ravi, Kiran for their love and affection to me.

Where would I be without my family? My parents deserve special mention for their inseparable support and prayers. With all their love, blessings and sacrifice only, this could be possible. Srinu anna, Krishana, Vijaya thanks for being supportive and caring. I thank my father -in-law and mother- in- law for their support.

Finally my appreciation is to my wife Radhika for her patience, care and love. My special wishes for my son Aryan Ravi who takes away all my tensions with his cheers and laughter. Collective and individual acknowledgments to all family members, friends and relatives.

P. Nageswara Rao

ABBREVIATIONS

1. Apaf-1	Apoptotic protease activating factor
2. CARD	Caspase recruitment domain
3. Cyt *c*	cytochrome *c*
4. IPTG	Isopropyl-beta-thio galactopyranoside
5. X-gal	5-Bromo-4-chloro-Indoly-β-D-Galactoside
6. DTT	1,4-Dithiothreitol
7. ATP	adenosine triphosphate
8. Mant-ATP	2'(3')-*O*-(*N*-methylanthraniloyl) ATP
9. CD	Circular dichorism
10. $\Delta G°$	Gibbs free energy
11. GdnHCl	guanidinium hydrochloride
12. SDS	Sodium dodecyl sulphate
13. PAGE	Poly acrylamide gel electrophoresis
14. PCR	Polymerase chain reaction
15. ALP	Alkaline phosphatase
16. ThT	Thioflavin T
17. CDNB	1-chloro-2,4-dinitrobenzene
18. bp	base pairs
19. kDa	kilo Dalton
20. TOF	time of flight

UNIVERSITY OF HYDERABAD

CHAPTER 1

Introduction to Apoptosis

1.1 Cell death and apoptosis

In the life cycle of every cell, there is time for growth and death. For all multi cellular organisms, cell death can occur by injury or through a purposeful and regulated process called apoptosis. In Greek the term 'apoptosis' means falling off leaves from trees. It was first coined in 1972 by Kerr and coworkers [1] to describe an alternative type of cell death different from necrosis. In necrosis, physical agents like trauma and toxic agents will cause cell injury and induce a dying process where cell structure and activity are destroyed, resulting in cellular and organelle swelling, cell membrane lysis, and release of cellular contents into surrounding tissues. This results in damage of surrounding cells and a strong inflammatory response in the corresponding tissue. As a consequence, necrotic cell death causes an inflammatory response with cytokine release by the surrounding macrophages. Apoptosis or programmed cell death (PCD) on the other hand, is a nontraumatic way to remove unwanted cells in a normal and controlled process induced by specific death signals. Apoptosis is an organized suicide program that begins when the mitochondria break down releasing cytochrome *c* into the cytoplasm. The cell then shrinks and develops blebs on its surface. The cytoskeleton is destroyed and nuclear DNA is degraded. Ultimately, the cell breaks apart into membrane-wrapped cellular fragments called “apoptotic bodies”. The apoptotic bodies are engulfed by macrophages and subsequently removed from the tissue without leading to an inflammatory response.

1.2 Role of apoptosis in multicellular organisms

Apoptosis is an important counterpart to mitosis and plays significant role in the normal development and homeostasis of multicellular organisms by removing

tissues and maintaining cell numbers. For example, billions of erythrocytes are released from the bone marrow every day, and it follows that a corresponding number must be eliminated to make way for these new arrivals. Apoptosis participates in sculpting the webbing between the fingers and toes of a human fetus or in the disappearance of a tadpole's tail as it develops into an adult frog [2]. In developing cells, apoptosis controls and adjusts the cell number to ensure healthy growth. In adult tissues apoptosis regulates the cell numbers by balancing cellular division and proliferation. These cells receive constant extracellular signals to maintain survival; without these signals, apoptosis will occur. When apoptosis is inhibited or over-stimulated, abnormal tissue degeneration or uncontrolled growth leads to conditions such as autoimmune disease and cancer [8]. Lack of cell death regulation is observed in cancerous cells which are able to survive and divide without extra cellular survival signals. Apoptosis also eliminates infected cells that are harmful to the body. For example virus infected cells are killed by cytotoxic T lymphocytes inducing apoptosis. This will prevent virus replication and the release of pathogenic particles to surrounding tissues. Once the viral pathogen is eliminated, activated cytotoxic T cells are down-regulated by apoptosis to prevent further destruction of neighboring cells [3]. Without this apoptotic regulation, an autoimmune response is initiated. The last 10-15 years of research in this area revealed complex web of molecules (the death machinery) that regulates apoptosis. The death machinery can be activated by diverse stimuli.

1.3 Pathways of apoptosis

The three important pathways of apoptosis are: the intrinsic or mitochondrial pathway of apoptosis, the extrinsic death receptor pathway, and the caspase independent pathway involving apoptosis inducing factor (AIF) [4]. In addition to

these three, there is another process in which the endoplasmic reticulum has been found to contribute to apoptosis through calcium-ion signaling.

1.3.1 *Intrinsic pathway*

As its name suggests, the intrinsic pathway (Figure 1) is initiated from within the cell. It is initiated by death stimuli like exposure to radiation (ultraviolet light or X-rays) and chemotherapeutic drugs that damage DNA, intracellular components such as oxidants, and the accumulation of improperly folded proteins. In the intrinsic pathway, mitochondria and Bcl-2 family proteins play key role. When the signals for cell survival are unfavorable, the mitochondrial membrane disintegrates and releases cytochrome *c* into the cytoplasm. The released cytochrome *c* binds to Apaf-1 and activates procaspase-9 [9-13]. The activated caspase-9 then initiates the apoptotic caspase cascade. The primary regulators of intrinsic pathway are Bcl-2 family proteins. The delicate balance between the pro-apoptotic and anti-apoptotic members of the Bcl-2 super family proteins regulates the permeability of the mitochondrial membrane. According to their function in apoptosis, the mammalian Bcl-2 family can be divided into pro-apoptotic and anti-apoptotic members. The pro-apoptotic members include Bax, Bcl-Xs, Bak, Bok/Mtd, which contain 2 or 3 Bcl-2 homology (BH) regions, and molecules such as Bad, Bik/Nbk, Bid, Hrk/DP5, Bim/Bod, and Blk, which contains only the BH3 region. The anti-apoptotic Bcl-2 family members include Bcl-2, Bcl-x_L, Bcl-w, A1/Bfl-1, Mcl-1, and Boo/Diva, which contain three or four regions with extensive amino acid sequence similarity to Bcl-2 (BH1-BH4). These integral membrane proteins are found on the outer mitochondrial membrane, endoplasmic reticulum, and other organelle surfaces [14]. In the healthy cell, caspases are inactive and pro-apoptotic Bcl-2 family members such as BH3-only proteins kept apart from pro-survival Bcl-2 molecules. In the presence of internal damage, BH3-only proteins act opposite of Bcl-2, first detecting damage and then interacting with

this membrane protein to elicit cell death. BH3 binds to Bcl-2 on mitochondrial surfaces and recruits pro-death proteins such as Bax and Bak. Bax is predominantly confined to the cytosol; upon a death stimulus however, it undergoes conformational changes and moves to the outer mitochondrial membrane during apoptosis. Bak, a protein that resides in the mitochondria, acts in a similar fashion, working with Bax to permealize the organelle's outer membrane [15]. This allows cytochrome *c* to be released from the mitochondrial intermembrane space into the cytosol of the cell. Cytochrome *c* in the cytosol binds to and activates the apoptotic protease activating factor (Apaf-1), causing a conformational change which results in the recruitment of procaspase-9. This combination forms the apoptosome complex which activates caspase-9 by allosteric change [7]. Caspase-9 is an initiator caspase and begins the apoptosis cascade by cleaving and activating other proteases, such as caspase-3 and caspase-7. Unlike caspase-9, caspases-3 and -7 are executioner caspases, which cleave downstream apoptotic substrates. This proteolytic cascade results in the degradation of structural proteins in the cytosol and chromosomal DNA in the nucleus. Membrane blebbing and phagocytosis of cellular fragments complete the apoptotic process.

1.3.2 *Extrinsic pathway*

The extrinsic pathway is also called the Death Receptor pathway (Figure 1) because of the involvement of the death receptor proteins expressed on the cell surface. Here, apoptosis is triggered by extracellular death stimuli which involve interactions between the members of the death receptor family and their complementary death ligand activators. Six distinct death receptors have been identified (TNF-R1, Fas/CD95/Apo-1, DR3, DR4 (TRAIL-R1), DR5 (TRAIL-R2) and DR6) whose triggering may initiate the extrinsic pathway [5, 6]. The death receptors are the transmembrane proteins expressed on the surface of the cells. The

death stimuli in the form of death ligands bind to the extracellular portion of the death receptors. Tumor necrosis factor-α and lymphotoxin (or tumor necrosis factor-β) are examples of death activators that bind to the TNF receptor. These ligands are cytokines secreted by macrophages and other immune cells. Another death activator is the Fas ligand (FasL) of the cytotoxic T cell which binds to the Fas (or CD95) receptor of a target cell. Upon binding by the cognate ligand, the death receptors trimerize and, in their intracellular portion, assemble a death-inducing signaling complex (DISC), where the FADD/MORT1 adaptor recruits 'initiator' caspases, as pro-caspase-8 [6]. In the DISC, pro-caspase-8 undergoes auto-proteolytic activation. This then activates downstream effector caspases, as caspase-3 and -7. For example, binding of Fas ligand to the Fas receptor leads to the recruitment of the adaptor molecule FADD to the cytoplasmic tail of Fas. The FADD in turn binds to the prodomain of procaspase-8 and results in the activation of caspase-8 which in turn activates caspase-3 via direct cleavage. In addition, caspase-8 cleaves Bid, a BH3 protein, promoting apoptosis by the mitochondrial pathway and caspase-9 activation [7]. This results in the amplification of the caspase cascade, and ultimately the cell death.

1.4 Caspases

Upon receiving a signal to induce apoptosis, the cell endures many regulated morphological changes such as degradation of cellular components. A family of cysteine proteases called caspases (cysteinyl aspartate specific proteases) is responsible for these actions and therefore mediates the process of apoptosis. The prime role of caspases in programmed cell death was discovered in the laboratory of Horvitz [16] that found the genes responsible for cell death in a nematode called *Caenorhabditis elegans*. In *C. elegans*, the 1090 somatic cells are formed during the development of an adult worm of which 131 die during the process and are engulfed

Apoptosis

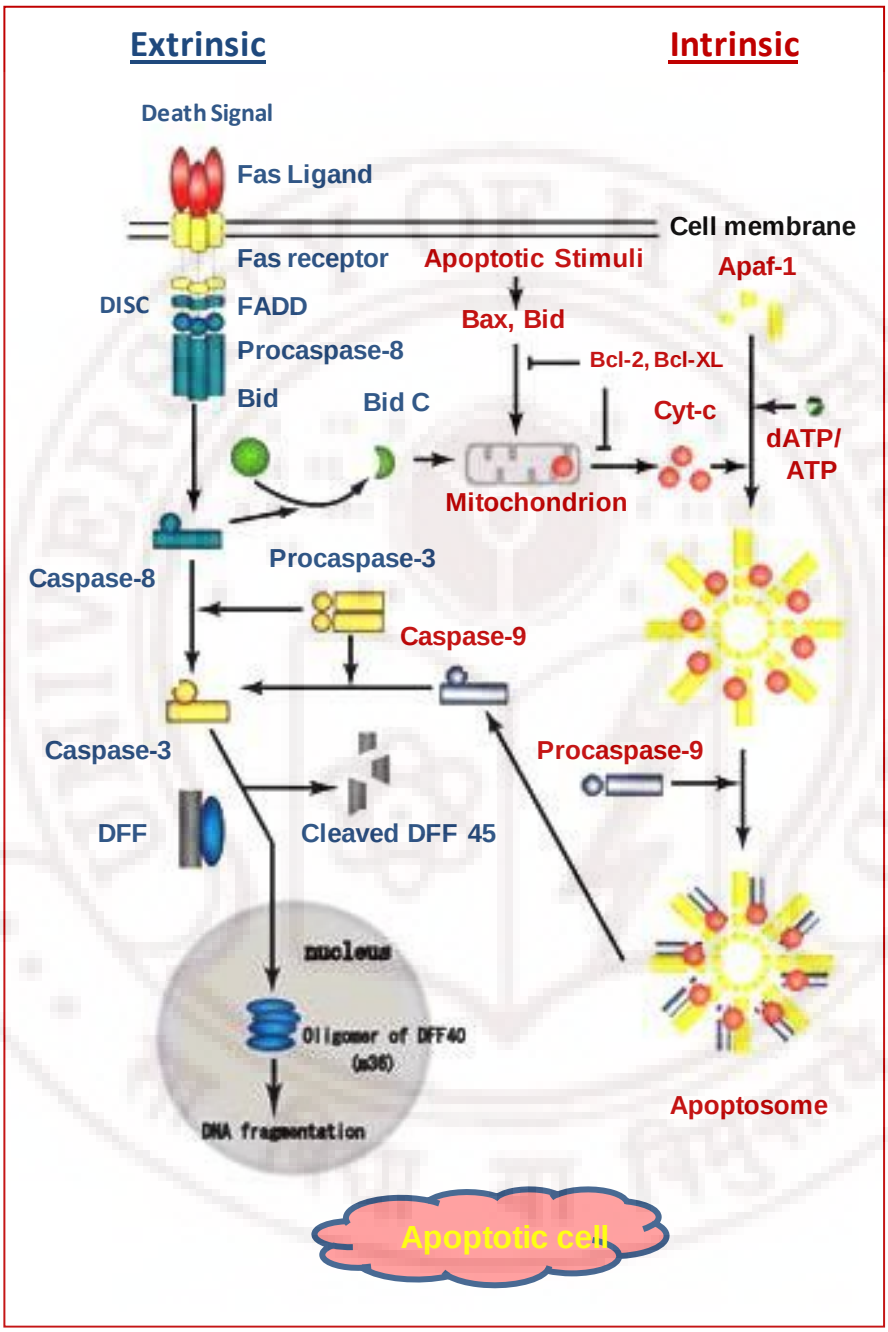

www.csml.org/.../apoptosis.png

Figure 1. Simplified model of major pathways of Apoptosis

by neighboring cells. Because these cell deaths occur at precise locations and times during worm development, they were considered to be genetically programmed. Finally, it was discovered that the genes *ced-3, ced-4 and ced-9* were responsible for cell death.

Caspases are proteases that use cysteine as the nucleophilic group for substrate cleavage and cleave peptide bonds on the carboxyl side of aspartic acid residues .To prevent premature activation of apoptosis, caspases are synthesized as zymogens. The activation of these caspases requires proteolytic processing of the zymogens. Caspases are composed of an N-terminal prodomain, a large subunit (p20), and a small subunit (p10). Active forms of caspases are heterotetramers containing two p20 and p10 heterodimers as well as two active sites. Most caspase activation occurs when an active initiator caspase cleaves an Asp-X bond of downstream zymogen between the p20 and p10 domains or between the prodomain and p20 domain [17]. There are two main classes of caspases, the upstream/initiator caspases and the downstream/executioner caspases. Upstream/initiator caspases are activated by dimerization with a protein [7]. This occurs through long N-terminal prodomains necessary for initiator caspases to associate with apoptotic complexes. The classic example of this is the activation of caspase-9 by Apaf-1. Upon mitochondrial permeabilization, cytochrome *c* binds to and causes a conformational change in Apaf-1. Procaspase-9 is then able to interact with Apaf-1 at its caspase activation and recruitment domain (CARD), forming the apoptosome complex and caspase-9 is activated. The apoptosome is then able to activate downstream caspases to begin further proteolysis and activate DNase to degrade nuclear material [4]. In the case of the extrinsic apoptotic pathway, caspase-8 is activated in a similar fashion through interaction with other proteins via its death effector domain (DED) and the subsequent formation of a multimeric complex called the death inducing signaling complex (DISC). Examples of downstream or "executioner" caspases are caspase-3, caspase-6,

and caspase-7, which remain inactive until cleaved by initiator caspases such as caspase-8 and caspase-9. Executioner caspases have shorter or no N-terminal prodomains and function to destroy various protein substrates in the cell [17]. Caspases do not randomly destroy any proteins in the cell. Instead, there are known to be about one dozen caspases in mammals, each designed to selectively cleave a specific set of substrates. The results of caspase cleavage vary depending on the substrate and where the cleavage occurs. Caspases activate other proteins by cleaving after the aspartate residue, but can inactivate target proteins as well.

1.5 Inhibitor of apoptosis proteins

In the healthy cell, inhibitors of apoptosis proteins (IAPs) keep caspases inactive by binding to them and preventing their enzymatic activity. Highly conserved in several species, IAPs bind to and inhibit caspases through their IAP baculovirus inhibitors repeat (BIR) domains which are necessary for their anti-apoptotic function. IAPs also promote caspase degradation and isolate caspases from their substrates [18]. IAPs called c-IAP-1, c-IAP-2, XIAP, and survivin are found in mammalian cells. While there are a number of IAPs, they are specific for and only interact with certain caspases. In mammalian cells, IAPs XIAP, c- IAP-1, and c-IAP-2 can only inhibit caspase-3, caspase-7, and caspase-9 but not caspase-1, caspase-6, caspase-8, and caspase-10. Also, survivin does not interact with caspase-8, but is vital to inactivate caspase-3 and caspase-7. Upon receiving death stimuli, pro-apoptotic proteins such as Diablo/Smac and Omi/Htr2 are released from mitochondria and inhibit IAP activity in the cytosol. This does not actively initiate apoptosis however, functions as one of many steps toward apoptosis.

1.6 The Cytochrome *c* mediated apoptosis

In 1995, the laboratory of Xiaodong Wang developed a cell free system to study the caspase activation. The laboratory found that addition of the nucleotide dATP/ATP induced activation of caspase-3, a major executioner caspase in HeLa cell cytosolic extracts. They found a 15 kDa protein required for this dATP-triggered caspase-3 activation; surprisingly it turned out to be cytochrome *c* [19]. For many years cytochrome *c* is known as an important molecule for energy production in mitochondria. Thus the involvement of cytochrome *c* in cell death was surprising. But the central role of cytochrome *c* in apoptosis was confirmed by two important findings. The first one was the identification of its downstream binding partner, Apaf-1, a homolog of *C. elegans* Ced-4 [20]. The second was the demonstration that Bcl-2 inhibits cell death by preventing cytochrome *c* release from mitochondria [21]. These observations support the concept that cytochrome *c* plays an essential role in apoptosis. Finally, the concept was solidified by the identification of cytochrome *c* and dATP-dependent formation of an Apaf-1/caspase-9 complex [22], which subsequently activates the effector caspases, caspase-3 and -7. So, Apaf-1 acts as an adaptor molecule to bring the procaspase-9 molecules into close proximity to form functional apoptosome which activates it into mature caspase-9.

1.6.1 *Structure and function of Apaf-1*

In 1997, Zou et al. [20] reported the purification, cDNA cloning and characterization of the human homolog of *C. elegans* Ced-4 gene, which was named Apoptotic Protease Activating Factor-1 (Apaf-1). The Apaf-1 mRNA is ubiquitously expressed in human adult and fetal tissues [33], and the corresponding 130 kDa cytoplasmic protein is able to bind cytochrome *c* and contributing to caspase-3 activation [20].

The Apaf-1 molecule contains three important functional domains. (1) The N-terminal CARD domain having the first 97 amino acids is similar to CED-3 of C. *elegans* and interacts with the prodomain of caspase-9. (2) The middle 320 amino acid stretch with homology for CED-4 of *C. elegans* is called CED-4/ATP binding domain. The conserved Walker's A- and B-box consensus sequences present in CED-4 domain facilitate dATP/ATP binding. CED-4 domain is important for oligomerization of Apaf-1. (3) The big C-terminal segment with 12-13 WD repeats is called WD-40 domain which is involved in negative regulation of Apaf-1 [23].

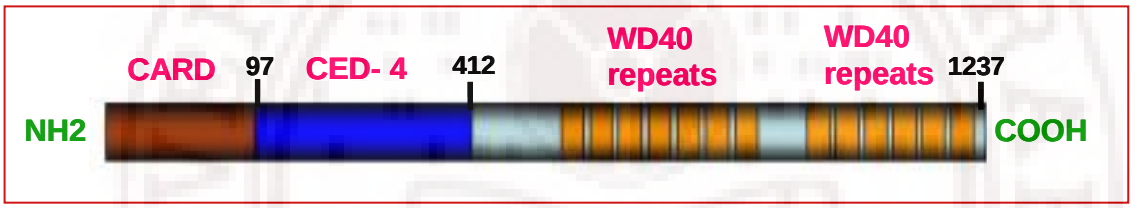

A. Anichini et al. Cancer Lett. 238(2006) 168-179

Figure 2. Domain organization in Apaf-1.

There are four differently spliced isoforms of Apaf-1 molecules: Apaf-1L, Apaf-1XL, Apaf-1M, and Apaf-1XS. These alternative Apaf-1 isoforms differ from the original Apaf-1 molecule in the number of WD40 repeats (12 or 13) and/or for the presence of additional 11 amino acid sequence inserted between the CARD and the Ced-4 homologous domains [24-26]. The original Apaf-1(S) clone (1194 amino acids), which contained neither the 11 WD-40 amino acid inserts, was essentially inactive in reconstituting a functional apoptosome [26-28]. The additional WD-40 repeat, which is found in Apaf-1XL and Apaf-1L, is essential for activity as only these isoforms are capable of supporting caspase activation [26].

1.6.1.1 *CARD domain of Apaf-1*

The Apaf-1 CARD belongs to the CARD family of apoptotic signaling motifs. The 97-residue CARD domain shares, 20% sequence homology with the prodomain of procaspase-9. The CARD-homology domain is present in several other caspase-activating proteins, such as CED-4and RAIDD/CRADD [30, 31] and in other initiator caspases, such as CED-3 and caspase-2/ICH-1 [32].

The NMR [33, 34] and X-ray crystallographic [35] analysis of Apaf-1 CARD and its mutants allowed greater insights in understanding the molecular three dimensional structure of Apaf-1 CARD and its interaction with the prodomain of caspase-9. The Apaf-1 CARD is a globular protein having seven closely packed antiparallel amphipathic α-helices. All these helices are tightly packed against a hydrophobic core which consists of conserved residues found in most CARD family proteins.

The N-terminal H1 helix has a 50° turn which is subsequently divided into two smaller helices called H1a and H1b. The helices H2, H3, H4 and H5 are parallel to each other and forms characteristic four- helix bundle. In Apaf-1 the H2, H3, H4 are more compact so H2, H3 come more close to each other. Helix 5 is connected to H4 by a tight turn and crosses the surface of H2, H4 at an angle of 50°. Helix 6 pairs with H5 and lies in the same plane.

The surface of Apaf-1 CARD contains two highly charged surface patches located on two adjacent sides of the molecule (Figure 3). On one side, a positively charged patch consists of five basic residues, Arg 13, Lys 42, Lys 58, Lys 62 and Lys 63, which are mainly located on helix H4 and the turn between H1a and H1b. On the adjacent side, three acidic residues on helices H2 and H3, Asp 27, Glu 40 and Glu 41, constitute a stripe of negatively charged surface. The basic residues create a concave surface, while the acidic ones form a convex surface. To facilitate this, procaspase-9

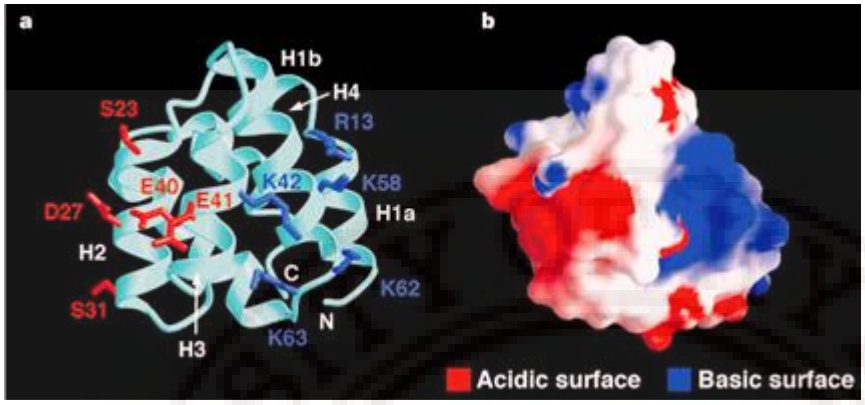

H. Qin et al. Nature 399 (1999) 547–555.

Figure 3. Structure of Apaf-1 CARD domain. a, In the structure, the acidic residues on helices H2/H3 and the basic residues on helices H1a/H1b/H4 are represented by red and blue sticks, respectively. b, Electrostatic surface potential of Apaf-1 CARD.

is recognized by Apaf-1 through CARD-CARD homophilic interaction. The Apaf-1 CARD interacts with the prodomain of caspase-9 in a 1:1 binding stoichiometry. Both Apaf-1 CARD and the procaspase-9 prodomain have similar globular fold, each consisting of seven antiparallel α-helices. These two domains interact through two complementary surfaces. The slightly concave surface of procaspase-9 formed by the positively charged helices H1a/H1b and H4 is recognized by Apaf-1 CARD through a convex surface formed by the negatively charged helices H2 and H3. The hinge region between the H1a/H1b helices in the prodomain is involved in interaction with the C-terminal end of H2 helix in the CARD.

The complex formation is mediated by a negatively charged surface in Apaf-1 CARD and a highly positively charged surface in the procaspase-9 prodomain. The acidic surface of Apaf-1 CARD at the interface contains three negatively charged residues, Asp 27, Glu 40 and Glu 41. The more extensive basic surface of the procaspase-9 prodomain consists of five arginine residues at positions 10, 11, 13, 52 and 56. These two surfaces are not only opposite in charge distribution, but also

complementary in shape, with the H1a/H1b/H4 helices of caspase-9 forming a concave surface for reception of the convex surface formed by the H2/H3 helices of Apaf-1. The residues participating in the interaction were identified by mutational analysis [35] of Apaf-1 CARD. Two mutations, Asp27Ala on helix H2 and Glu40Ala on helix H3 of Apaf-1 CARD eliminated the interaction with the wild-type procaspase-9 prodomain. A third mutation, Ser31Ala, weakened but failed to abolish the interaction. Together, these three mutations define the core of the observed acidic surface on the structure of Apaf-1 CARD. But the mutations on the basic surface patch have no effect on the interaction. On the procaspase-9 prodomain, two mutations, Arg13Ala at the hinge region between H1a and H1b helices and Arg56Ala on helix H4, prevented interaction with wild-type Apaf-1 CARD. Two additional mutations, Arg11Ala at the end of helix H1 and Arg52Ala on helix H4, also significantly reduced the interaction. In contrast, seven mutations affecting negatively charged face had no detectable effect on Apaf-1/procaspase-9 complex formation [35].

The interaction between oppositely charged surfaces is mediated by electrostatic interactions. But in case of Apaf-1 CARD and caspase-9, it is mediated not only by electrostatic interactions but also by hydrogen bonding and van der Waals forces. That is why the binding remains undisrupted at high ionic strength. There are a total of eleven intermolecular hydrogen bonds at the interface, constituting two networks. The most extensive network involves eight hydrogen bonds and five residues, Asp 27 and Glu 40 from Apaf-1, and Arg 13, Arg 52 and Arg 56 from procaspase-9. This network makes a large contribution to the stability of the Apaf-1/procaspase-9 complex. Apart from hydrogen bonding, the presence of significant hydrophobic interactions in the buried hydrophobic core of the two proteins stabilizes the binding. This is supported by the titration experiments and NMR analysis by Wagner and co-workers [33].

1.6.1.2 *ATP binding domain*

After the CARD domain, the 320 amino acid stretch follows which is called CED-4 or ATP binding domain. This domain shows 22% identity and 48% similarity with CED-4 of *C .elegans* [20]. The two longest conserved amino stretches of CED-4 at positions 141-157 and 227 are called Walker's A- and B-box consensus sequences [37] for nucleotide binding.

The 2.2 Å crystal structure [36] of ADP bound, WD-40 deleted Apaf-1 (Figure 4) by Yigong Shi and co-worker explained the nucleotide binding and oligomerization of Apaf-1 and further activation of Procaspase-9. The WD40 deleted Apaf-1 consists of 586 amino acid residues. The crystal structure of ADP-bound Apaf-1 has five distinct domains: CARD, three-layered α/β domain, helical domain I, winged-helix domain, and helical domain II (Figure 4). The N-terminal CARD domain contains six α- helices, α1- α6 arranged in a Greek-key topology. The three layered α/β domain (residues 108-284) consists of five parallel β- strands β1- β5, in the centre sandwiched by four α- helices on each side. The helical domain I, containing α16- α19 is followed by an unexpected winged-helix domain. The extended helical domain II is exclusively of α- helices, α25- α32, arranged in a right-handed super-helical conformation.

The structural homology search showed that Apaf-1 belonged to AAA (ATPase associated with various cellular activities) family of ATPases. The presence of a short helical domain following the α/β fold is a hallmark of the AAA+ family of ATPases, in which the helical domain contributes to nucleotide binding energetically.

The CARD domain of Apaf-1 interacts with the prodomain of caspase-9 and this interaction is crucial for the recruitment and subsequent activation of caspase-9 [3, 4]. The N-terminal CARD stacks against the α/β fold and the winged-helix domain through a large interface involving helices α 2, α 4 and α 5 of the CARD domain. The interactions between CARD and the α/β fold and the winged-helix domain involve a

network of 13 inter-domain hydrogen bonds and some van der Waals interactions. In the ADP bound Apaf-1 structure, the binding pocket for ADP is formed at the junction of four domains, CARD, α/β fold, helical domain I and winged-helix domain. Through extensive interactions, ADP seems to serve as an organizing centre to bring together these four adjoining domains and locks Apaf-1 in a closed conformation.

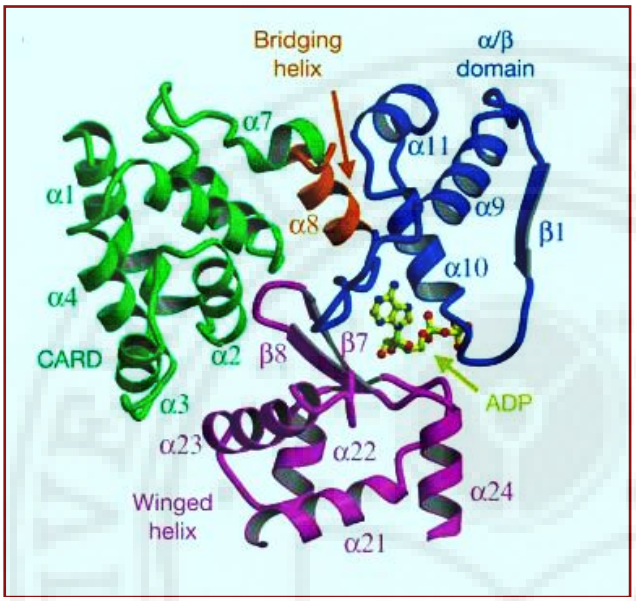

S.J. Riedl, et al. Nature 434 (2005)926-933.

Figure 4. A schematic diagram of the interdomain packing between CARD (green), the α/β fold (blue) and the winged-helix domain (magenta). The bridging helix (red), which forms a single folding unit with the α/β fold, closely stacks against helix α5 of the CARD domain.

The CARD domain of WD-40 deleted Apaf-1 in the closed conformation is able to interact with caspase-9 in the absence of dATP/ATP with a stoichiometry of 1:1. The complex shows four-fold elevated catalytic activity of caspase-9. But in the presence of ATP, the activity drastically enhanced by two orders of magnitude. This is because the only accessible narrow channel for solvent exposure to ADP is blocked by CARD domain. Upon interaction of the CARD domain with prodomain of caspase-9, the nucleotide binding pocket becomes more accessible to dATP.

1.6.1.3 *WD-40 domain.*

The C-terminal large domain after the CED-4 domain is called WD-40 domain because of the presence of multiple WD-40 repeats. The original Apaf-1(S) contains 11 WD-40 repeats but functionally inactive in reconstituting a functional apoptosome [26-28]. The cytochrome *c* released from mitochondria is thought to bind to the WD-40 region of Apaf-1. Only those Apaf-1 isoforms like Apaf-1XL with additional WD-40 repeats are able to bind cytochrome *c* and participates in caspase-3 activation. The sequence homology search of Apaf1-1 showed that it is similar with the WD-40 protein family. The WD-40 proteins normally participate in protein-protein interactions. A typical WD repeat contains a 44–60 residue sequence with a GH dipeptide, 11–24 residues from the N-terminus and separated by a conserved core sequence from the WD dipeptide at the C-terminus [38]. The best-characterized WD repeat protein is the Gβ subunit of heterotrimeric G proteins, which has a seven bladed β-propeller structure. Each blade of the propeller is a four-stranded anti-parallel β sheet, which is made up of three strands from one WD repeat and another strand from the next repeat. Usually, β-propeller structures contain 4–8 blades. Although proteins have been described with as many as 16 WD repeats, it is not known whether this results in one large propeller or two smaller 8-bladed propellers. If the latter structure is favored, then it may be that the WD repeat domain in Apaf-1 is arranged as two asymmetric (7- and 6-bladed) β-propellers. The closed circular structure of β-propellers is extremely rigid and such proteins do not readily undergo conformational changes. There is no obvious function or enzymatic activity of the WD-40 repeats, other than protein–protein interactions with other molecules. Interestingly, cytochrome oxidase cd1 also contains a rigid 8-bladed propeller in which the cytochrome *c* moiety is located at and above the axis of the propeller [39].

1.6.2 *Apoptosome formation and activation of caspase-9*

Caspases are produced as inactive zymogens. The intrachain cleavage makes them catalytically active. This is very effective in the case of effector caspases only. The intrachain cleavage simply is not enough for many initiator caspases like caspase-9. They require an apoptosome complex [55-56] for their complete activity. The unprocessed procaspase-9 is catalytically inactive and the processed free caspase-9 is only marginally active. But the processed caspase-9 when present in apoptosome is very highly active. So the apoptosome acts as holoenzyme for caspase-9 activity.

In mammalian apoptosome, the Apaf-1 molecule is the primary component which oligomerizes in the presence of dATP/ATP and cytochrome *c*, and is responsible for activation of caspase-9. [27, 28, 40, 41]. In Drosophila, the activation of Dronc requires an octameric protein complex of Dark [42] or Dapaf-1, a homologue of Apaf-1. In *C. elegans*, the activation of CED-3 caspase zymogen is facilitated by the CED-4 complex [43] which exhibits significant sequence homology to Apaf-1.

There are three important steps involved in the apoptosome formation. First, the cytochrome *c* released from mitochondria binds to the WD-40 domain of Apaf-1. Second, the hydrolysis of dATP/ATP and nucleotide exchange. Third, procaspase-9 is recruited into apoptosome. The molecular and kinetic assembly of apoptosome is not completely understood and there are still many unanswered questions. The Apaf-1 homolog of *C-eleagan's* CED-4 does not have the WD-40 domain. So the exact function of WD-40 domain is not completely understood. But it is expected to act as a negative regulator of Apaf-1. This is evident when the WD-40 deletion mutant of Apaf-1 is constitutively active and capable of processing caspase-9 in the absence of dATP and cytochrome *c* [44, 45]. These studies suggest that cytochrome *c* binds to Apaf-1 possibly to the WD-40 region. So in Apaf-1, the CARD domain is normally

blocked by the WD repeats, and dATP and cytochrome *c* cause Apaf-1 to undergo conformational changes that expose the CARD domain and allow recruitment of caspase-9. Fluorescence polarization studies have shown that cytochrome *c* can bind to recombinant Apaf-1 in a 2:1 stoichiometry with high affinity ($K_a = 10^{11}\ M^{-1}$) that is markedly reduced ($K_a = 4 \text{ X } 10^{7}\ M^{-1}$) in the presence of normal intracellular K^+ concentrations [46, 47]. So the WD-40 domain might be consisting two propeller structures, each of which can bind a cytochrome *c* molecule. Mutational epitope studies indicate [48] the involvement of lysine rich interface close to the heme pocket and the opposite surface of cytochrome *c*. The bound cytochrome *c* induces the dATP/ATP binding.

There is some controversy as to the role of the nucleotide-binding sites in Apaf-1. In one study, a P-loop (Walker A box) mutant, Apaf-1 K160R, failed to associate with Apaf-1 and inhibited recruitment and processing of caspase-9 [41]. However, in other studies this mutation did not markedly affect the ability of Apaf-1 to process caspase-9 [44]. Initial studies with the non-hydrolyzable ATP analogue ATP-γS did not support Apaf-1 self-association or binding to procaspase-9 indicating that ATP hydrolysis was required for formation of the apoptosome [41]. Studies with [α-32P] dATP were initially reported to show that nucleotides bound to Apaf-1 were hydrolysed and that ATP-γS strongly inhibited caspase-3 activation [27]. Similar results were also reported by other groups and appeared to confirm that dATP/ATP binding to Apaf-1 was accompanied by hydrolysis [28]. A very recent study with recombinant Apaf-1 expressed in insect cells revealed the exact molecular mechanism involved in nucleotide binding and oligomerization of Apaf-1 [58]. Apaf-1 produced in insect cells contains dATP as cofactor. Upon binding with cytochrome *c*, the bound dATP undergoes one round of hydrolysis to dADP. This hydrolysis step is important. It serves two purposes: providing energy for the conformational changes required for Apaf-1 oligomerization, and allowing the exogenous dATP/ATP exchange. When

Apaf-1 is incubated with cytochrome *c* in the absence of dATP/ATP, it does oligomerize but they are the non functional aggregates. These aggregates are similar to Apoptosome complex. But they fail to activate caspase-3. So hydrolysis and nucleotide exchange are important steps in the formation of active and functional apoptosome. The hydrolysis happens only in one round. Exogeneously added dATP will then bind Apaf-1, but remains unhydrolysed during apoptosome formation. So WD-40 repeats play an autoinhibitory role.

The conformational change that takes place upon binding with cytochrome *c* and dATP, causes seven to eight molecules of Apaf-1 to interact with each other and form a wheel-like structure with molecular weight in the range of 700 kDa -1.4 MDa. This is the functional Apoptosome that will eventually recruit the procaspase-9 in 1:1 stoichiometry through CARD-CARD homophilic interactions. The formation of apoptosome is a rapid process. The assembled apoptosome complex appears to be relatively stable in terms of its ability to process exogenous caspases [49]. However, caspase-9 is recruited and rapidly processed [27,28, 49], and the processed caspase-9 can be detected as the free form as well as bound to the apoptosome complex. However, it is now clear that the active form of caspase-9 is the Apaf-1 bound holoenzyme [50].

But, how the recruited procaspase-9 will become active? This can be explained by induced proximity model, in which the initiator caspases autoprocess themselves when brought into close proximity of each other [51]. A refinement of the induced proximity model is the proximity-driven dimerization model [52]. Based on this model, the heptameric Apaf-1 apoptosome may recruit multiple copies of inactive procaspase-9 into close proximity of one another. The high concentration of procaspase-9 monomers in the apoptosome are thought to favor dimerization and hence activation [53.59]. This model is consistent with the observed second-order activation of caspase-9 by a miniapoptosome [60]. In addition, a fusion protein

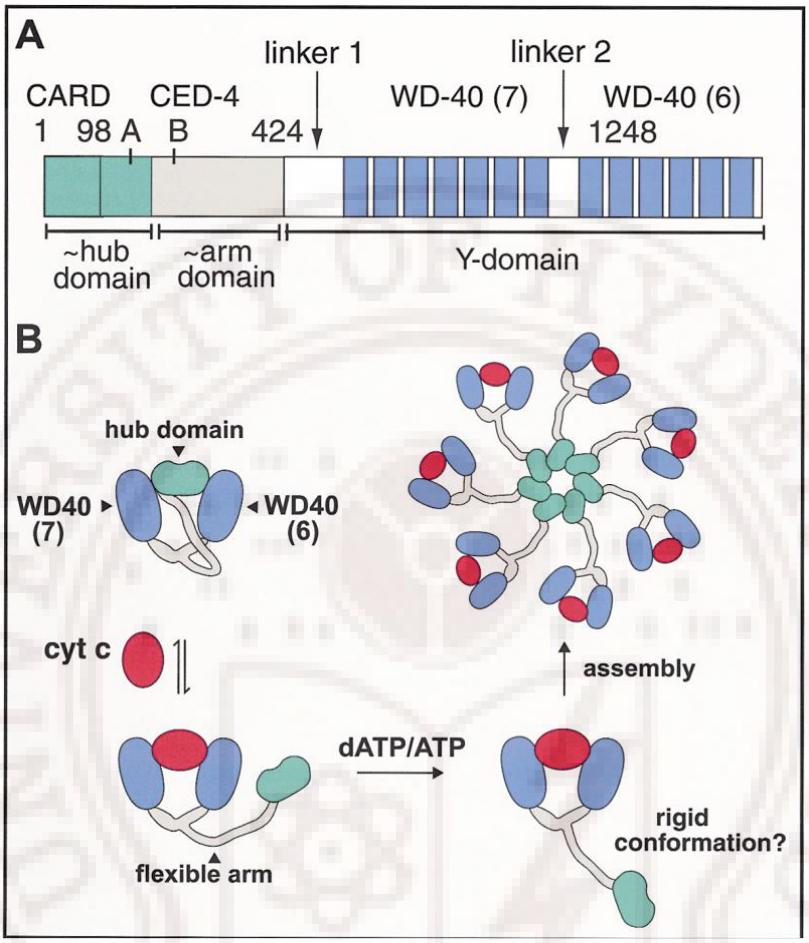

D. Acehan et al. Molecular cell. 9 (2002) 423-432.

Figure 5. The Role of Apaf-1 Sequence Motifs in the Assembly of an Apoptosome (A) The relative positions of the CARD, CED4 homology motif, WD40 repeats, and linker regions .The approximate positions of the hub, the arm, and the Y domains are indicated and color-coded. The positions of the Walker A and B nucleotide binding motifs are shown. Thus, the nucleotide binding pocket may be located in close proximity to the hub, where it may regulate assembly. (B) Apaf-1 normally adopts an auto inhibited conformation in healthy cells (top left). In actuality, only one globular region of the hub domain may interact directly with the β propellers. Cytochrome *c* then displaces the hub domain (left side), which allows Apaf-1 to bind dATP/ATP (bottom). Upon nucleotide binding, a second conformational change may promote assembly (right side).

between a dimeric leucine zipper and caspase-9 led to significant enhancement of its catalytic activity, which suggests that the dimerization of caspase-9 might be sufficient for its activation [61]. In contrast to these studies, an engineered caspase-9, which exists as a constitutive homodimer in solution, exhibited a much lower level of catalytic activity compared to the apoptosome-activated caspase-9 [62]. This observation was taken to imply an induced conformation model for the apoptosome-mediated activation of caspase-9, in which caspase-9 binding to the apoptosome was thought to result in an altered active site conformation and consequent activation of caspase-9.

The three dimensional structure of the apoptosome, [53,54] determined by electron cryomicroscopy (cryo-EM), gives insights into apoptosme assembly and caspase-9 activation. The apoptosome is a wheel-shaped structure composed of seven molecules of Apaf-1. In the apoptosome complex, Apaf-1 interacts with adjacent Apaf-1 molecules with their N-terminal CARD domains to form a central hub region.

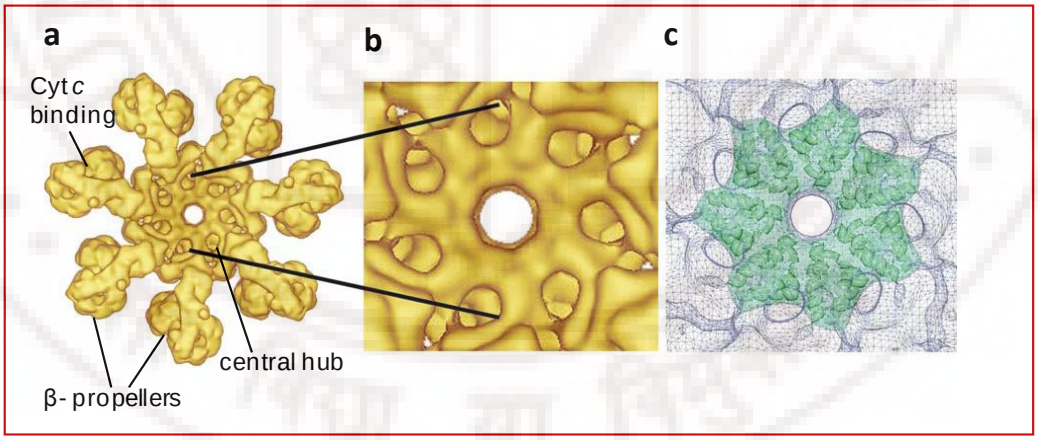

X. Yu et al. Structure 13 (2005). 1725–1735.

Figure 6. A 3D model of apoptosome assembly by 12.8 A° resolution electron cryomicroscope. (a) The bottom view of Apoptosome with cyt-*c* central hub region, the β-propellers, and cytochrome *c* binding region. (b) The ring at the center of the apoptosome, visible in an expanded view of the bottom surface. (c) Seven CARDs form a central ring within the apoptosome are shown as green.

The ring outside the hub is formed of the C-terminal extended WD40 repeats. On the basis of electron density it is clear that one molecule of cytochrome *c* will bind to one molecule of Apaf-1. Before cytochrome *c* binds to Apaf-1, the latter stays in a rigid conformation. Upon cytochrome *c* binding the rigid conformation becomes flexible and facilitates the dATP/ATP binding. The nucleotide binding brings about the conformational changes for oligomerization of seven Apaf-1 molecules to form the apoptosome which then recruits procaspase-9.

Recent studies show that formation and function of the apoptosome can be regulated by a variety of factors including intracellular levels of K^+, inhibitor of apoptosis proteins (IAPs), heat shock proteins and Smac/Diablo. These various factors thus ensure that the apoptosome complex is only fully assembled and functional, when the cell is irrevocably destined to die.

1.7. Major objectives of this work

The survey presented above identifies deficiency in at least two aspects: structural complexity not only of the interprotein complexes but also at the individual molecular level, and the thermodynamics and kinetics of the protein-protein interactions in the upstream segment of the intrinsic apoptotic pathway. The present investigations began with the primary objective of quantifying the cytochrome *c* apoptotic protein associations by both equilibrium and kinetic methods. To meet with the basic requirement of the studies, enormous effort was made to clone, bacterially overexpress, and purify Bcl-2, Bcl-x_L, and various truncated forms of Apaf-1. The work with Bcl-2 was discontinued, as the purified protein was found to be highly unstable with the tendency to disintegrate. The thesis describes cloning, expression, purification, and aspects of cytochorme *c*-Apaf-1, Apaf-1-ATP, and cytochrome *c*-Bcl-x_L interactions. It also reports on the amyloid fibrillation of the CARD domain of human Apaf-1.

1.8 References

[1] J. F. Kerr, A. H. Wyllie, A. R. Currie, Apoptosis: A basic biological phenomenon with wide-ranging implications in tissue kinetics. Br J Cancer 26 (1972) 239-257.

[2] E. H. Baehrecke, How death shapes life during development. Nat Rev Mol Cell Bio. 3 (2002) 779-787.

[3] B. Fadeel, and S. Orrenius, Apoptosis: a basic biological phenomenon with wideranging implications in human disease. J Int Med. 258 (2005) 479-517.

[4] J. M. Adams, Ways of dying: multiple pathways to apoptosis. Genes & Dev. 17 (2003) 2481-2495.

[5] V.N. Ivanon, A. Bhoumik, Z. Ronai, Death receptors and melanoma resistance to apoptosis. Oncogene 22 (2003) 3152–3161.

[6] N.N. Danial, S.J. Korsmeyer. Cell death: critical control points. Cell 116 (2004) 205–219.

[7] Z. Jin, and W. S. El-Deiry, Overview of cell death signaling pathways. Cancer Bio Ther. 4 (2005) 139-163.

[8] C. B. Thompson, Apoptosis in the pathogenesis and treatment of disease. Science 267 (1995) 1456–1462.

[9] W.C. Earnshaw, L.M. Martins, and S.H. Kaufmann, Mammalian caspases: Structure, activation, substrates, and functions during apoptosis. Annu Rev Biochem. 68 (1999) 383-424.

[10] A. Strasser, L. O'Conner, and V.M. Dixit, Apoptosis signaling. Annu Rev Biochem. 69 (2000) 217-245.

[11] I. Budihardjo, H. Oliver, and M. Lutter, et al., Biochemical pathway of caspase activation during apoptosis. Annu Rev Cell Dev. 15 (1999) 269-290.

[12] C. Adrain, and S.J. Martin, The mitchondrial apoptosome: A killer unleashed by the cytochrome seas. Trends in Biochem Sci. 26 (2001) 390-397.

[13] N.N. Danial, and S.J. Korsmeyer Cell death: Critical control points. Cell 116 (2004) 205-219.

[14] T. Kaufmann, S. Schlipf, J. Sanz, K. Neubert, R. Stein, C. Borner, Characterization of the signal that directs Bcl-xL, but not Bcl-2, to the mitochondrial outer membrane. J Cell Bio. 160 (2003) 53-64.

[15] D. D. Newmeyer, and S. Ferguson-Miller, Mitochondria: releasing power for life and unleashing the machineries of death. Cell 112 (2003) 481-490.

[16] R. E. Ellis, J.Y. Yuan, H.R. Horvitz, Mechanisms and functions of cell death. Annu.Rev.Cell Biol. 7 (1991) 663-698.

[17] M. O. Hengartner, The biochemistry of apoptosis. Nature 407 (2000) 770-776.

[18] G. S. Salvesen, andC. S. Duckett, IAP proteins: blocking the road to death's door. Nat Rev Mol Cell Bio 3 (2002) 401-410.

[19] X. Liu, C. N. Kim, J. Yang, R. Jemmerson, and X. Wang, Induction of Apoptosis program in cell-free extracts: Requirement for dATP and cytochrome *c*. Cell 86 (1996) 147-157.

[20] H. Zou, W. J. Henzel, X. Liu, A. Lutschg, and X. Wang, Apaf-1, a human protein homologous to C. elegans CED-4, participates in cytochrome *c* dependent activation of caspase-3. Cell 90 (1997) 405-413.

[21] J. Yang, X. Liu, K. Bhalla, C. N. Kim, A. M. Ibrado, J. Cai, T.-I. Peng, D. P. Jones, and X. Wang, Prevention of apoptosis by Bcl-2: Release of cytochrome *c* blocked. Science 275 (1997) 1129-1132.

[22] P. Li, D. Nijhawan, I. Budihardjo, S. M. Srinivasula, M. Ahmad, E. S. Alnemri, and X. Wang, Cytochrome *c* and dATP-dependent formation of Apaf-1/caspase-9 complex initiates an apoptotic protease cascade. Cell 91 (1997) 479-489.

[23] C. Adrain, E.A. Slee, M.T. Harte, S.J. Martin, Regulation of apoptotic protease activating factor-1 oligomerization and apoptosis by the WD-40 repeat region. J. Biol. Chem. 274 (1999) 20855-20860.

[24] W.N. Fu, S.M. Kelsey, A.C. Newland, L. Jia, Apaf-1XL is an inactive isoform compared with Apaf-1L. Biochem. Biophys. Res. Commun. 282 (2001) 268–272.

[25] C. Hahn, B. Hirsch, D. Janke, H. Durkop, H. Stein, Three new types of Apaf-1 in mammalian cells. Biochem. Biophys. Res. Commun. 261 (1999) 746–749.

[26] M.A. Benedict, Y. Hu, N. Inohara, G. Nunez, Expression and functional analysis of Apaf-1 isoforms. Extra WD-40 repeat is required for cytochrome *c* binding and regulated activation of procaspase-9. J. Biol. Chem. 275 (2000) 8461–846.

[27] H. Zou, Y. Li, X. Liu, X. Wang, An Apaf-1 cytochrome *c* multimeric complex is a functional apoptosome that activates procaspase-9. J. Biol. Chem. 274 (1999) 11549–11556.

[28] A. Saleh, S.M. Srinivasula, S. Acharya, R. Fishel, E.S. Alnemri, Cytochrome *c* and dATP-mediated oligomerization of Apaf-1 is a prerequisite for procaspase-9 activation. J. Biol. Chem. 274 (1999) 17941–17945.

[29] K. Hofmann, & P. Bucher, The CARD domain: a new apoptotic signaling motif. Trends Biochem. Sci.22 (1997) 155–156.

[30] H. Duan, & V. M. Dixit, RAIDD is a new 'death' adaptor molecule. Nature 385 (1997) 86–89.

[31] M. Ahmad, et al., CRADD, a novel human apoptotic adaptor molecule for caspase-2, and FasL/tumor necrosis factor receptor-interacting protein RIP. Cancer Res. 57 (1997) 615–619.

[32] E. S. Alnemri, et al., Human ICE/CED-3 protease nomenclature. Cell 87 (1996) 171.

Apoptosis

[33] P. Zhou, J. Chou, R. S. Olea, J. Yuan, & G. Wagner, Solution structure of Apaf-1 CARD and its interaction with caspase-9 CARD: a structural basis for specific adaptor/caspase interaction. Proc. Natl Acad. Sci. USA 96 (1999)11265–11270.

[34] C.L. Day, C. Dupont, M. Lackmann, D.L. Vaux, and M.G.Hinds, Solution structure and mutagenesis of the caspase recruitment domain (CARD) from Apaf-1. Cell Death and Diff. 6 (1999) 1125 – 1132.

[35] H. Qin, S. M. Srinivasula, G. Wu, T. Fernandes-Alnemri, E. S. Alnemri, and Y. Shi, Structural basis of procaspase-9 recruitment by the apoptotic protease-activating factor- 1. Nature 399 (1999) 547–555.

[36] S.J. Riedl, W. Li, Y. Chao, R. Schwarzenbacher, Y. Shi, Structure of the apoptotic protease activating factor 1 bound to ADP. Nature 434 (2005)926-933.

[37] J.E. Walker, M. Saraste, M.J. Runswick, and N.J. Gay, Distantly related sequence in the α- and β- subunits of ATP synthase, myosin kinase and other ATP- requiring enzymes and a common nucleotide binding fold. EMBO J.1 (1982) 945-951.

[38] T.F. Smith, C. Gaitatzes, K. Saxena, E.J. Neer, The WD repeat: a common architecture for diverse functions, Trends Biochem. Sci. 24 (1999) 181–185.

[39] P.A. Williams, V. Fulop, E.F. Garman, N.F. Saunders, S.J. Ferguson, and J. Hajdu, Heme-ligand switching during catalysis in crystals of a nitrogen-cycle enzyme, Nature 389 (1997) 406–412.

[40] K. Cain, D. G. Brown, C. Langlais, and G. M. Cohen, Caspase activation involves the formation of the aposome, a large (1700 kDa) caspase-activating complex. J. Biol. Chem. 274 (1999) 22686–22692.

[41] Y. Hu, M. A. Benedict, L. Ding, and G. Nunez, Role of cytochrome *c* and dATP/ATP hydrolysis in Apaf-1-mediated caspase-9 activation and apoptosis. EMBO J. 18 (1999) 3586–3595.

[42] A. Rodriguez, H. Oliver, H. Zou, P. Chen, X. Wang, and JM. Abrams, Dark is a Drosophila homologue of Apaf-1/CED-4 and functions in an evolutionarily conserved death pathway. Nat. Cell Biol. 1 (1999) 272–279.

[43] A. M. Chinnaiyan, K. O'Rourke, B. R. Lane, and V. M. Dixit, Interaction of CED-4 with CED-3 and CED-9: A molecular framework for cell death. Science 275 (1997) 1122–1126.

[44] S.M. Srinivasula, M. Ahmad, T. Fernandes Alnemri, and E.S. Alnemri, Autoactivation of procaspase-9 by Apaf-1-mediated oligomerization. Mol. Cell 1 (1998) 949–957.

[45] Y.M. Hu, L.Y. Ding, D.M. Spencer, G. Nunez, WD-40 repeat region regulates Apaf-1 self-association and procaspase- 9 activation, J. Biol. Chem. 273 (1998) 33489–33494.

[46] C. Purring, H. Zou, X.D. Wang, G. McLendon, Stoichiometry, free energy, and kinetic aspects of cytochrome *c*: Apaf-1 binding in apoptosis. J. Am. Chem. Soc. 121 (1999) 7435–7436.

[47] C. Purring-Koch, G. McLendon, Cytochrome *c* binding to Apaf-1: the effects of dATP and ionic strength. Proc.Natl. Acad. Sci. USA 97 (2000) 11928–11931

[48] T. Yu, X. Wang, C. Purring-Koch, Y. Wei, G.L. McLendon, A mutational epitope for cytochrome *c* binding to the apoptosis protease activation factor-1, J. Biol. Chem. 276 (2001) 13034–13038.

[49] K. Cain, S.B. Bratton, C. Langlais, G. Walker, D.G. Brown, X.M. Sun, et al., Apaf-1 oligomerizes into biologically active approximately 700-kDa and

inactive approximately 1.4-MDa apoptosome complexes, J. Biol. Chem. 275 (2000) 6067–6070.

[50] J. Rodriguez, Y. Lazebnik, Caspase-9 and Apaf-1 form an active holoenzyme, Genes Dev. 13 (1999) 3179–3184.

[51] G. S. Salvesen, and V. M. Dixit, Caspase activation: The induced-proximity model. Proc. Natl. Acad. Sci. USA 96 (1999) 10964–10967.

[52] K. M. Boatright, and G. S. Salvesen, Mechanisms of caspase activation. Curr. Opin. Cell Biol. 15 (2003) 725–731.

[53] D. Acehan, X. Jiang, D. G. Morgan, J. E. Heuser, X. Wang, and C. W. Akey, Three-dimensional structure of the apoptosome: Implications for assembly, procaspase-9 binding and activation. Mol. Cell. 9 (2002) 423–432.

[54] X. Yu, D. Acehan, J. F. Menetret, C. R. Booth, S. J. Ludtke, S. J. Riedl, Y. Shi, X. Wang, and C. W. Akey, A structure of the human apoptosome at 12.8 A° resolution provides insights into this cell death platform. Structure 13 (2005). 1725–1735.

[55] X. Jiang, X. Wang, Cytochrome *c*-mediated apoptosis. Annu. Rev. Biochem. 73 (2004) 87-106

[56] K. Cain, SB. Bratton, GM. Cohen, The Apaf-1 apoptosome: a large caspase-activating complex. Biochimie. 84 (2002) 203-14.

[57] Y. Shi, Apoptosome Assembly. Methods in Enzymology 442 (2008) 141-156.

[58] H. E. Kim, F. Du, M. Fang, andX. Wang, Formation of apoptosome is initiated by cytochrome *c* induced dATP hydrolysis and subsequent nucleotide exchange on Apaf-1. Proc. Natl. Acad. Sci. USA 102 (2005) 17545–17550.

[59] M. Renatus, H. R. Stennicke, F. L. Scott, R. C. Liddington, and G. S. Salvesen, Dimer formation drives the activation of the cell death protease caspase 9. Proc. Natl. Acad. Sci. USA 98 (2001) 14250–14255.

[60] C. Pop, J. Timmer, S. Sperandio, and G. S. Salvesen, The apoptosome activates caspase-9 by dimerization. Mol. Cell 22 (2006) 269–275.

[61] Q. Yin, H. H. Park, J. Y. Chung, S. C. Lin, Y. C. Lo, L. S. da Graca, X. Jiang, and H. Wu, Caspase-9 holoenzyme is a specific and optimal procaspase-3 processing machine. Mol. Cell 22 (2006) 259–268.

[62] Y. Chao, E. N. Shiozaki, S. M. Srinivasula, D. J. Rigotti, R. Fairman, and Y. Shi, Engineering a dimeric caspase-9: A re-evaluation of the induced proximity model form caspase activation. PLoS Biol. 3 (2005) e183.

CHAPTER 2

Cloning, Expression, Refolding, and ATP-Binding Properties of a WD40-Deleted Apaf-1 Isoform

2.1 Abstract

The apoptotic protease activating factor (Apaf-1) is central to the regulatory mechanism by which procaspase-9 is activated in the cytochrome *c*-mediated pathway of apoptosis. For a detailed biochemical and structural investigation of Apaf-1 function, we have cloned and expressed in *E. coli* inclusion bodies the WD40-deleted protein ($^{\Delta WD40}$Apaf-1) from HepG2 cell. The construct contains an N-terminal His_6 tag derived from the cloning vector so that the mass of the protein and the tag together is 51,594 Da, as determined by TOF/TOF mass spectrometric analysis. An optimized refolding protocol has allowed protein recovery in highly pure form. Basic fluorescence and CD probes indicate that the refolded protein retains secondary and tertiary structures, and unfolds in the presence of higher concentration of denaturant. The equilibrium ATP binding property of the protein has been measured by changes in fluorescence emission due to the fluorescent ATP analog, mant-ATP (2'(3')-*O*-(*N*-methylanthraniloyl) adenosine 5'-triphosphate). The results demonstrate a tight Apaf-1–ATP interaction, the binding affinity being 380 nM.

2.2 Introduction

In the mitochondrial pathway of apoptosis [1], Apaf-1 is the central player in the upstream events of cytochrome *c* dependent activation of procaspase-9 [2,3]. Apaf-1 consists of a CED-4 homologous domain that straddles a *Ca*spase *R*ecruitment *D*omain (CARD) in the N-terminal region and a 12 or 13 WD-40 repeats domain in the C-terminus [2,4]. The CED-4 domain is also called ATPase domain, owing to its

apparent ATP hydrolysis activity [2,5-7]. The biochemical mechanisms by which Apaf-1 involves itself to assembling a functional apoptosome, a generic term for the initial platform provided by Apaf-1 and cytochrome *c* in the presence of ATP/dATP leading to the activation of caspases- 9 and 3 [2,3,8], are astonishingly complex, and remains largely unknown. In the pursuit of this aspect at molecular and atomic level, Apaf-1 itself offers a major challenge by its large size and isoformic existence [3, 9]. Notwithstanding the largeness, electron cryomicroscopic methods have been applied to view the gross structural and topological features of the apoptosome, and the oligomerization of Apaf-1 [10-12]. More recently, a mathematical model for Apaf-1 heptamer assembly process has also been proposed [13]. Of the three domains of Apaf-1, atomic-level structural descriptions have been provided for the CARD domain alone by NMR [14] and together with the ATPase domain by x-ray crystallography [7].

Depending on the mode of mRNA splicing, multiple Apaf-1 splice variants can exist [3], but not all isoforms thus produced can activate procaspase-9 [9]. It has been demonstrated that the isoform with an 11-amino acid insert between the CARD and ATPase domain, and an extra WD-40 sequence in the WD-40 domain are essential for ATP hydrolysis-mediated cytochrome *c* binding, and regulation of procaspase-9. According to this model, the cytochrome *c*-binding region in the C-terminal WD-40 domain of functionally active Apaf-1 isoforms remains unavailable for binding until a conformational change possibly driven by ATP hydrolysis in the CED-4 domain unmasks the binding site [9]. However, Apaf-1 lacking the WD-40 domain can bind and hydrolyze ATP/dATP. Localization of ADP in the crystal structure of the CED-4 domain indicates that ATP $\rightarrow$ ADP + P_i reaction is possibly driven by the domain itself [7]. Thus, several regulatory and mechanistic issues, including the regulation of nucleotide binding and hydrolysis, and the CARD's role

toward these, can be investigated using recombinant Apaf-1 lacking the WD-40 domain.

Here, the RT-PCR approach is employed to clone a gene corresponding to the N-terminal 1-419 amino acid sequence of Apaf-1 from HepG2 cell line. The gene construct excludes the WD-40 repeat domain ($^{\Delta WD40}$Apaf-1), and the CARD domain features a 4-residue deletion. The protein overexpressed in *E. coli* is invariably localized in the cytoplasmic inclusion body. The protein was refolded, purified, and characterized in terms of quantification of its equilibrium interaction with ATP.

2.3 Materials and methods

2.3.1 *Cloning and generation of expression construct for $^{\Delta WD40}$Apaf-1*

Total RNA was isolated from ~ 5 million HepG2 cells by standard procedures that use TRI Reagent (Sigma), chloroform, and isopropanol. The isopropanol-pelleted RNA was washed with 75% ethanol, dissolved in nuclease-free water, and subjected to agarose gel electrophoresis to confirm the integrity of the isolated RNA. cDNA was prepared by using the SuperscriptII kit (Invitrogen). Approximately 5 µg of total RNA was added to the RT-PCR mix. Oligo dT primed cDNA synthesis was achieved by incubating the reaction mix at 47 ^{o}C for 30 min. The first strand that was made using SuperscriptII was used for PCR amplification of $^{\Delta WD40}$Apaf-1. The primers were

*Bam*H1

CARD-F: 5′ CG**GGATCC**ATGGATGCAAAAGCTCGAA 3′

CED4-R: 5′CC**CTCGAG**CTAAAGAGACTTATTTACAAACTC 3′

*Xho*1

The 50 μl PCR reaction mixture contained 5 μL 10X PCR buffer, 1 μL CARD-F primer (10 pmol), 1 μL CED4-R primer (10 pmol), 2 μL cDNA, 1 μL of 2.5U/μL EasyA Taq DNA polymerase (Stratagene), and 40 μL water. PCR amplification involved the initial denaturation at 94°C for 2 min, followed by 30 cycles each consisting of a 30-sec final denaturation at 94°C, a 30 sec annealing at 54 °C, and a 1 min initial extension at 72 °C. The final extension following the 30 cycles was allowed for 15 min at 72 °C. The amplified PCR product, electrophoresed and eluted from agarose gel, was ligated into a TA vector, pTZ57 R/T (MBI-Fermentas). The positive clones, selected by Blue-white colony screening and colony PCR, were used to isolate plasmids employing QIAprep spin miniprep kit (Qiagen). The plasmids were sequenced, and the clone containing the correct sequence was digested with *Bam*H1 and *Xho*1. The digested fragment was then ligated into *Bam*H1 and *Xho*1 sites of pRSETa vector (Invitrogen), and transformed into DH5α *E. coli* cells. Positive clones were selected by colony PCR, and confirmed by digestion.

2.3.2 *Protein expression*

The protein was expressed in LB medium containing ampicillin (100 mg/ml). To obtain the protein in the soluble fraction, several cell growth conditions generated by varying temperature and IPTG concentration were tried out. Typically, 20 ml of an overnight grown culture was added to a 2-L medium, and incubated with vigorous shaking at a temperature in the 5–37 °C range. At OD600 = 0.5 of the culture, protein expression was induced with IPTG in the 0.1–1 mM range. The growth was continued until the steady state was reached. Noting no trace protein in the soluble fraction under all conditions employed, we eventually chose to induce protein expression at 37 °C with 1 mM IPTG, and let the cells grow for 5 h after induction. Cells were

harvested by centrifugation at 4000g for 10 min at 4 °C, washed with TE buffer (10 mM Tris–HCl, 1 mM EDTA pH 8.0), and frozen stored at –80 °C.

2.3.3 *Preparation of inclusion bodies*

The cell pellet was resuspended in 30 ml Buffer A (20 mM Tris–HCl, 100 mM NaCl, 1 mM PMSF, pH8.0, containing 10 μL of 1 mg/ml DNaseI), and sonicated at 4 °C with 10 cycles, each cycle consisting of 30 s on and 60 s off times. The lysate was treated with deoxycholic acid (4 mg per gram weight of E. coli), stirred for 30 min at room temperature, and centrifuged at 10,000 rpm for 15 min at 4 °C. The pellet was resuspended in 9 volumes of Buffer B (20 mM Tris, 100 mM NaCl, 10 mM EDTA, 0.5% Triton X-100, pH 8.0), stirred at room temperature for 5 min and centrifuged at 10000 rpm for 15 min at 4 °C. The step was repeated. Inclusion bodies were then washed with 10 volumes of 20 mM Tris–HCl containing 100 mM NaCl at pH 8.0 three times to remove the Triton X-100. Washed inclusion bodies are now 95% pure.

2.3.4 *Refolding of $^{\Delta WD40}$Apaf-1*

Three procedures were applied to refold the protein from inclusion body aggregates, and the compositions of unfolding and refolding buffers varied slightly from one procedure to another. The basic buffer for solubilization of inclusion body was Buffer C (6.0 M GdnHCl, 20 mM Tris–HCl, 500 mM NaCl, pH 7.5). For refolding by the use of classical gel filtration procedure, ~ 25 mg of the inclusion body preparation (by wet weight) was solubilized in 5 ml of Buffer C with 1 mM EDTA, 1 mM DTT and 50 mM L-arginine at pH 7.4, and incubated at 25 °C for 90 min. The unfolded protein solution, cleared after centrifugation, was diluted five-fold by drop wise addition into 20 ml of the same buffer containing no GdnHCl. The refolded protein solution, now in ~1.2 M GdnHCl was faintly hazy, and was kept in

cold for 90 min. The solution was then centrifuged at 15000 rpm for 15 min, and 20 ml of it was chromatographed in a 1.6 X 100 cm (diameter and height, respectively) Sephadex G75 column pre equilibrated in the refolding buffer. Fractions each of 1.5 ml size were collected at a flow rate of 20 ml/h, and analyzed by SDS-electrophoresis and silver staining. In the second refolding procedure, nickel affinity column was used to separate $^{\Delta WD40}$Apaf-1 from other proteins present in the refolded protein solution. Inclusion bodies were solubilized in Buffer C with 1 mM PMSF and 5 mM β-mercaptoethanol, pH 8.0, incubated for 2 h, and refolded by 20-fold dilution into Buffer C containing no GdnHCl but 0.4 M L-arginine, 0.5 M urea, and 1 mM β-mercaptoethanol, pH 7.5. The solution was kept in cold for 24 h, and then dialyzed extensively against the same refolding buffer (pH 8.0) that excluded L-arginine and β-mercaptoethanol. After discarding the precipitate by centrifugation, the solution was loaded onto a Ni-NTA His bind column (Novagen) equilibrated with the dialysis buffer, and washed with the same buffer. The protein, eluted by passing 20 mM Tris, 150 mM NaCl, and 300 mM imidazole, pH 8.0, was dialyzed or centrifuged in Amicon 5 kDa cutoff filter devices to remove imidazole. Although nothing wrong in itself, this procedure for imidazole removal was time consuming under our laboratory conditions. We, therefore, used 20 mM Tris, 150 mM NaCl, 50 mM EDTA, pH 8 for protein elution.

The third refolding procedure involved on-column folding. The inclusion body preparation was unfolded in Buffer C with 1 mM PMSF and 5 mM b-mercaptoethanol, pH 8.0, and then incubated for 2 h. Thirteen milliliters of this unfolded protein solution (protein concentration: ~1 mg ml $^{-1}$) was loaded onto a 10 ml Ni-NTA-His bind column equilibrated in the same unfolding buffer. The column was washed with five volumes of 20 mM Tris, 300 mM NaCl, containing 6 M urea, pH 8.0. After refolding by five volume column washes with 20 mM Tris, 150

mM NaCl, pH 8.0, the protein was eluted with the same buffer containing 50 mM EDTA. The eluted protein solution was then dialyzed or centrifuge-filtered using the same buffer at pH 7.5 containing no EDTA.

2.3.5 *Western blot*

Purified $^{\Delta WD40}$Apaf-1 as well as the *E. coli* extract proteins were run on 10% SDS–PAGE, transferred onto a PVDF membrane (Amersham), incubated overnight at 4 °C with anti-Apaf-1 rabbit polyclonal IgG (Upstate),washed with TBS, incubated for 1 h at room temperature with 2° antibody (anti-rabbit conjugated with alkaline phosphatase), and developed with BCIP-NBT solution.

2.3.6 *Mass spectrometry*

2 μL of the purified protein solution (~0.21 μg) was mixed with 2 μL of 2% TFA and 2 μL of the matrix solution (2,5 dihydroxyacetophenone with 10 mM di-ammonium citrate). Mass measurements were performed on an Autoflex III TOF/TOF spectrometer (Bruker) in the positive linear mode of operation. ~1000 single spectra were added. Spectra were processed using 10 Da Gauss filter smoothing and baseline subtraction.

2.3.7 *Fluorescence and CD measurements*

Fluorescence and CD spectra of $^{\Delta WD40}$Apaf-1 were recorded with 2 μM protein in 20 mM Tris, 100 mM NaCl, pH 7.5, 25 °C. For fluorescence, a photon counting instrument (FluoroMax-3, Jobin-Yvon) was used (excitation: 280 nm, 1.5 nm slit).

CD spectra were taken in a JASCO J715 spectropolarimeter with the protein solution contained in 2 mm path length cylindrical cell. Sixteen scans were averaged.

2.3.8 *Interaction of $^{\Delta WD40}$Apaf-1 and ATP measured by fluorescence*

The titration of MANT-ATP (Invitrogen) with $^{\Delta WD40}$Apaf-1 was followed by the decrease in fluorescence of the former (excitation: 356 nm). A set of samples containing a fixed concentration of MANT-ATP (1 or 5 μM) and variable concentration of $^{\Delta WD40}$Apaf-1 was prepared in 50 mM Tris, 50 mM NaCl, 10 mM $MgCl_2$, pH 7, and equilibrated at 25 °C for 1 hr. With this procedure of equilibrium titration experiment, where different premixed samples are used instead of repeated addition of aliquots of the titrant to a single protein solution, no correction for dilution effects are required, and the data obtained are also more accurate. Fluorescence at 444 nm, which is the emission maximum for MANT-ATP, was used for binding analysis. The concentration of free $^{\Delta WD40}$Apaf-1 in the titration mixture is given by

$$[^{\Delta WD40}\mathrm{Apaf\text{-}1}]_{free} = \frac{[\mathrm{MANT-ATP}]\times \Delta F}{\Delta F_{\infty}} \quad (1)$$

in which, $\Delta F=F_x-F_o$ and $\Delta F_\infty=F_\infty-F_o$, where F_o, F_x, and F_∞ are 444-nm fluorescence of solutions containing MANT-ATP alone, MANT-ATP in the presence of x concentration of $^{\Delta WD40}$Apaf-1, and MANT-ATP in the presence of infinite or saturating concentration of $^{\Delta WD40}$Apaf-1, respectively. The association constant, K_{ass}, was extracted from the equation

Recombinant ^{WD40}Apaf-1

$$\log\left[\frac{\Delta A}{A_\infty - A_x}\right] = \log K_{ass} + \log[^{WD40}\text{Apaf} - 1]_{free} \quad (2)$$

The *x*-intercept of the plot of log $[\Delta F/(F_\infty - F_x)]$ vs log[$^{\Delta WD40}$Apaf-1] gives the value of pK_a for the interaction between MANT-ATP and $^{\Delta WD40}$Apaf-1.

2.4 Results and discussion

2.4.1 *4-residue deletion in the CARD domain of $^{\Delta WD40}$Apaf-1*

To clone the $^{\Delta WD40}$Apaf-1 gene containing the N-terminal 1-419 amino acids, we used RNA from HepG2 cells (Figure. 1). The gene sequence aligned to the HeLa Apaf-1 sequence (also called Apaf-1S) originally described by Zou *et al* [4] and also cloned later by others [9], however, indicated a deletion involving four consecutive amino acids (VRNE) in the CARD domain (Figure 2). In the past, several studies have reported Apaf-1 isoforms [2, 3, 6, 9]. The occurrence of full-length Apaf-1 isoforms in tumor cell lines have been attributed to alternative splicing that can create an 11-residue insert straddled by the CARD and ATPase domains or an additional WD40 repeat between the fifth and sixth repeats of the WD40 domain, or both. We observe the 11-residue insert, not present in the Apaf-1S isoform but in the Apaf-1 gene that we have cloned. Accordingly, following the nomenclature of Benedict *et al*. [9], the $^{\Delta WD40}$Apaf-1 may be termed Apaf-1XL (1-419) or N+. A survey of all the isoforms conducted by the same authors has indicated that only Apaf-1 isoforms with the additional WD40 insert bind cytochrome *c* and activate procaspase-9. However, the 11-residue insert between the CARD and ATPase domains are essential for dATP/ATP binding and subsequent hydrolysis, thereby facilitating the binding of

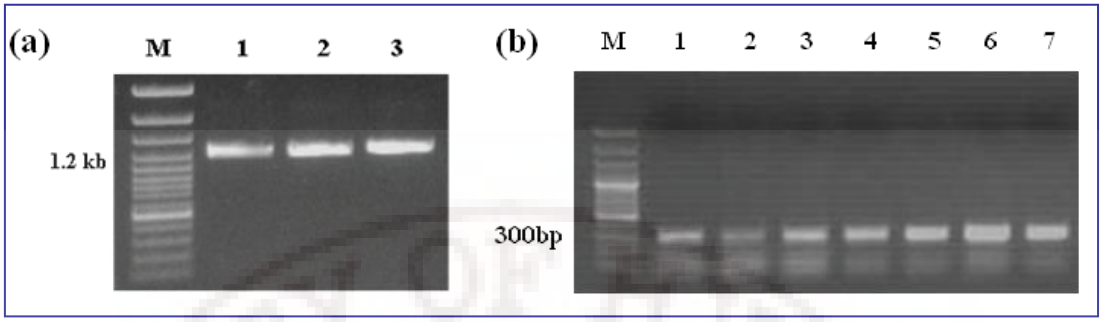

Figure 1. (a) Agarose gel electrophoresis of PCR amplified Apaf-1 (1-419): 100 bp DNA ladder (lane M), and PCR product (lanes 1-3). (b) Agarose gel electrophoresis showing colony PCR for recombinant pRCETa-Apaf-1 (1-419): Lane M: 100 bp DNA ladder, lanes (1-7) 300 bp PCR amplified Apaf-1 sequence. (For colony PCR, the CARD primers of Apaf-1 were used).

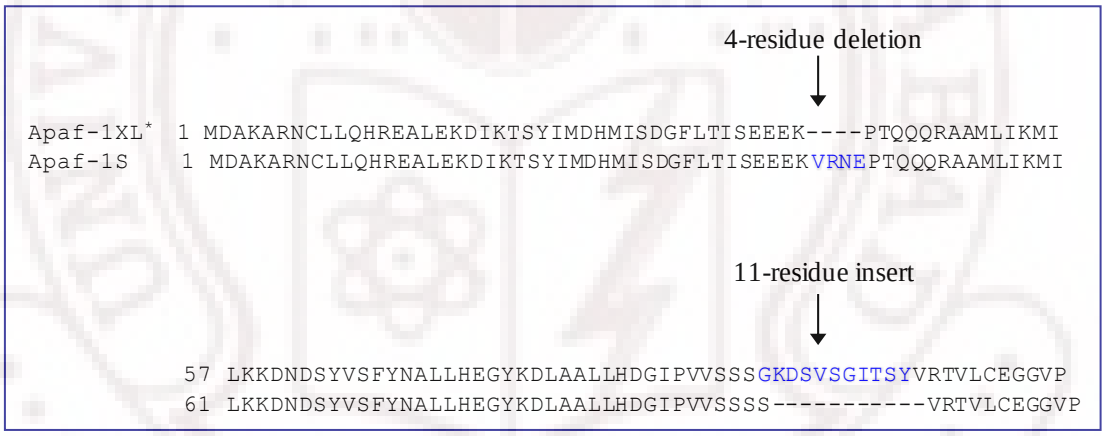

Figure 2. Principal features of the amino acid sequence of the cloned protein, Apaf1-XL* (called $^{\Delta WD40}$Apaf-1 in the text) showing the 4-residue deletion in the CARD domain, and the 11-residue insert between the CARD and ATPase domains. Apaf-1S isoform is incapable of activating procaspase-9 in a cytochrome *c* and dATP/ATP-dependent manner [3]. The rest of the sequence up to the end of the ATPase domain is same for the two isoforms. The difference between them in theWD40 domain is discussed in the text.

cytochrome *c*. This implies that only those isoforms that carry the 11-residue insert could bind dATP/ATP [7], and any other deletion or insertion elsewhere should not alter the functional activity significantly so long as the changes do not disorder the protein conformation critically. Indeed, the 4-residue deletion in the CARD domain of Apaf-1 from HepG2 cell line does not influence the structure and function of the protein. In fact, $^{\Delta WD40}$Apaf-1 studied here preserves both the conformational integrity and the ATP binding property (see below).

2.4.2 *Refolding of $^{\Delta WD40}$Apaf-1 from the inclusion body fraction*

In *E. coli* production of recombinant $^{\Delta WD40}$Apaf-1, the protein is invariably localized in the cytoplasmic inclusion body fraction. We tested the expression under several growth conditions of temperature in the 5–37 °C range with variable use of IPTG concentration up to 1 mM, but could not localize the protein in the soluble fraction. Therefore, cells were grown at 37 °C, and protein production was induced by

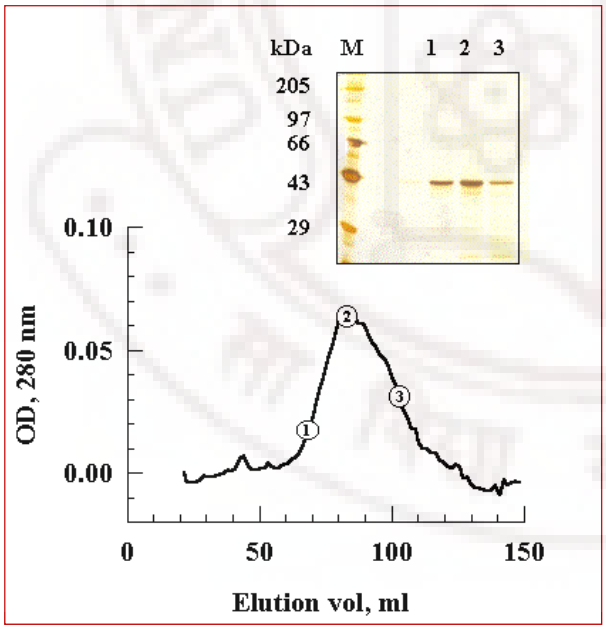

Figure 3. Sephadex G-75 isolation of $^{\Delta WD40}$Apaf-1 from the protein mixture refolded at pH 7.5 by the first procedure (5-fold dilution of the protein solution initially unfolded in 6 M GdnHCl) described in the text. Lanes 1-3 in the SDS gel correspond to the eluted fractions labeled 1-3 within circles.

adding IPTG to a final concentration of 1 mM. The insoluble aggregates of the inclusion body fraction were extensively washed, and solubilized in Buffer C that contained 6 M GdnHCl and other solvent additives (described under Materials and methods) depending on the refolding protocol considered.

Figure 3 shows the isolation by gel filtration of $^{\Delta WD40}$Apaf-1 from the refolded protein solution. Nearly complete homogeneity of the protein isolate, more surely from the left half of the elution peak, is seen in the silver-stained SDS gel (inset). Because smaller volume of sample is preferred for gel filtration work, the initial unfolded protein solution (in 6 M GdnHCl) was diluted only five-fold, so that the refolded protein solution had finally ~ 1.2 M GdnHCl. This is a subdenaturing condition, where the protein may or may not have actually refolded to the globally native state. In any case, when present in such subdenaturing amounts, GdnHCl can stabilize the folding structures by chain stiffening or entropic effect due to the cross-linking action of $GdnH^+$ cations, and electrostatic effect due to the interaction of Cl^-, and also possibly of $GdnH^+$, with charged groups of the protein [15–17]. Use of ~1 M GdnHCl in the refolding buffer is a common practice in the refolding of inclusion bodies [18, see also ref 19]. Indeed, we noticed more precipitation when the refolding was done by ten-fold dilution (~0.6 M GdnHCl, finally) of the unfolded inclusion body solution. Use of 50 mM arginine in the unfolding and refolding solutions did not alter the qualitative extent of precipitation during refolding. Gel filtration eventually removes the residual GdnHCl and arginine.

When refolded by 20-fold dilution of the unfolded protein solution so that the final concentration of GdnHCl in the refolded solution became 0.3 M, a sizable fraction of the protein precipitated, indicating that the protein-stabilizing action of the

denaturant weakens as its concentration is lowered in the bid to shift the condition from subdenaturing to native-like [15]. We then worked on the solvent condition to minimize precipitation during refolding to a final GdnHCl of 0.3 M (20 mM Tris–HCl, 500 mM NaCl). This was done by checking light scattering at 500 nm as a function of pH and L-arginine content of the refolding buffer. For the experiment with L-arginine alone, the pH of the refolded protein solution was 7.5. Effects of arginine on protein refolding and purification have been extensively investigated by Arakawa and coworkers [20–22]. Figure 4 indicates that precipitation is minimum when the pH is in the 7.5–8 range, and L-arginine concentration is 0.4 M or more. This concentration of L-arginine was previously found optimum in the refolding of recombinant mouse Bcl-2(1-203) also [23]. DTT in the 0-10 mM range does not influence protein precipitation (data not shown). Thus, for isolation of the refolded

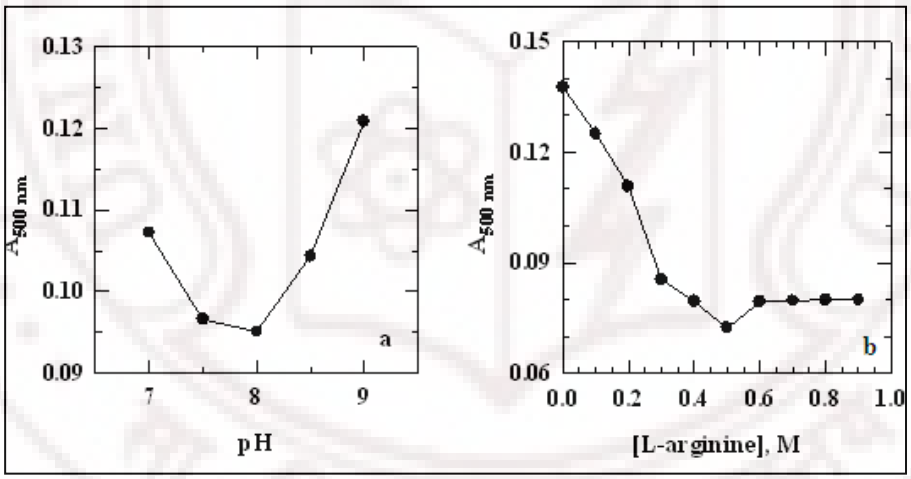

Figure 4. Effect of (a) pH, and (b) L-arginine concentrations on protein solubilization in the refolded protein solution, monitored by light scattering at 500 nm. In these experiments, the unfolded protein solution (6.0MGdnHCl, 20 mM Tris–HCl, 500 mM NaCl, pH 7.5) was diluted 20- fold into the same buffer containing no GdnHCl and the pH adjusted to different values. For the variable L-arginine experiment, pH of the refolded protein solution was 7.5.

protein by nickel-column chromatography, we carried out refolding to a final GdnHCl of 0.3 M at pH 8.0 in the presence of 0.4 M L-arginine. Elution was achieved by using imidazole or EDTA as described under Materials and methods. Figure 5a shows the EDTA elution result by silver-stained SDS gel electrophoresis.

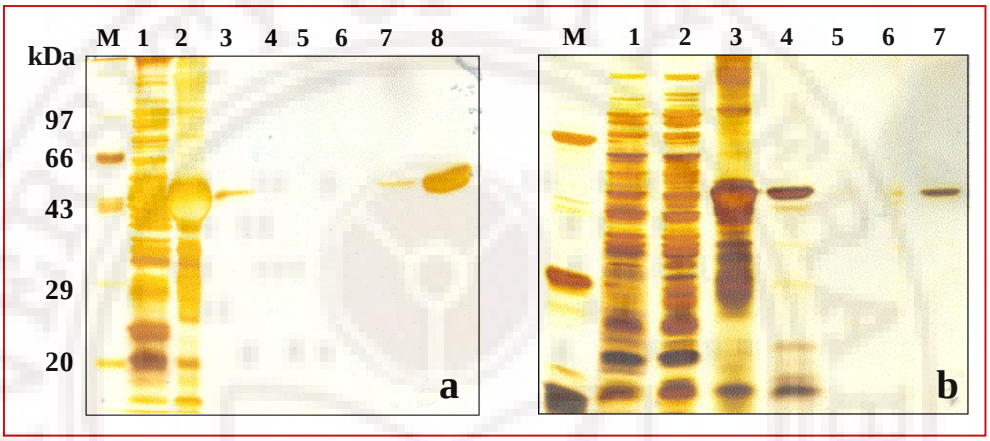

Figure 5. (a) Silver-stained SDS–PAGE analysis of the Ni-NTA resin affinity chromatographic elution of the protein refolded by 20-fold dilution of the initial 6 M GdnHCl-containing unfolded protein solution. The refolding buffer contained 0.4 M L-arginine at pH 8. Elution was performed with 50 mM EDTA. Details of the buffer composition are given in the text. Lane labels are: M, marker; 1, whole cell lysate; 2, unprocessed inclusion bodies; 3, the refolded inclusion body solution; 4, flow-through fraction from the column; 5 and 6, wash fractions; 7 and 8, elution fractions.

(b) Silver-stained SDS–PAGE analysis of Ni-resin on-column refolding. The unfolded protein (in 6 M GdnHCl) was allowed to bind to the column at pH 8, washed, and eluted as described in the text. Lane labels are: M, marker; 1, uninduced cell lysate; 2, induced cell supernatant; 3, the inclusion body fraction from induced cells; 4, the 6 M GdnHCl-unfolded inclusion bodies; 5, flow-through from the column; 6, wash fraction; 7, the eluted fraction.

Recombinant ^{WD40}Apaf-1

The identity and purity of $^{\Delta WD40}$Apaf-1 is further confirmed by the Western blot developed with polyclonal anti-Apaf-1 (Figure 6b). For removal of EDTA and Ni^{2+}, the eluted protein solution was extensively dialyzed against 20 mM Tris, 150 mM NaCl, pH 7.5

We then looked at the quantitative aspect of this procedure by starting with 1 L culture that yielded 1.6 g wet weight cells. The details of steps and procedure involved were same as described above. Protein content was estimated at various

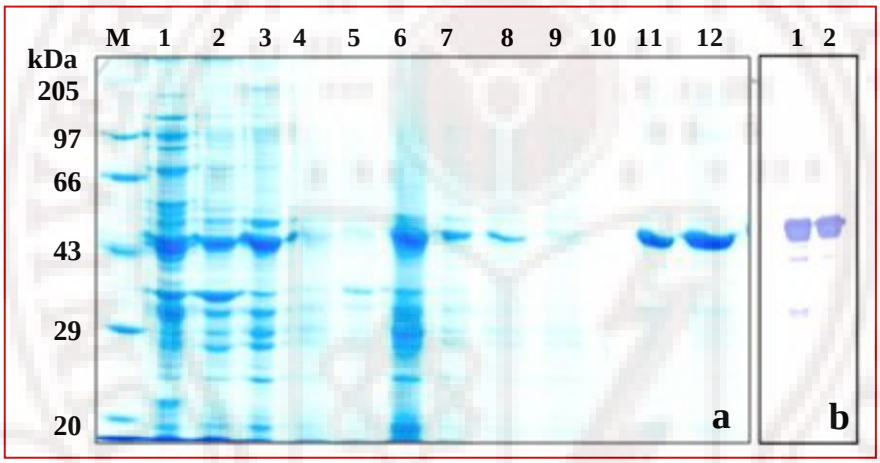

Figure 6. (a) Coomassie-stained SDS–PAGE analysis of refolding and purification. Lane labels are: M, marker; 1, whole cell lysate; 2, lysate pellet; 3, washed inclusion bodies; 4, protein debris precipitated from the solubilized (unfolded) inclusion bodies; 5, solubilized inclusion bodies; 6, refolded inclusion body solution; 7, the refolded protein solution after dialysis; 8, flow-through fraction from the Ni-NTA column; 9, wash fraction; 10 and 11, elution fractions. (b) Polyclonal anti-Apaf-1 blot of $^{\Delta WD40}$Apaf-1 obtained from the crude cell lysate (lane 1), and the purified protein (lane 2).

Table 1
Protein content and fractional purity at various stages of solubilization and purification of $^{\Delta WD40}$Apaf-1

Stage/sample	Amount of protein (mg)[a]	Fractional purity [b]
Washed cell lysate pellet	69	0.13
Solubilized inclusion bodies	13.2	0.2
Post refolding from inclusion bodies	7.9	Not estimated
The dialyzed refolded protein	4.1	50.6
Post Ni NTA chromatography	1.2	1.0

[a] The experiment was started with 1.6 g of wet weight cells obtained from 1 L culture.
[b] The fractional purity is relative to the purity of the protein (>95%) after Ni-NTA chromatography

stages of purification, although large errors were obtained in those steps that involved one or both GdnHCl and L-arginine. Excluding these, the amount of protein determined at different stages is listed in Table 1. As discussed above, $^{\Delta WD40}$Apaf-1 is localized exclusively in the inclusion body fraction. The protein amount in this fraction is 13.2 mg, and that after Ni-NTA elution finally is 1.2 mg (Table 1), indicating ~ 9% recovery. The percent purity at different stages was estimated by coomasie stained SDS gel electrophoresis (Figure. 6a). The lane descriptions and other details are given in the legend to the Figure. For each lane, the integrated density of the $^{\Delta WD40}$Apaf-1 band was divided by the amount of protein loaded in that lane, because the volume and the amount of protein loaded in different lanes were not uniform. This yielded the fractional content of $^{\Delta WD40}$Apaf-1 in the protein solution at various stages of purification. To normalize finally, the fractional contents of $^{\Delta WD40}$Apaf-1 for all lanes were divided by the fractional content corresponding to the

highest purity preparation. The error propagated through these estimations is in the 2–8% range. Table 1 provides the fractional purity at some of the stages of purification. The 0–1 scaling of purity should be considered relative to the purity of the protein eluted from Ni-NTA column (>95%).

2.4.3 *Mass, and basic conformational characterization*

Fig. 7 shows the Gauss filter-smoothed mass spectrum (TOF/TOF) of $^{\Delta WD40}$Apaf-1. The singly charged ($[M_1+H]^+$) fundamental peak corresponds to a mass of 51,594 Da. The molecular weight calculated for the 454- amino acid $^{\Delta WD40}$Apaf-1 is 51534, fairly consistent with the experimental mass data. Part of the observed mass difference of 60 could be due to incorrectly determined side chain charges used in calculations. The experimental mass should be more reliable. Of the 454-residues in the expressed protein, 35 residues in the N-terminus, including the six histidines

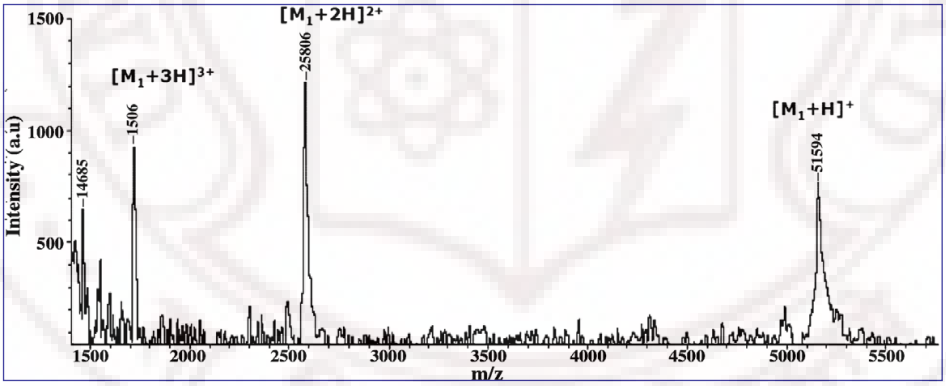

Figure 7. Molecular mass of the His_6-tagged $^{\Delta WD40}$Apaf-1 is 51,594 as indicated by mass spectrometry. The calculated mass is 51,662.

(MRGSHHHHHHGMASMTGGQQMGRDLYDDDDKDRWI), are due to the pRSETA vector. The calculated molecular weight of the actual 419-amino acid polypeptide is 47,436 Da at pH 7. Figure 8a shows the 280-nm excited tryptophan fluorescence spectra of the native and 6 M GdnHCl-unfolded proteins. The emission maximum of the native-state spectrum centered at 345 nm shifts to ~ 358 nm when the protein unfolds. The unfolding also accompanies a very significant quenching of fluorescence. Figure 8b presents the far-UV CD spectrum of purified $^{\Delta WD40}$Apaf-1, clearly indicating substantial secondary structure content. These results suggest that the 4-residue deletion mutation (Figure. 2) in the N-terminal part of the CARD domain of HepG2 Apaf-1 is unlikely to disorder the molecular conformation greatly.

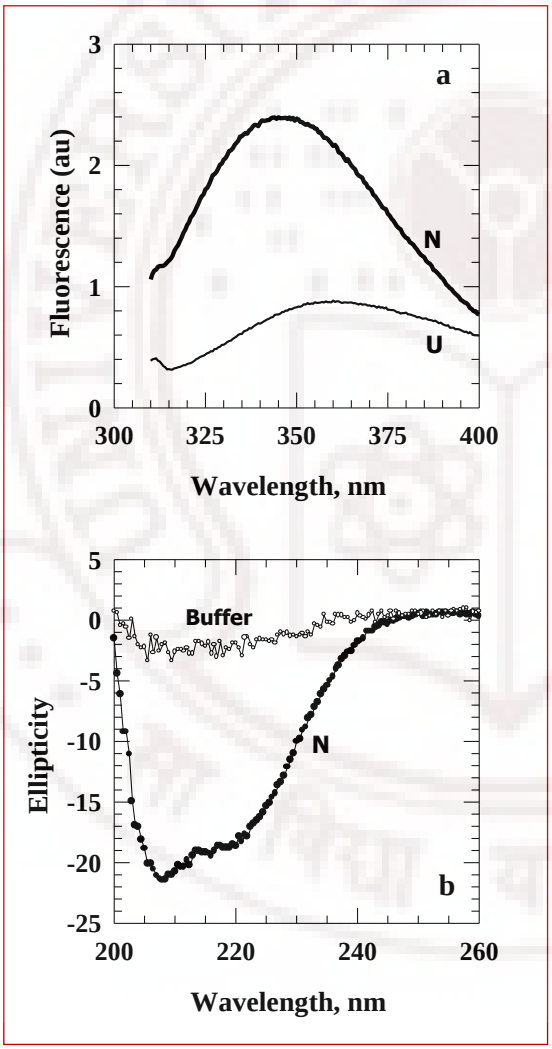

Figure 8. (a) Fluorescence spectra of the refolded native protein (N) with a peak wavelength of 345 nm. The N protein can be unfolded by the addition of 6 M GdnHCl. Fluorescence then (U) is quenched and the emission maximum red-shifts to 358 nm.

(b) The far-UV CD spectrum of the refolded protein (N) also indicates the presence of native-state secondary structures. All spectra were taken in 20 mM Tris, 100 mM NaCl, pH 7.5, 25°C.

2.4.4 *Binding of ATP to $^{\Delta WD40}$Apaf-1*

To study the equilibrium binding of ATP to $^{\Delta WD40}$Apaf-1, we used a fluorescent analog of the nucleotide, mant-ATP, whose fluorescence emission is quenched detectably when bound to proteins. Earlier studies of nucleotide binding to Apaf-1 employed [α-^{32}P]dATP for quantification by scintillation counting [5,7]. Because of high sensitivity, the fluorescence method provides more accurate data, and facilitates the measurement of rapid binding kinetics. The fluorescence emission due to a fixed concentration of mant-ATP is quenched when titrated by increments of the protein concentration as indicated in Figure. 9a. Figure. 9b plots the binding analysis as described under Materials and Methods.

The *x*-intercept of the linear fit of the data yields the association constant, K_{ass}=2.63 μM^{-1} (binding affinity, K_{diss}=1/K_{ass}=380 nM), indicating tight binding of ATP for $^{\Delta WD40}$Apaf-1. The slope of the plot (n = 0.6) indicates a 1:1 interaction, and the Gibbs free energy for ATP–Apaf-1 interaction ($\Delta G° = -RT \ln K_{ass}$) is ~ 8.7 kcal mol^{-1} at 25°C. There appear certain ambiguities in past reports regarding nucleotide binding to Apaf-1. For example, the earlier demonstration that ADP, dADP, ATP, and dATP bind to purified Apaf-1 [2] was somewhat inconsistent with a later study where Apaf-1 showed little nucleotide binding activity [5]. Similarly, it is not entirely clear whether cytochrome *c* enhances dATP binding [5] or not [2]. Our study demonstrates that ATP does bind to purified $^{\Delta WD40}$Apaf-1 in the absence of any other cofactor, and the binding affinity value of 380 nM suggests a substantially high affinity. This value for ATP–$^{\Delta WD40}$Apaf-1 interaction is inconsistent with earlier values of 1.72 and 0.86 μM for dATP–Apaf-1 interaction in the presence of cytochrome *c* and

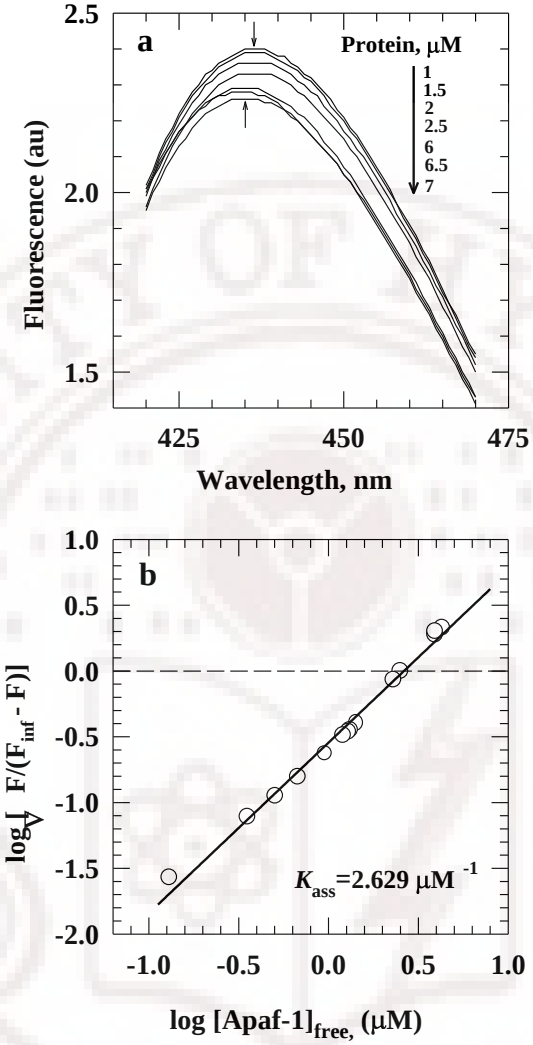

Figure 9. (a) Quenching of mant-ATP fluorescence in the presence of increasing concentration of the protein indicates ATP binding. Spectra were recorded after equilibrating the ATP-protein mixture at 25 °C for 1 h in 50 mM Tris, 50 mM NaCl, 10 mM MgCl2, pH 7. (b) The final plot for analysis of ATP binding data as described under Materials and methods (Eqs. 1 and 2). The equilibrium association constant, K_{ass} = ~2.63 μM^{-1}, is calculated from the *x*-intercept of the straight line (pK_{ass}). The binding affinity, K_{diss}=1/K_{ass}=380 nM. The slope of the line (n = 0.6) indicates a 1:1 binding interaction.

cytochrome *c* plus caspase-9, respectively, measured by scintillation counting of radioactive dATP [5]. In fact, Apaf-1 prefers dATP to ATP [24–26], and therefore the affinity of dATP for Apaf-1 should be ~ 5-fold more than that of ATP [5]. The reasons for the observed lack of consistency, and the other molecular details of Apaf-1–nucleotide interaction, including the influence of the WD40 domain, will be addressed in detail in due course of the study. It is likely that slow oligomerization and/or aggregation of Apaf-1 is partly responsible for the inconsistencies and the disparate in vitro results. In our study, the purified $^{\Delta WD40}$Apaf-1 is monomeric, as reflected by its elution volume in the Sephadex G75 chromatogram (Figure. 3) Since the ATP binding experiments were performed with freshly prepared protein (without storage in between), it is likely that a large fraction of the protein was in monomeric form. At this stage, we cannot provide quantitative data for time dependent oligomerization. Although the binding results presented here demonstrate that the 4-residue deletion in the CARD domain of HepG2 Apaf-1 does not abrogate ATP binding, it might affect other details—the rate constants for binding interaction, and hydrolysis to ADP and Pi, for example. As mentioned in the introduction, knowledge of such mechanistic issues is central to understand the regulatory role of Apaf-1 in cell death. These studies should have applications in the induction of caspase activated apoptosis in therapeutics.

2.5 Summary and conclusion

Apaf-1XL isoform from HepG2 cell line carries a 4-residue deletion in the CARD domain. The N-terminal His_6- tagged protein, termed $^{\Delta WD40}$Apaf-1, over expressed in *E. coli* is localized exclusively in the cytoplasmic inclusion body fraction, unaffected by growth conditions in the 5–37 °C range of temperature and induction by IPTG concentrations from 0.1 to 1 mM. The protein is refolded best by 20- fold dilution of the initial 6 M GdnHCl-unfolded inclusion body preparation into a

buffer system composed of 20 mM Tris–HCl, 500 mM NaCl, 0.5 M Urea, 0.4 M L-arginine, pH 7.5–8. Highly pure protein can be isolated by Ni^{2+}-resin chromatography with 20 mM Tris, 150 mM NaCl, 50 mM EDTA, pH 8.0 as the elution buffer. The protein thus purified displays fluorescence and far-UV CD spectra characteristic of folded proteins. The interaction of $^{\Delta WD40}$Apaf-1 with ATP has been studied by the use mant-ATP whose fluorescence decreases as it binds to the protein. The 1:1 ATP–$^{\Delta WD40}$ Apaf-1 interaction is characterized by the equilibrium dissociation constant, K_{diss}, of 380 nM, and $\Delta G° = -RT \ln K_{ass} = 8.7$ kcal mol^{-1} (25°C), indicating tight affinity.

2.6 References

[1] X. Jiang, X. Wang, Cytochrome *c*-mediated apoptosis, Annu. Rev. Biochem. 73 (2004) 87-106.

[2] H. Zou, Y. Li, X. Liu, X. Wang, An Apaf-1·cytochrome *c* multimeric complex is a functional apoptosome that activates procaspase-9, J. Biol. Chem. 274 (1999) 11549-11556.

[3] Y. Hu, M.A. Benedict, L. Ding, G. Núñez, Role of cytochrome *c* and dATP/ATP hydrolysis in Apaf-1-mediated caspase-9 activation and apoptosis. EMBO J. 18 (1999) 3586-3595.

[4] H. Zou, W. J. Henzel, X. Liu, A. Lutschg, X. Wang, Apaf-1, a human protein homologous to C. elegans CED-4, participates in cytochrome *c* dependent activation of caspase-3. Cell 90 (1997) 405-413.

[5] X. Jiang, X. Wang, Cytochrome *c* promotes caspase-9 activation by inducing nucleotide binding to Apaf-1. J. Biol. Chem. 275 (2000) 31199-31203.

[6] A. Saleh, S.M. Srinivasual, S. Acharya, R. Fishel, E.S. Alnemri, Cytochrome *c* and dATP-mediated oligomerizationof Apaf-1 is a prerequisite for procaspase-9

activation. J. Biol. Chem. 274 (1999) 17941-17945.

[7] S.J. Riedl, W. Li., Y. Chao., R. Schwarzenbacher, Y. Shi, Structure of the apoptotic protease-activating factor 1 bound to ADP. Nature 434 (2005) 926-933.

[8] X. Wang, The expanding role of mitochondria in apoptosis. Genes Dev. 15 (2001) 2922-2933.

[9] M.A. Benedict, Y. Hu. N. Inohara, G. Núñez, Expression and functional analysis of Apaf-1 isoforms: extra WD-40 repeat is required for cytochrome *c* binding and regulated activation of procaspase-9. J. Biol. Chem. 275 (2000) 8461-8468.

[10] D. Acehan, X. Jiang, D.G. Morgan, J.E. Heuser, X. Wang, C.W. Akey, Three dimensional structure of the apoptosome: implications for assembly, procaspase-9 binding and activation. Mol. Cell 9 (2002) 423-432.

[11] X. Yu. D. Acehan, J. Ménétret, C.R. Booth, S.J. Ludtke, S.J. Riedl, Y. Shi, X. Wang, C.W. Akey, A structure of the human apoptosome at 12.8Å resolution provides insights into this cell death platform. Structure 13 (2005) 1725-1735.

[12] X. Yu. L. Wang, D. Acehan, X. Wang, C.W. Akey, Three-dimensional structure of a double apoptosome formed by the Drosophila Apaf-1 related killer. J. Mol. Biol. 355 (2006) 577-589.

[13] J. Nakabayashi, A. Sasaki, A mathematical model for apoptosome assembly: the optimal cytochrome *c*/Apaf-1 ratio. J. Theor. Biol. 242 (2006) 280-287.

[14] P. Zhou, J. Chou, R.S. Olea, J. Yuan, G. Wagner, Solution structure of Apaf-1 CARD and its interaction with caspase-9 CARD: a structural basis for specific adaptor/caspase interaction. Proc. Natl. Acad. Sci. USA 96 (1999) 11265-11270.

[15] A.K. Bhuyan, Protein stabilization by urea and guanidine hydrochloride. Biochemistry 41 (2002) 13386-13394.

[16] R. Kumar, N.P. Prabhu, M. Yadaiah, A.K. Bhuyan, Protein stiffening and entropic stabilization in the subdenaturing limit of guanidine hydrochloride. Biophys. J. 87 (2004) 2656-2662.

[17] A. Zarrine-Afsar, A. Mittermaier, L.E. Kay, A.R. Davidson, Protein stabilization by specific binding of guanidinium to a functional arginine-binding surface on an SH_3 domain. Protein Sci. 15 (2006) 162-170.

[18] A.P.J. Middelberg, Preparative protein refolding. Trends. Biotech. 20 (2002) 437-443.

[19] K. Tsumoto, D. Ejima, I., Kumagai, T. Arakawa, Practical considerations in refolding proteins from inclusion bodies. Protein Express. Purif. 28 (2003) 1-8.

[20] T. Arakawa, K. Tsumoto, K. Nagase, D. Ejima, The effects of arginine on protein binding and elution in hydrophobic interaction and ion-exchange chromatography. Protein Express. Purif. 54 (2007) 110–116.

[21] K. Tsumoto, D. Ejima, K. Nagase, T. Arakawa, Arginine improves protein elution in hydrophobic interaction chromatography: The cases of human interleukin-6 and activin-A. J. Chromatogr. A 1154 (2007) 81–86.

[22] T. Arakawa, K. Tsumoto, Y. Kita, B. Chang, D. Ejima, Biotechnology applications of amino acids in protein purification and formulations. Amino Acids (2007) doi: 10.1007/s00726-007-0506-3.

[23] B.A. Vance, C.M. Zacharchuk, D.M. Segal, Recombinant mouse Bcl-2(1-203): two domains connected by a long protease-sensitive linker. J. Biol. Chem. 271 (1996) 30811–30815.

[24] X. Liu, C.N. Kim, J. Yang, R. Jemmerson, X. Wang, Induction of apoptotic program in cell-free extracts: requirement for dATP and cytochrome *c*. Cell 86 (1996) 147–157.

[25] L.M. Leoni, Q. Chao, H.B. Cottam, D. Genini, M. Rosenbach, C.J. Carrera, I. Budihardjo, X. Wang, D.A. Carson, Induction of an apoptotic program in cell-

free extracts by 2-chloro-20 deoxyadenosine 50 triphosphate and cytochrome *c*. Proc. Natl. Acad. Sci. USA 95 (1998) 9567–9571.

[26] D. Genini, I. Budihardjo, W. Plunkett, X. Wang, C.J. Carrera, H.B. Cottam, D.A. Carson, L.M. Lepni, Nucleotide requirement for the in vitro activation of the apoptosis protein-activating factor-1 mediated caspase pathway. J. Biol. Chem. 275 (2000) 29–34.

CHAPTER 3

Bacterially expressed recombinant WD40 domain of human Apaf-1

3.1 Abstract

The apoptotic protease activating factor (Apaf-1) is a protein that upon binding to cytochrome *c* and in the presence of dATP/ATP oligomerizes to assume the role of an adaptor platform for activating the caspase-9 zymogen. In order to study the biochemical and structural details of Apaf-1 function, we have generated an expression construct from pcDNA 3-Apaf-1XL for production of the WD40 domain (^{WD40}Apaf-1) in *E .coli*. The WD40 domain expressed contains 825 amino acids in addition to an N-terminal His_6 tag derived from the cloning vector. The expressed protein is invariably localized in the inclusion body fraction of *E. coli*. A simple protocol involving Sephadex G100 chromatography developed for purifying the protein starting from inclusion bodies has allowed protein recovery in highly pure form. Basic fluorescence and CD spectra indicate that the refolded protein retains extensive secondary and tertiary structures. Immunoprecipitation studies have provided qualitative information about the binding interaction of ^{WD40}Apaf-1 and cytochrome *c*. The binding interaction has been quantified by spectrophotometric titration of cytochrome *c* with recombinant ^{WD40}Apaf-1. The results demonstrate a fairly tight binding for cytochrome c and ^{WD40}Apaf-1 interaction, the binding affinity being 390 nM. The analysis indicates a 2:1 or possibly 3:1 stoichiometry for cytochrome *c* and ^{WD40}Apaf-1 binding interaction.

3.2 Introduction

A key upstream event in the mitochondrial pathway of apoptosis is the cytochrome *c* dependent activation of procaspase-9 so that the processed caspase-9 can propagate the death signal by triggering events leading to activation of downstream caspases [1,2]. Apaf-1 is the protein that mediates the initial event of caspase-9 activation [3,4]. By binding to cytochrome *c* translocated from mitochondria, Apaf-1 is thought to self-associate in the presence of dATP/ATP to produce a homo-multimer that contains at least 8 subunits of Apaf-1 [3]. This homo-multimeric complex in which cytochrome *c* and dATP are presumably still bound to each Apaf-1 subunit is generically dubbed the 'apoptosome' [3-6] − an assembly that recruits procaspase-9 and activates it into caspase-9 [3, 4, 7]. The initiating events and structural mechanism by which Apaf-1 multimerizes to assemble a functional apoptosome is inexplicably complex, and to a large extent the size and form of Apaf-1 itself generates the complexity. Apaf-1 contains a CED-4 homologous domain that straddles a *Ca*spase *R*ecruitment *D*omain (CARD) in the N-terminal region and a C-terminal WD-40 domain containing 12 or 13 WD-40 repeats depending on the isoform [3,4, 8, 9]. The oligomerization of Apaf-1 and gross structural and topological details of the apoptosome have been viewed by electron cryomicroscopy [10-12]. A theoretical model for Apaf-1 heptamer assembly has also been reported [13]. However, there exists an acute dearth of atomic-level structural descriptions of Apaf-1 and its multimeric complex, although NMR solution structure of the CARD domain [14] and a 2.2 Å crystal structure of an ADP-bound CARD and CED-4 homologous domains together [15] have been reported.

The WD40 domain at the C-terminal part accounts for approximately 66% of Apaf-1 primary sequence. The finding of at least 12 WD-40 repeats in this domain aroused interest right from the seminal stage of Apaf-1 description [8]. WD-repeat

proteins invariably assume a β-propeller fold and are thus structurally related, but their functions remain poorly understood [16, 17]. Nonetheless, the large content of Asp in the WD40 domain of Apaf-1 together with the finding that Apaf-1 binds to cytochrome *c*, a basic protein rich in Lys, points to the possibility that Asp-Lys charge-charge interactions form the basis for Apaf-1 binding to cytochrome *c*. There is no definite structural support for this possibility except for the demonstration that ionic strength has a profound effect on the interaction [18]. In view of the importance and interest in the structure, binding epitope, and functional regulation of Apaf-1, it is imperative that recombinant WD40 domain is made available. Proteins, the size of the WD40 domain (825 amino acid residues for the present study) are often difficult to produce in bacterial overexpression system.

This study develops an expression construct for *E. coli* expression of ^{WD40}Apaf-1. The gene construct excludes the contiguous CARD and CED-4 homologous domains whose cloning and *E. coli* expression has already been described in Chapter 2 [also, ref 19]. This Chapter reports on the cloning, *E. coli* expression, refolding, and cytochrome *c* binding properties of the WD40 repeat domain of the human Apaf-1XL isoform, called ^{WD40}Apaf-1 henceforth.

3.3 Materials and methods

3.3.1 *Cloning and generation of expression construct for ^{WD40}Apaf-1*

The gene sequence encoding the 2.5 kb ^{WD40}Apaf-1 (amino acid residues 424–1248) region was specifically amplified from pcDNA3-Apaf-1XL, a generous gift from Gabriel Nunez's laboratory, by standard PCR reaction. The forward and reverse primers flanking the WD40 region of Apaf-1XL were:

Recombinant ^{WD40}Apaf-1

*Bam*H1

WD40-F: 5′ CG**GGATCC**TTATTCTGTGATCGGAATGG 3′

WD40-R: 5′ CC**CTCGAG**TTATTCTAAAGTCTGTAAAATATA 3′

*Xho*1

Restriction sites were included at the 5' end of each primer to facilitate cloning into pRSETa vector (Invitrogen), and the region of ~ 2.5 kb corresponding to ^{WD40}Apaf-1 was amplified using MBI-Fermentas long PCR enzyme mix. The 50 µL reaction mixture contained 5.0 µL 10X long PCR buffer, 10 pmole each of forward and reverse primers, 100 ng of pcDNA 3-Apaf-1 XL as template, and 2.5 U/µL of long PCR enzyme mix. The PCR amplification involved initial denaturation at 94 °C for 2 min, followed by 30 cycles each consisting of a 30 s denaturation at 94 °C, a 30 s annealing at 55 °C, and a 2.5 min extension at 72 °C. To facilitate TA cloning, the final extension was allowed for 15 min at 72 °C. The amplified PCR product was analyzed by agarose gel electrophoresis. The 2.5 kb ^{WD40}Apaf-1 fragment was sliced from the gel, eluted by using Qiagen gel extraction column, ligated into the TA vector pTZ57R/T (MBI-Fermentas), and transformed into DH5α *E. coli* cells. The cells were plated onto agar plates containing 100 µg/mL ampicillin. Positive recombinant clones of ^{WD40}Apaf-1 were selected by colony PCR. Plasmids were isolated and digested with *Bam*H1 and *Xho*1 restriction enzymes. The digested fragments were run on 1.0% agarose gel, and the digested 2.5 kb ^{WD40}Apaf-1 was sliced from the gel and eluted by gel extraction columns. This was ligated between the *Bam*H1 and *Xho*1 sites of pRSETa expression vector (Invitrogen). The recombinant pRSETa–^{WD}40Apaf-1 clones were selected by colony PCR, and confirmed by restriction digestion.

3.3.2 *Protein expression*

The recombinant pRSETa–^{WD40}Apaf-1 plasmids were sequenced before transforming into *E.coli* BL21 DE3 cells. Many singly isolated colonies were selected and screened for soluble expression of ^{WD40}Apaf-1. Unfortunately, we could not obtain any soluble expression of the protein. Use of different *E. coli* strains, and variable growth conditions, including temperature and IPTG concentration, did not ameliorate the situation. Facing this difficulty, we decided to proceed with inclusion bodies.

3.3.3 *Cell growth and harvest, cell lysis, and inclusion body washing*

These steps were carried out using procedures already described for $^{\Delta WD40}$Apaf-1 [19] with minor modifications. Briefly, *E. coli* BL21 DE3 cells containing the pRSETa–^{WD40}Apaf-1 plasmid were grown in LB medium containing ampicillin (100 μg/mL). Typically, 10 mL of an overnight grown culture was added to a 1 L medium, and grown upto OD_{600} = 0.5 at 37 °C. Protein expression was then induced by adding IPTG to a final concentration of 1 mM, and growth was continued for 5 h. Cells were harvested by centrifugation at 4000g for 10 min at 4 °C, washed with TE buffer (10 mM Tris–HCl, 1 mM EDTA pH 8.0), and frozen-stored at –80 °C. For lysis, 2 g of the cell pellet (wet weight) obtained from 1 L culture was suspended in 20 mL of the lysis buffer (20 mM Tris–HCl, 100 mM NaCl, 1 mM PMSF, pH 8.0, containing 10 μL of 1 mg/mL DNaseI), and sonicated at 4 °C with 10 cycles, each cycle consisting of 30 s on and 60 s off times. The lysate was treated with deoxycholic acid (4 mg per gram weight of *E. coli*), stirred for 30 min at room temperature, and centrifuged at 10,000 rpm for 15 min at 4 °C. The pellet was resuspended in ~ 9 volumes of a buffer consisting of 20 mM Tris, 100 mM NaCl, 10 mM EDTA, 0.5% Triton X-100, at pH 8.0, stirred at room temperature for 5 min and centrifuged at 10,000 rpm for 15 min at 4 °C. The step was repeated. Inclusion bodies

were then washed with ~ 10 volumes of 20 mM Tris–HCl containing 100 mM NaCl at pH 8.0 three times to remove the Triton X-100. In the effort to remove the unwanted materials as far as possible, a final wash was given with ~10 volumes of 20 mM Tris–HCl containing 2.5 M GdnHCl at pH 8.0. Washed inclusion bodies are now ~ 95% pure.

3.3.4 *Finding optimal pH for refolding*

To measure the optimal pH for refolding, the inclusion bodies were first unfolded in buffer A (50 mM Tris–HCl, 0.15 M NaCl, 5 mM EDTA, 5 mM DTT, 6.0 M GdnHCl, pH 8.0), incubated for 2 h at room temperature, and spun at 20,000g for 15 min. The supernatant was then diluted 10-fold by adding buffer B (refolding buffer: 0.5 M NaCl, 0.25 M arginine, 0.5 M urea, 1 mM EDTA, and 1 mM DTT in 50 mM Tris–HCl for the 7–10.5 range of pH values, and in 50 mM sodium acetate for the 4.0–6.5 range of pH values). In all of these refolding trials, the final protein concentration was ~ 100 μg/mL. The refolded proteins samples were incubated for 2 h at 4 °C. The refolding efficacy was determined spectrophotometrically by turbidity measurement at 450 nm. By observing a dramatic decrease in turbidity at pH > 8.5, we decided to refold the protein at pH 8.8. It should be noted that attempts to refold the protein at lower pH values showed little success. However, in the steps followed for purification of the refolded protein, pH 8.0 was employed (see below). The multitude of refolding conditions checked by the turbidity measurement also suggested the inclusion of 400 mM arginine and 2 mM DTT in the refolding buffer. The buffer B mentioned above then would contain 0.4 M arginine, 2 mM DTT, and 0.1% glycerol.

3.3.5 *Preparative refolding and purification of ^{WD40}Apaf-1*

Inclusion bodies containing ~34 mg protein were solubilized in 2.5 mL of the unfolding buffer (buffer A as described above). Following 4 h of incubation at room temperature, the solution was centrifuged at 20,000g for 15 min at 4 °C. For refolding, the supernatant was diluted 10-fold by slow addition of the refolding buffer (buffer B: 50 mM Tris, 0.5 M NaCl, 0.5 Murea, 0.4 M arginine, 2 mM DTT, 0.1% glycerol, pH 8.8), and equilibrated overnight at 4 °C. The solution appeared a little turbid the following morning, but was clear when centrifuged at 20,000g for 15 min at 4 °C. For purification of the refolded protein, two approaches were employed. In one, the supernatant obtained from the protein solution refolded at pH 8.8 was loaded onto a Ni–NTA column equilibrated in 20 mM Tris, 0.5 M NaCl, 0.5 M urea, 1 mM β- mercaptoethanol, pH 8.0, washed thoroughly with the same buffer, and eluted with 20 mM Tris containing 0.25 M imidazole at pH 8.0. Here, although the refolding was carried out at pH 8.8 outside the column, pH 8.0 was chosen to meet with the condition for Ni–NTA chromatography. Eluted fractions were pooled and dialyzed against 20 mM Tris containing 50 mM NaCl, pH 8.0. In the other procedure, the refolding was carried out at pH 8.8, and the supernatant obtained was simply chromatographed using a 200 mL (100 X 1.6 cm) Sephadex G100 column equilibrated in 20 mM Tris containing 50 mM NaCl, pH 8.0. Here again, we chose pH 8.0 for gel filtration to avert undesirable exposure of the protein to the actual refolding pH. As discussed later, the gel filtration method produces not only higher purity protein, but is also more reliable and reproducible. The eluted fractions were pooled and concentrated by centrifugal filters (Amicon). Signs of aggregation however, appear whenever the protein concentration exceeds ~ 500 μg/mL.

3.3.6 *Western blot*

A mixture of 50 μg each of horse heart cytochrome *c* and ^{WD40}Apaf-1 in 0.5X PBS was incubated at 4 °C overnight with constant shaking. To the mixture, 1 μg of anti-cytochrome *c* monoclonal antibody (Novagen) was added and incubated for 3–4 h at 4 °C. Then 100 μL of 50% protein A agarose beads were added and incubated for 3 h at 4 °C with shaking. The beads were centrifuged at 2000 rpm for 1 min and the pellet was washed three times with 0.5x PBS taking 0.5 mL for each wash. To the washed beads, 60 μL of 2X sample-loading dye was added, boiled for 5 min to dissociate the immuno complex, and the beads were collected by centrifugation. The protein-containing supernatant was separated by 12% SDS-PAGE, and transferred onto a PVDF membrane. One set of membranes was probed with anti-His and the other with anti cytochrome *c* mouse monoclonal antibody. The membranes were incubated with corresponding 2° antibodies (anti-mouse IgG-conjugated with alkaline phosphatase) and developed with BCIP-NBT solution.

3.3.7 *Mass spectrometry*

The sample for mass spectrometric measurement was prepared by in-gel tryptic digestion. Briefly, the coomassie-stained SDS/PAGE band containing pure ^{WD40}Apaf-1 was excised from the gel, destained with a 1:1 (v/v) solution of ACN and 2 μg/μL NH_4HCO_3, and dried with ACN. The protein still in the gel piece was reduced with DTT in 25 mM L^{-1} NH_4HCO_3 for 1 h at 50 °C, and alkylated for 45 min at room temperature using 55 mM L^{-1} iodoacetamide in 25 mM L^{-1} NH_4HCO_3. The gel piece was then dehydrated with ACN, rehydrated with a minimal volume of 50 mM L^{-1} NH_4HCO_3 containing trypsin (10 ng μL^{-1}), and incubated at 37 °C for 16 h. The peptides were extracted twice with 50% (v/v) acetonitrile containing 1% (v/v) TFA. The peptide mixture was concentrated under vacuum. The tryptic peptides were dissolved in 2 μL of 50% (v/v) ACN containing 1% (v/v) TFA, and mixed with

2 μL of 1% cyano-4- hydroxycinnamic acid (HCCA) dissolved in 50% ACN and 1% TFA. About 1 μL of this solution was applied on MALDI target plates. Spectra were taken using a MALDI TOF/TOF Autoflex spectrometer (Bruker Daltonics) in reflectron mode. MS/MS of selected peptides were performed by LIFT (a device integrated in the mass spectrometer for raising the potential energy of the ions). The spectra were calibrated by Pepmix (Bruker Daltonics).

3.3.8 *CD and fluorescence measurement*

Spectra of the purified protein in native and GdnHCl-unfolded states were taken at 22 °C. The buffer was 20 mM Tris, 10 mM NaCl, pH 7, and the final protein concentration in the samples was ~3 (±1) μM. To unfold the protein, the desired concentration of GdnHCl was incorporated in the buffer. For fluorescence, a photon counting instrument (FluoroMax-3, Jobin-Yvon) was used (excitation: 280 nm, 1.5 nm slit). CD spectra were taken in a JASCO J715 spectropolarimeter with the protein solution contained in 2 mm path length cylindrical cell. Sixteen scans were averaged.

3.3.9 *Determination of equilibrium constant for the binding of ^{WD40}Apaf-1 to cytochrome c*

These experiments involved equilibrium titration of reduced cytochrome *c* by ^{WD40}Apaf-1. A set of samples containing 0.8 μM cytochrome *c* and variable concentration of ^{WD40}Apaf-1 in the 0– 1.4 μM range was prepared in 20 mM Tris, 10 mM NaCl, 1 mM DTT, pH 7. This procedure for titration where separate samples are used for each increment of the titrant avoids dilution effects. Samples were incubated for ~ 4 h at 22 °C before recording baseline-corrected optical absorption spectra in the 500–390 nm wavelength region using a Cary 100 (Varian) spectrophotometer. Absorbance at 415 nm, which is the Soret maximum for DTT-

reduced cytochrome *c*, was used for binding analysis. The concentration of free ^{WD40}Apaf-1 in the titration mixture is given by

$$[^{WD40}\text{Apaf} - 1]_{\text{free}} = \frac{[cyt\ \text{c}] \times \Delta \text{A}}{\Delta \text{A}_{\infty}} \quad (1)$$

in which, $\Delta A = A_x - A_o$ and $\Delta A_\infty = A_\infty - A_o$, where A_o, A_x, and A_∞ are 415-nm absorbance of solutions containing cytochrome *c* alone, cytochrome *c* in the presence of *x* concentration of ^{WD40}Apaf-1, and cytochrome *c* in the presence of saturating concentration of ^{WD40}Apaf-1, respectively. The pK_a value for cytochrome *c*-^{WD40}Apaf-1 interaction is extracted from the *x*-intercept of the plot of log $[\Delta A/(A_\infty - A_x)]$ vs log $[^{WD40}\text{Apaf-1}]_{\text{free}}$ according to the equation

$$\log\left[\frac{\Delta \text{A}}{\text{A}_{\infty} - \text{A}_x}\right] = \log \text{K}_{\text{ass}} + \log[^{WD40}\text{Apaf} - 1]_{\text{free}} \quad (2)$$

3.4 Results and discussion

3.4.1 *A 43-residue insert in the ^{WD40}Apaf-1*

The 2.5 kb gene sequence used to create the expression construct of ^{WD40}Apaf-1 has been amplified from pcDNA 3-Apaf- 1XL (Figure. 1a). The Apaf-1 protein has been found in multiple isoforms [3–5,9,19], and the occurrence of full-length isoforms in tumor cell lines is believed to arise from alternative splicing of the gene that can generate an 11-residue insert between the CARD and ATPase domains or a 43-residue insert almost in the middle of the WD40 domain, or both [9]. The Apaf-1XL isoform carries both inserts [4], and thus has 1248 amino acids instead of 1194 for the canonical Apaf-1 first identified in HeLa cells [8]. Hence, the construct generated in this study codes for the entire WD40 domain (amino acid residues 424–1248) with the additional 43 residues inserted between residues 811 and 812.

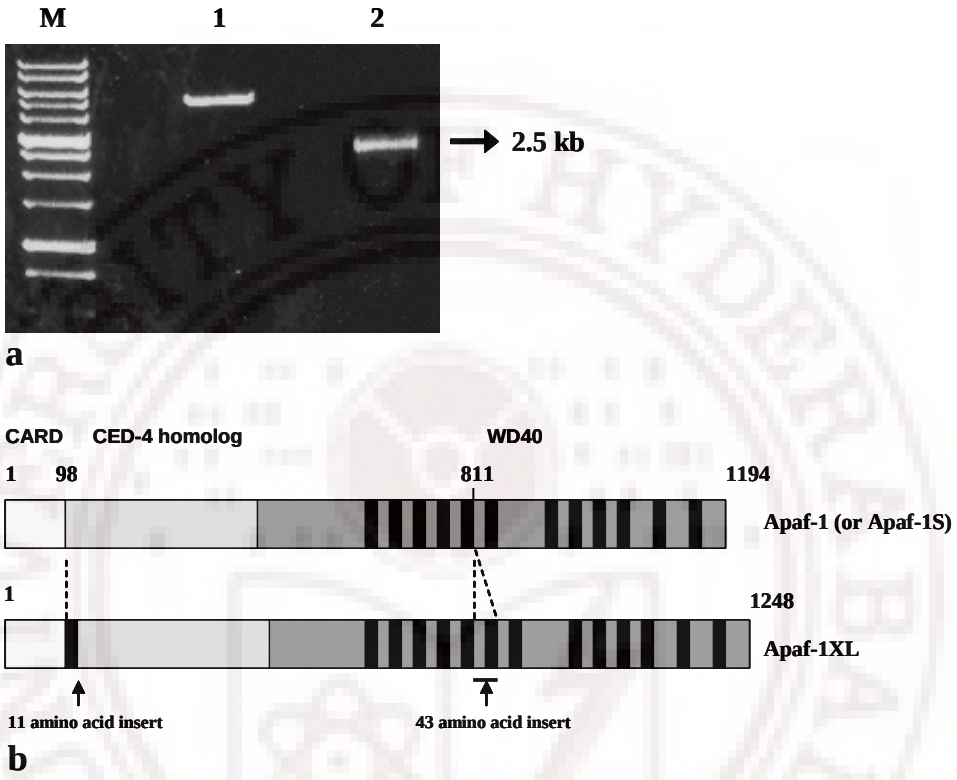

Figure 1. (a) 1% Agarose gel electrophoresis of PCR amplified ^{WD40}Apaf-1: 1000 bp DNA ladder (lane M), and PCR product (lanes 1 and 2). (b) Schematic of the Apaf-1 domains. The amino acid inserts in the Apaf-1XL isoform are also shown. The 43 amino acids insert in the WD40 domain of the latter introduces an additional WD-40 repeat. In the present work, the expression construct for the WD40 domain of Apaf-1XL (called ^{WD40}Apaf-1 in the text) is generated.

With reference to the 12 WD40 repeats in the WD40 domain of the originally described Apaf-1 from HeLa cells [8], the ^{WD40}Apaf-1 studied here contains the last three amino acids of a WD40 repeat followed by another WD40 repeat (Figure 1b), thus accounting for the additional 43 residues in the WD40 domain of Apaf-1XL [4].

Recombinant ^{WD40}Apaf-1

Since the additional WD40 repeat has been demonstrated essential for cytochrome *c* binding function of Apaf-1 [9], obtaining the recombinant WD40 domain containing all 13 WD40 repeats provides an opportunity to investigate whether the CARD and ATPase domains are determinants of the cytochrome *c* binding efficacy of Apaf-1.

3.4.2 *Refolding and purification of ^{WD40}Apaf-1 from the inclusion body fraction*

A recombinant protein, the size of ^{WD40}Apaf-1 (825 residues) is normally not expected to be localized in the *E. coli* soluble fraction. We nonetheless tested several conditions of temperature, growth time, and IPTG concentration under which ^{WD40}Apaf-1 could possibly be found in the soluble fraction, but the protein is invariably localized in the cytoplasmic inclusion body fraction. Therefore, to maximize the protein content in the inclusion bodies, we grew cells at 37 °C and induced protein production by using 1 mM final concentration of IPTG.

The details of buffer systems and the protein refolding procedure from the inclusion body fraction are described under Materials and methods. In search for optimal protein folding conditions, we refolded the protein at various final pH values and in the presence of variable concentration of DTT in the refolding buffer, and measured the turbidity of the refolded protein solutions. From the observation of a sharp decrease in turbidity for pH > 7.5 (Figure. 2a), we set the refolding pH to 8.8. A higher pH value (>9) was not chosen with the view that the structural and energetic stability of the protein may deteriorate. But the pH midpoint of 8.4, determined from the calculated transition (the solid line through the data points), raises curiosity with regard to the involvement of the specific residue(s). The value of 8.4 distinctively stands out for the pKa of the cysteine side chain, and since there are at least 24 cysteines in ^{WD40}Apaf-1, it would appear that protonation of the cysteine side chains

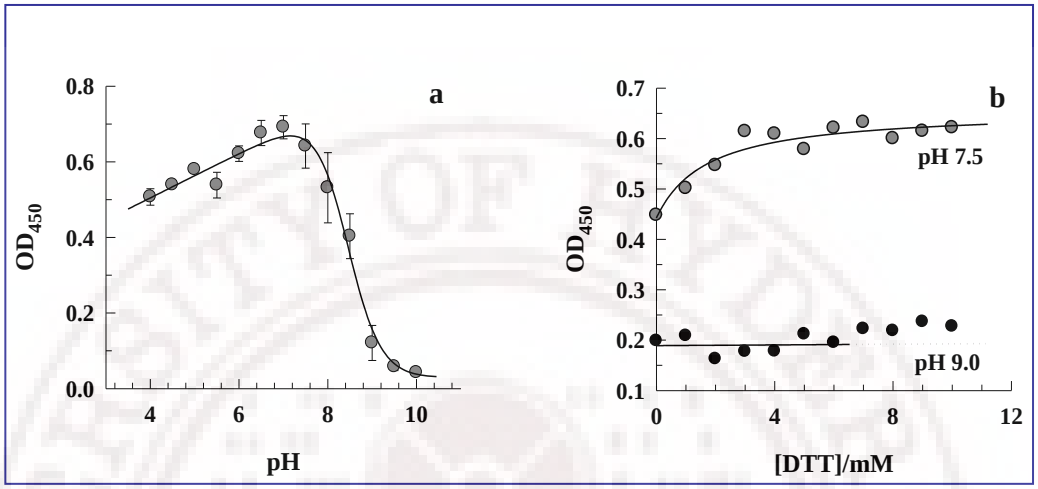

Figure 2. Effects of pH and DTT on protein solubilization in the refolded protein solution monitored by light scattering at 450 nm. The buffers used for solubilization of inclusion bodies and subsequent refolding are described in the text. (a) Turbidity dramatically decreases when the protein is refolded to a final pH>7.5 (see text). Error bars were generated from three sets of independent measurements. The solid line through the data represents a pH-titration fit with a midpoint of 8.35. (b) Presence of DTT in the refolding buffer enhances turbidity at pH 7.5 but shows no effect at pH 9. The solid lines in this panel have been drawn by inspection only.

may be somehow associated with the observed turbidity or the yield of the refolded protein.

In further study of the turbidity problem, we included DTT in the refolding buffer. For refolding at pH 7.5, the turbidity increased with increments of DTT up to ~ 4 mM and remained constant thereafter, but DTT had little effect on the turbidity when refolding was carried out at pH 9 (Figure. 2b). DTT ensures complete reduction of dissociated cysteine side chains at pH 9 also, and yet no turbidity appears and the protein folds correctly (see below). These observations suggest that disulfide formation is not associated with folding, although no information on the structure and

the content of disulfides in ^{WD40}Apaf-1 is available at the present.

Another set of experiments (results not shown) also appeared to point to the absence of disulfides. We have generated expression construct for ^{WD40}Apaf-1 with a GST (glutathione S-transferase) tag. After refolding the fused protein from the inclusion bodies at pH 7.5, the refolded protein solution was dialyzed against a buffer containing the GSH–GSSG redox couple that is known to facilitate generation of disulfides. The dialyzed protein was assayed for GST activity by using the synthetic substrate analog CDNB (1-chloro-2,4-dinitrobenzene). No GST activity was detected under any condition of redox potential generated by variable GSH: GSSH ratio. One of the reasons for the absence of GST activity is misfolding of the whole or parts of the fused protein, for which we do not have any direct experimental proof. If correct folding is assumed, then the lack of GST activity would mean that disulfides are redundant or absent in ^{WD40}Apaf-1.

With this information, we chose to refold the protein using buffer B containing 0.4 M arginine and 1 mM DTT at pH 8.8. In the Ni–NTA column purification, the eluted protein fraction contained three additional proteins clearly visible in the silver-stained SDS/PAGE gel (Figure. 3). Imidazole gradient elution also did not eliminate these proteins from the fraction containing ^{WD40}Apaf-1.

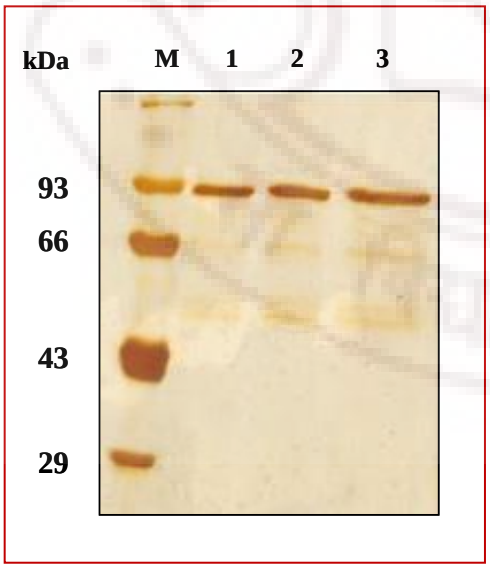

Figure 3. Silver-stained SDS–PAGE analysis of the Ni–NTA resin affinity chromatographic elution of ^{WD40}Apaf-1 initially refolded from GdnHCl-solubilized inclusion bodies. Lane labels are: M, molecular weight markers; 1, 2, and 3, different elution fractions containing low molecular weight contaminants.

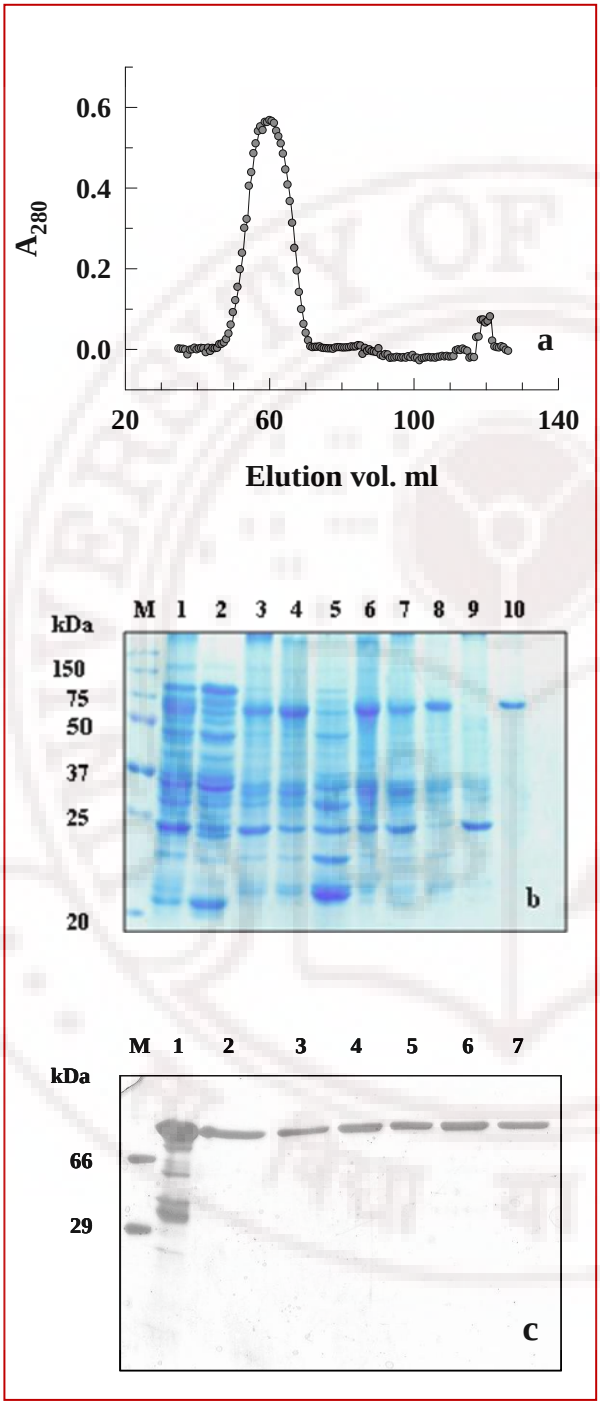

Figure 4. (a) Sephadex G100 gel filtration of the refolded protein solution. The GdnHCl solubilized protein was refolded by 10-fold dilution with buffer B (50 mM Tris, 0.5 M NaCl, 0.5 M urea, 0.4 M arginine, 2 mM DTT, 0.1% glycerol, pH 8.8), and the refolded protein solution was chromatographed using 20 mM Tris, 50 mM NaCl, pH 8 as the eluting buffer.

(b) Coomassie-stained SDS/PAGE of proteins at various stages of isolation. Lane labels: M, molecular weight markers; 1, whole cell lysate; 2, supernatant from the cell lysate; 3, precipitated material from the cell lysate; 4, Triton X-100-washed inclusion bodies; 5, supernatant after washing the inclusion bodies in 2.5 M GdnHCl; 6, pelleted inclusion bodies washed in 2.5 M GdnHCl; 7, inclusion bodies solubilized in 6 M GdnHCl (buffer A); 8, the soluble proteins in the refolded protein solution; 9, the insoluble proteins in the refolded protein solution; 10, the Sephadex G100-purified ^{WD40}Apaf-1.

(c) Silver-stained SDS/PAGE analysis of a repeat experiment. Lane labels are: M, marker proteins; 1, solubilized inclusion bodies; 2, supernatant from the refolded protein solution; 3–7, various fractions across the major peak in the gel filtration profile (Figure. 4a).

Fortunately, the contaminating proteins are smaller enough (45–70 kDa) than ^{WD40}Apaf-1 (Figure. 3), so we chromatographed the refolded protein solution on a Sephadex G100 column for which the equilibrating and running buffer was simply 20 mM Tris containing 50 mM NaCl, pH 8.0. The results shown in Figure. 4 clearly indicate virtually complete purification of ^{WD40}Apaf-1 (Figure. 4c). Another major advantage of the gel filtration procedure at pH 8.0 is that the ^{WD40}Apaf-1 solution obtained is devoid of anything other than 20 mM Tris and 50 mM NaCl. The eluted protein fraction can thus be used for structural and functional studies without any further processing. We should add a note of caution here that ^{WD40}Apaf-1 is prone to aggregation in the buffer system (20 mM Tris, 50 mM NaCl, pH 8) used for gel filtration as well as for later studies. We suspect this is part of the reason for the loss of some protein in the column matrix (Figure. 4b and Table 1).

Table 1
Protein content and fractional purity at various stages of solubilization and purification of ^{WD40}Apaf-1.

Stage/sample	Amount of protein[a] (mg)	% purity[b]
Cell lysate	226	10–15
Insoluble pellet from the cell lysate	70	Not estimated
Washed inclusion bodies	34	30–40
GdnHCl-solubilized inclusion bodies	25	Not estimated
GdnHCl-unfolded solution→refolded	20	60
WD40Apaf-1 eluted from Sephadex G100 column	3–7	~100

[a] Starting with 4 gm of wet weight cells harvested from 2 L of culture.
[b] The figures in this column represent estimates only, and therefore may have large errors.

To avoid the aggregation problem, we recommend processing and handling of less than ~5 μM protein (~ 500 μg/mL). Also, concentrating the protein solution should be avoided. Hence, the gel filtration elute was directly aliquotted and stored at –20 °C. The recovery and fractional purity of ^{WD40}Apaf-1 at various stages of purification are given in Table 1.

3.4.3 *Mass spectrometric identification and basic conformational characterization*

Figure 5 shows the mass spectrum for tryptic peptides of the purified protein. That the protein is theWD40 domain of human Apaf-1was established by peptide mass fingerprint search in primary sequence database (NCBI) using the Mascot search engine (Matrix Science). In the search, 61 tryptic peptide mass values were tested

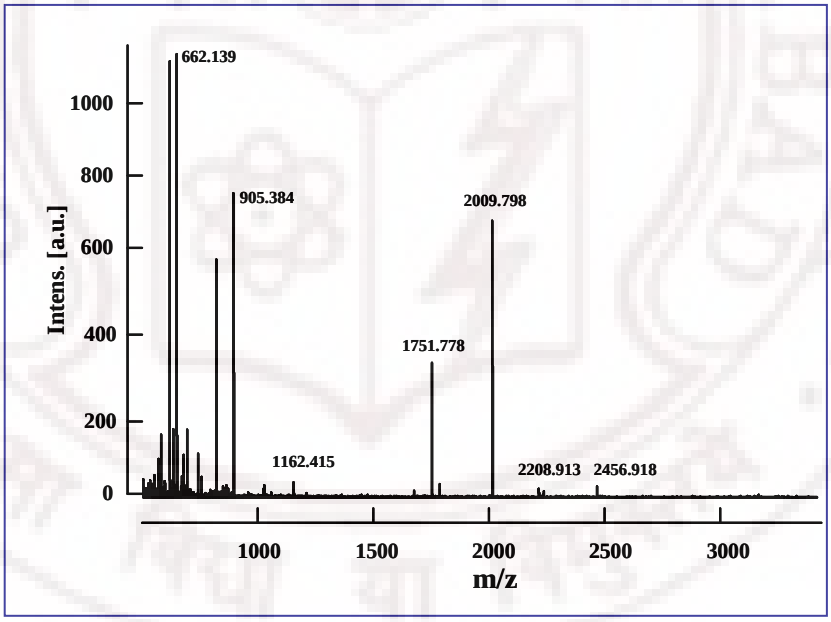

Figure 5. Mass spectrum of tryptic peptides of ^{WD40}Apaf-1. Spectra were recorded in a MALDI TOF/TOF in reflectron mode. MS/MS of selected peptides were determined by LIFT. The protein identity was established by a mass fingerprint search in primary sequence database (NCBI) using the Mascot search engine.

constraining the mass tolerance to 0.5 Da, and 20 peptide mass values matched with sequence coverage of 13%. Of the calculated 860 amino acid residues in our expressed ^{WD40}Apaf-1, 35 are extrinsic to the protein. These residues are: MRGSHHHHHHGMASMTGGQQMGRDLYDDDDKDRWI; the six consecutive histidines form the tag and the remaining residues are due to the pRSETa vector. The calculated molecular mass of the cloned protein is 97.9 kDa, and the pI value is 5.84.

The folded conformation of the protein was checked by fluorescence and CD spectra taken with ~3 µM proteins in 20 mM Tris, 10 mM NaCl, pH 7 at 25 °C. The tryptophan-excited fluorescence spectra of ^{WD40}Apaf-1 produced in Figure. 6a show that when the native protein is unfolded by ~4.5 M GdnHCl included in the buffer, there is nearly 3-fold enhancement of fluorescence intensity accompanied by a red shift of the emission maximum from ~325 to ~340 nm, suggesting quenched native-state fluorescence due to tertiary packing and a large solvent exposure of the fluorophores in the unfolded state. In an earlier study with the WD40-deleted Apaf-1

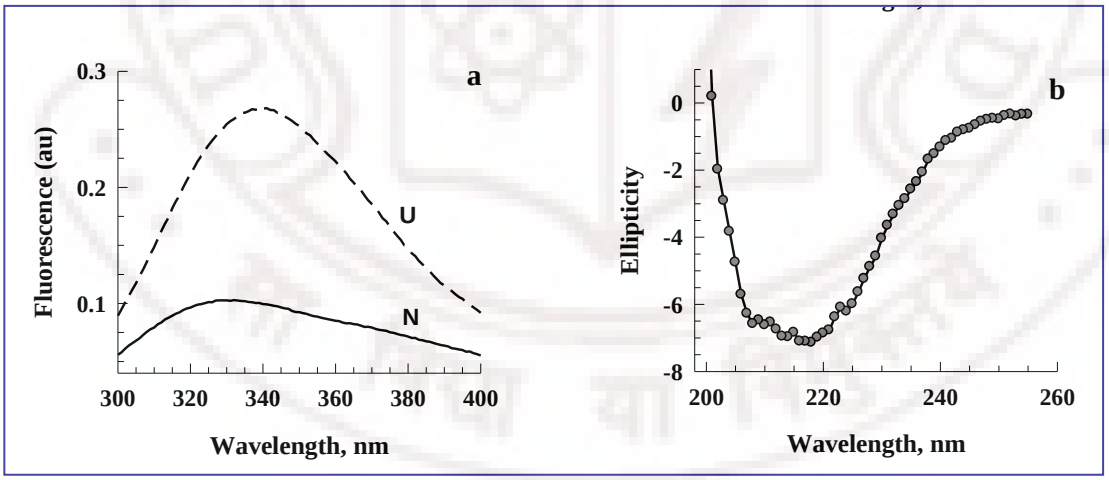

Figure 6. (a) Fluorescence emission spectra of the native (N) and 4.5 M GdnHCl unfolded ^{WD40}Apaf-1 (U) in 20 mM Tris, 10 mM NaCl, pH 7. The peak wavelengths are 325 and 340 nm, respectively, (b) The far-UV CD spectrum of the purified ^{WD40}Apaf-1.

isoform from HepG2 tumor cell line, we found that the tryptophan fluorescence is substantially quenched when the protein is unfolded, which together with the present results appears to suggest domain-independent folding-unfolding of Apaf-1.

The far-UV CD spectrum of ^{WD40}Apaf-1(Figure. 6b) indicates substantial content of secondary structure, suggesting that the protein we have purified is likely to be folded and functionally active. The content of secondary structure does not provide a full proof for correct folding of the protein, nor does it guarantee functional activity of the protein. However, demonstration of functional activity provides adequate proof for correct folding of the protein. The test for the functional activity of ^{WD40}Apaf-1 presented below indeed suggests that the protein is correctly folded.

3.4.4 *Binding of cytochrome c to ^{WD40}Apaf-1*

Central to the functioning of Apaf-1 is its ability to bind to cytochrome *c*. The finding of WD40 repeats in the C-terminal domain of Apaf-1 [9] immediately led to the belief that it is the WD40 domain of Apaf-1 that interacts with cytochrome *c* [20,21]. WD40 repeats are generally known to be involved in protein–protein interactions [16,17], and given that cytochrome *c* is highly basic (19 lysines in the total of 104), it could be reasonably expected that a number of Asp–Lys interactions are involved in the binding of ^{WD40}Apaf-1 and cytochrome *c*. The interaction of cytochrome *c* and ^{WD40}Apaf-1 can of course be verified qualitatively by coimmunoprecipitation and immunoblot analyses (data not shown). To determine the equilibrium binding affinity, we titrated 0.8 μM cytochrome *c* with ^{WD40}Apaf-1 in the 0–1.4 μM range. The buffer was 20 mM Tris containing 10 mM NaCl and 1 mM DTT at pH 7, and the titration was followed by the Soret optical absorption spectrum of the DTT-reduced cytochrome *c* (Figure. 7a). As described earlier [19,22], for quantitative in vitro binding analyses involving cytochrome *c* we rely on the spectrophotometric

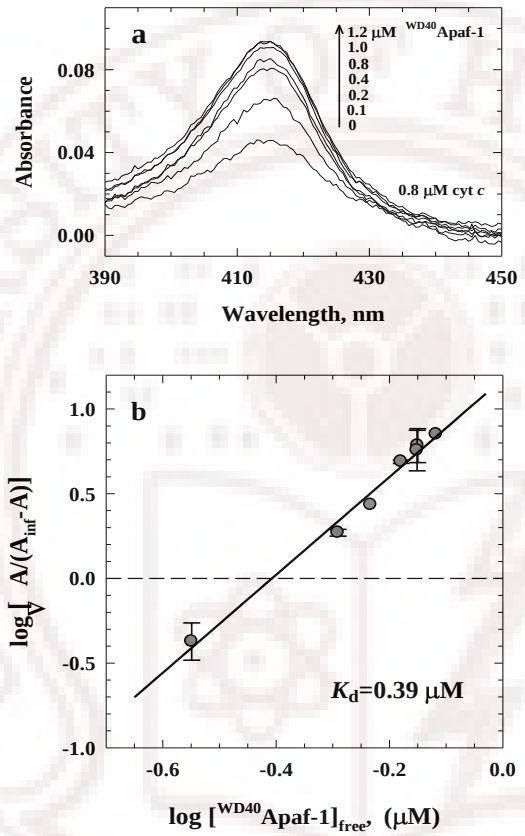

Figure 7. (a) Absorption spectra of 0.8 μM cytochrome *c* in the presence of different concentrations of ^{WD40}Apaf-1 in 20 mM Tris, 10 mM NaCl, 1 mM DTT, pH 7. (b) The final plot for analysis of binding data, as described under Materials and methods. The equilibrium association constant, K_{ass}=2.56 μM^{-1}, is calculated from the *x*-intercept of the straight line (pK_{ass}). The error bars were determined from three independent experiments. The binding affinity, K_{diss}=1/K_{ass}=390 nM. The slope of the line (n=2.85±0.05) indicates a 3:1 binding stoichiometry for the interaction of cytochrome *c* with ^{WD40}Apaf-1. A discussion of the binding stoichiometry is presented in the text.

method because emission quenching due to the heme group of cytochrome *c* introduces large artifacts in the fluorometrically obtained titration results. Figure 7b shows the binding analysis where the *x*-intercept of the linear fit of the data yields the association constant, K_{ass} = 2.56 μM^{-1} (binding affinity, $K_{diss} = 1/K_{ass}$ = 390 nM). The data can be analyzed equally well by a nonlinear fit for single-site binding (inset, Figure. 7b), in which case the binding affinity is 122 nM. As discussed below, the linear analysis is more meaningful for extraction of binding stoichiometry.

Thus, we should consider the linear analysis and take K_{diss} = 390 nM, which is at least four-orders of magnitude larger than the value of 0.01 nM reported in an earlier study of the interaction of full length Apaf-1 with cytochrome *c* under low ionic strength conditions [23]. We believe, 0.01 nM is overly low (much stronger binding), even for the full-length Apaf-1. In a revisit to the problem, Purring-Koch and McLendon estimated 25 nM for the K_{diss} value under physiological conditions [18]. A contextual question is: what factor(s) could produce a binding affinity difference between the full-length Apaf-1 and ^{WD40}Apaf-1, if any considerable difference exists? There is a thought that the cytochrome *c*-binding region in the WD40 domain of functionally active Apaf-1 isoforms remains unavailable for binding until a conformational change possibly driven by ATP hydrolysis in the CED-4 domain unmasks the binding site [9]. Since protein function is also known to be governed by motional dynamics, major difference in the flexibility of the full-length Apaf-1 and ^{WD40}Apaf-1 can affect cytochrome *c* binding parameters

It is interesting that the slope of the straight line in Figure. 7b is 2.8, indicating a 3:1 or at least 2:1 stoichiometry for the binding of cytochrome *c* to ^{WD40}Apaf-1. For the interaction of zinc substituted cytochrome *c* with baculovirally expressed full-length Apaf-1, a 2:1 binding stoichiometry was found [18]. Our results raise the possibility that each ^{WD40}Apaf-1 molecule may have provision for even three cytochrome *c* molecules under the conditions of ionic strength and pH employed here.

The value of 390 nM for the binding affinity does not reflect a rather tight binding. Such a complex could dissociate with a half time of seconds. As discussed elsewhere in the context of protein–protein interaction [24], weaker affinity often reflects broad binding specificity and floppy binding surfaces, suggesting that the binding epitope on Apaf-1 is dynamically flexible. The nature and the identity of the Apaf-1 surface involved in cytochrome *c* binding are unknown. Studies using mutant cytochrome *c* implicated not only lysines but also other residues of cytochrome *c* that are important for Apaf-1 binding [25]. Indeed, the cytochrome *c* epitope for Apaf-1 binding is suggested to be large and extensive [25, 26], suggesting that the Apaf-1 epitope may contain other residues in addition to Asp. The atomic details of the binding epitopes for both proteins are unknown, and we hope to address these in future work.

3.5 Summary and conclusion

In *E. coli* expression, the recombinant WD40 domain of human Apaf-1 (^{WD40}Apaf-1) is invariably localized in the inclusion body fraction. The protein, refolded at pH 8.8 by diluting the GdnHCl-solubilized inclusion bodies, can be purified to a very high homogeneity by Sephadex G100 gel filtration in 20 mM Tris, 50 mM NaCl, pH 8. The protein obtained thus can be used directly for structural and functional studies. Since the protein is prone to aggregation, concentrations exceeding ~5 μM should be avoided during gel filtration and all subsequent uses. The protein thus purified displays fluorescence and far-UV CD spectra typical of folded proteins. The binding of cytochrome *c* to ^{WD40}Apaf-1 is not rather tight. The value of 390 nm for the binding affinity is suggestive of a possibly floppy binding surface on Apaf-1. The binding stoichiometry suggests binding of 2 or 3 molecules of cytochrome *c* per molecule of ^{WD40}Apaf-1.

3.6 References

[1] E.A. Slee, M.T. Harte, R.M. Kluck, B.B. Wolf, C.A. Casiano, D.D. Newmeyer, H-G. Wang, J.C. Reed, D.W. Nicholson, E.S. Alnemri, D.R. Green, S.J. Martin, Ordering the cytochrome *c*-initiated caspase cascade: hierarchical activation of caspases-2, -3, -6, -7, -8, and -10 in a caspase-9−dependent manner. J. Cell. Biol. 144 (1999) 281-292.

[2] X. Jiang, X. Wang, Cytochrome *c*-mediated apoptosis. Annu. Rev. Biochem. 73 (2004) 87-106.

[3] H. Zou, Y. Li, X. Liu, X. Wang, An Apaf-1·cytochrome *c* multimeric complex is a functional apoptosome that activates procaspase-9. J. Biol. Chem. 274 (1999) 11549-11556.

[4] Y. Hu, M.A. Benedict, L. Ding, G. Núñez, Role of cytochrome *c* and dATP/ATP hydrolysis in Apaf-1-mediated caspase-9 activation and apoptosis. EMBO J. 18 (1999) 3586-3595.

[5] A. Saleh, S.M. Srinivasula, S. Acharya, R. Fishel, E.S. Alnemri, Cytochrome *c* and dATP-mediated oligomerization of Apaf-1 is a prerequisite for procaspase-9 activation. J. Biol. Chem. 274 (1999) 17941-17945.

[6] J. Rodriguez, Y. Lazebnik, Caspase-9 and Apaf-1 form an active holoenzyme. Genes Dev. 13 (1999) 3179-3184.

[7] X. Wang, The expanding role of mitochondria in apoptosis. Genes Dev. 15 (2001) 2922-2933.

[8] H. Zou, W. J. Henzel, X. Liu, A. Lutschg, X. Wang, Apaf-1, a human protein homologous to *C. elegans* CED-4, participates in cytochrome-*c* dependent activation of caspase-3. Cell 90 (1997) 405-413.

[9] M.A. Benedict, Y. Hu., N. Inohara, G. Núñez, Expression and functional analysis of Apaf-1 isoforms: extra WD-40 repeat is required for cytochrome *c* binding and regulated activation of procaspase-9. J. Biol. Chem. 275 (2000) 8461-8468.

[10] D. Acehan, X. Jiang, D.G. Morgan, J.E. Heuser, X. Wang, C.W. Akey, Three dimensional structure of the apoptosome: implications for assembly, procaspase-9 binding and activation. Mol. Cell 9 (2002) 423-432.

[11] X. Yu., D. Acehan, J. Ménétret, C.R. Booth, S.J. Ludtke, S.J. Riedl, Y. Shi, X. Wang, C.W. Akey, A structure of the human apoptosome at 12.8Å resolution provides insights into this cell death platform. Structure 13 (2005) 1725-1735.

[12] X. Yu, L. Wang, D. Acehan, X. Wang, C.W. Akey, Three-dimensional structure of a double apoptosome formed by the Drosophila Apaf-1 related killer. J. Mol. Biol. 355 (2006) 577-589.

[13] J. Nakabayashi, A. Sasaki, A mathematical model for apoptosome assembly: the optimal cytochrome *c*/Apaf-1 ratio. J. Theor. Biol. 242 (2006) 280-287.

[14] P. Zhou, J. Chou, R.S. Olea, J. Yuan, G. Wagner, Solution structure of Apaf-1 CARD and its interaction with caspase-9 CARD: a structural basis for specific adaptor/caspase interaction. Proc. Natl. Acad. Sci. USA 96 (1999) 11265-11270.

[15] S.J. Riedl, W. Li., Y. Chao, R. Schwarzenbacher, Y. Shi, Structure of the apoptotic protease-activating factor 1 bound to ADP. Nature 434 (2005) 926-933.

[16] T.F. Smith, C. Gaitatzes, K, Saxena, E.J. Neer, The WD repeat: a common architecture for diverse functions. Trends. Biochem. Sci. 24 (1999) 181-185.

[17] D. Li, R. Roberts, WD-repeat proteins: structure characteristics, biological

function, and their involvement in human diseases. Cell Mol. Life Sci. 58 (2001) 2085-2097.

[18] C. Purring-Koch, G. McLendon, Cytochrome *c* binding to Apaf-1: the effects of dATP and ionic strength. Proc. Natl. Acad. Sci. U.S.A. 97 (2001) 11928-11931.

[19] P.N. Rao, M. Yadaiah, K.P. Roy, H. Potu, A.K. Bhuyan, Cloning, *E. coli* expression, refolding, and ATP-binding properties of a WD40-deleted Apaf-1 isoform. Protein Express. Purif. 56 (2007) 220-228.

[20] Y. Hu, L. Ding, D.M. Spencer, G. Núñez, WD-40 repeat region regulates Apaf-1 self-association and procaspase-9 activation. J. Biol. Chem. 273 (1998) 33489-33494.

[21] C. Adrian, E.A. Slee, M.T. Harte, S.J. Martin, Regulation of apoptotic protease activating factor-1 oligomerization and apoptosis by the WD-40 repeat region. J. Biol. Chem. 274 (1999) 20855-20860.

[22] M. Yadaiah, P.N. Rao, H. Potu, A.K. Bhuyan, High-affinity binding of Bcl-x_L to cytochrome *c*: possible relevance for interception of translocated cytochrome *c* in apoptosis. Biochim. Biophys. Acta 1774 (2007) 1370-1379.

[23] C. Purring, H. Zou, X. Wang, G. McLendon, Stoichiometry, free energy, and kinetic aspects of cytochrome *c*:Apaf-1 binding in apoptosis. J. Am. Chem. Soc. 121 (1999) 7435-7436.

[24] S.C. Sahu, A.K. Bhuyan, A. Majumdar, J.B. Udgaonkar, Backbone dynamics of barstar: a ^{15}N NMR relaxation study. Proteins: Struct. Funct. Genet. 41 (2000) 460-474.

[25] T. Yu, X. Wang, C. Purring-Koch, Y. Wei, G.L. McLendon, A mutational epitope for cytochrome *c* binding to the apoptosis protease activating factor-1. J. Biol. Chem. 276 (2001) 13034-13038.

[26] A.G. Martin, H.O. Fearnhead, Apocytochrome *c* blocks caspase-9 activation and Bax-induced apoptosis. J. Biol. Chem. 277 (2002) 50834-50841.

CHAPTER 4

Interaction of horse cytochrome *c* with recombinant human Bcl-x_L

4.1 Abstract

The Bcl-2 family of proteins orchestrates the release of cytochrome *c* from mitochondria by several preferential and selective interactions with the latter, and the released cytochrome *c* interacts with Apaf-1 to produce the apoptosome. Although evidences for these interactions have come primarily from immunochemical data, quantitative *in vitro* studies involving pure proteins have been scarcely reported. In an attempt to investigate if any pro-survival protein from the Bcl-2 family could intercept cytochrome *c* after its translocation from mitochondria, the work presented in this Chapter reports on the interaction of cytochrome *c* with bacterially expressed human Bcl-x_L at pH 7, studied by optical absorption of cytochrome *c* as a function of titrating concentrations of Bcl-x_L. The association constants, K_{ass}, for Bcl-x_L-cytochrome *c* interaction at 22ºC, pH 7, is 8.4(±4) $\times 10^6$ M^{-1} (binding affinity, $K_{diss}=1/K_{ass}\approx 120$ nM), decreases at high ionic strength. The rates for binding of Bcl-x_L to cytochrome *c*, studied by stopped-flow kinetics at pH 7, show that the bimolecular rate constant for binding, $k_{bi}= 0.24\times 10^6$ M^{-1} s^{-1}. Values of the thermodynamic and kinetic parameters for Bcl-x_L-cytochrome *c* interaction are very similar to those known for regulatory protein-protein interactions in apoptosis.

4.2 Introduction

As discussed earlier in the introductory chapter, cytochrome *c* translocated from mitochondria assists in the assembly of an apoptosome required for activation of caspase-9 and subsequent activation of other caspases [1-3]. The rapid release of cytochrome *c* from mitochondria is believed to arise from effects of pro-apoptotic

proteins of the Bcl-2 family, including Bax, Bak, and Bad, which form pores on the outer mitochondrial membrane to facilitate release of cytochrome *c* [4-9]. Alternatively, these proteins may function to cause a loss of mitochondrial membrane potential that can lead to membrane permeabilization [10-14].

The pro-survival members of the Bcl-2 family proteins, including Bcl-x_L, Bcl-2, and Bcl-w, counter the release of cytochrome *c* from mitochondria by less understood mechanisms. Numerous studies have established that Bcl-x_L participates in a number of protein-protein interactions to exert its pro-survival effect. In the intrinsic apoptotic pathway, Bcl-x_L blocks cytochrome *c* release by preventing Bax from disrupting the integrity of the outer mitochondrial membrane [15, 16], and in the extrinsic apoptotic pathway initiated by death ligands, Bcl-x_L can prevent death by blocking Bid redistribution downstream of caspase-8 [17]. In hypoxia/reoxygenation-induced apoptosis, Bcl-x_L has been found to interfere with the assembly of death-inducing signal complex (DISC), block the translocation of both Bax and Bid to mitochondria, and inhibit the activation of caspase-8 [18].

Thus, Bcl-x_L appears to prevent cell death through diverse protein-protein interactions, seemingly in a case specific manner. However, there is no known mechanism by which cytochrome *c* translocated to cytosol can be intercepted, such that the apoptosome is not assembled. There have been reports that Bcl-x_L can block the formation of the apoptosome by associating itself with Apaf-1 and caspase-9 to produce an antiapoptotic ternary complex [19, 20]. In another earlier immunoprecipitation study, cytochrome *c* was found to interact specifically with Bcl-x_L as a cellular response to ionizing radiation and genotoxic stress [21]. The present study is basically aimed at providing quantitative data on the interaction between the two proteins. To characterize the affinity of this interaction so that Bcl-x_L could possibly be implicated for arresting cell death by inhibiting the cytosolic cytochrome *c*, we have investigated the interaction between bacterially over expressed full-length

human Bcl-x_L and horse cytochrome *c* using coimmunoprecipitation and classical biochemical methods. Cytochrome *c* displays very high binding affinity for Bcl-x_L, which closely matches the reported affinities of BH3 peptides/domains for Bcl-x_L. The bimolecular binding rate of Bcl-x_L to cytochrome *c* is also within the range set by dimerization of Bcl-2 family proteins, and by BH3-Bcl-2 protein interactions.

4.3 Materials and methods

4.3.1 *Production and purification of Bcl-x_L*

A pET-16b (Novagen) vector coding for full length human Bcl-x_L with N-terminal His_6 tag was kindly provided by Dr. Apurva Sarin, and the plasmid was transformed into *E. coli* BL21(DE3) cells. The cells were grown in LB media to a A_{600} of 0.5. Protein expression was induced with 0.8 mM IPTG at 30ºC and 180 rpm. Cells were harvested at 10000 rpm for 10 min. The cell pellet, washed with PBS, was resuspended in 1:5 W/V buffer A (50 mM Tris, pH 8.0, 0.2 M NaCl, 0.2 mM PMSF, 5 mM β-mercaptoethanol, 5 mM imidazole, and 1% glycerol), and stirred for 15 min at 4 ºC. The cells were disrupted by pulsed sonication, and the lysate was spun at 15000 rpm for 30 min. The soluble fraction was loaded onto a Ni-NTA-His bind column (Novagen) equilibrated with buffer A. The column was washed with 45 mM imidazole in buffer A until the A_{280} reached 0.001, and the protein was eluted with 200 mM imidazole in the same buffer. The protein fractions were pooled, concentrated, and loaded onto a Sephadex G-75 (Amersham) gel filtration column preequilibrated with buffer B (50 mM Tris, pH 8.0, 50 mM NaCl, 1 mM DTT, 2 mM EDTA, and 0.2 mM PMSF) at 4 ºC. Of the two major peaks, the one corresponding to the monomeric protein was collected and loaded onto an anion-exchange DEAE-cellulose column (Whatman) equilibrated with buffer B. The column was washed with 10-volumes of buffer B, and the protein was eluted with a 50-400 mM NaCl gradient applied linearly. The protein-containing fractions were pooled and dialyzed

extensively against 1X PBS at 4ºC. Protein purity was determined to be >99% by SDS/PAGE silver staining. The protein concentration was determined spectrophotometrically using ε_{280}= 41940 M^{-1} cm^{-1} in 6 M guanidine hydrochloride.

4.3.2 *Determination of equilibrium constant for the binding of Bcl-x_L to cytochrome c*

Titration experiments were carried out holding cytochrome *c* constant at one of the concentrations in the 1-4 μM range. A set of samples containing a fixed concentration of cytochrome *c* and variable concentration of Bcl-x_L (0-8 μM) was prepared in a pH 7 buffer composed of 50 mM phosphate, 4 mM DTT, and a given concentration of NaCl. This procedure of equilibrium titration annulled dilution effects. Samples were incubated for ~4 hours at 22°C before recording baseline-corrected optical absorption spectra in the 600-400 nm wavelength region using a Cary 100 (Varian) spectrophotometer.

Absorbance at 415 nm, which is the Soret maximum for DTT-reduced cytochrome *c*, was used for binding analysis. The concentration of free Bcl-x_L in the titration mixture is given by

$$[Bcl-x_L]_{free} = \frac{[cyt\ c]\times \Delta A}{\Delta A_\infty} \quad (1)$$

in which, $\Delta A = A_x - A_o$ and $\Delta A_\infty = A_\infty - A_o$, where A_o, A_x, and A_∞ are 415-nm absorbances of solutions containing cytochrome *c* alone, cytochrome *c* in the presence of *x* concentration of Bcl-x_L, and cytochrome *c* in the presence of infinite or saturating concentration of Bcl-x_L, respectively. The association constant, K_{ass}, was extracted from the equation

$$\log\left[\frac{\Delta A}{A_\infty - A_x}\right] = \log K_{ass} + \log[Bcl-x_L]_{free} \quad (2)$$

The *x*-intercept of the plot of log [$\Delta A/(A_\infty - A_x)$] vs log [Bcl-$x_L$] gives the value of p$K_a$ for cytochrome *c*-Bcl-x_L interaction.

4.3.3 *Equilibrium binding of the Bad BH3 domain to cytochrome c*

In this set of experiment, 475 nM cytochrome *c* was titrated out by a fluorescein-labeled Bad BH3 peptide (Calbiochem). The titration was followed by both Soret optical absorbance due to cytochrome *c* as described above, and 535-nm fluorescence emission due to the BH3 peptide (excitation: 485 nm). Absorbance data were analyzed using equations 1 and 2. The binding parameters from the fluorescence data were extracted from the equation

$$y(x) = \frac{c}{1+10^{n(x-K_{diss})}} \qquad (3)$$

where, *n* is the number of peptides bound to cytochrome *c*, K_{diss} is apparent dissociation constant, and *c* is the total change in fluorescence normalized to unity. In the concentration range of the peptide (0-7 μM) used for the titration experiment, there was no inner filter effect on the fluorescence emission, since the optical absorbance of the peptide at the excitation wavelength was less than 0.32 in this range of concentrations.

4.3.4 *Stopped-flow kinetics of interaction of Bcl-x_L with cytochrome c*

All solutions for kinetic experiments were prepared in 50 mM phosphate, 4 mM DTT, and 50 mM NaCl, pH 7. In a two-syringe mixing procedure, a solution of 24 μM cytochrome *c* was mixed with Bcl-x_L solutions of variable concentration in the 2-12 μM range. The mixing ratio was 1:7. These experiments were done in a Bio-Logic SFM 400 instrument. The temperature was regulated at 22°C using an external

circulating water bath. The traces were analyzed using a single-exponential function: $y(t)=A_\infty+A\ exp(-kt)$, where A is the amplitude, A_∞ denotes the baseline signal at long times, and k is the observed rate constant. The bimolecular binding rate was calculated from the slope of the plot of the observed rate constant as a function of Bcl-x_L concentration.

4.4 Results

The nickel column-eluted Bcl-x_L was gel-filtered on a Sephadex G75 column and the monomer fraction isolated was chromatographed on a DEAE anion-exchange column. As confirmed by silver-stained SDS/PAGE, more than 99% pure protein was obtained (Figure 1).

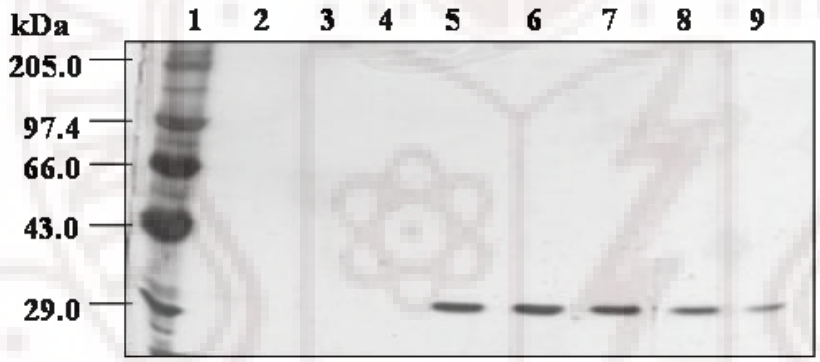

Figure 1. Silver-stained SDS electrophoresis of different fractions from the peak corresponding to DEAE column-eluted Bcl-x_L (0.23 M NaCl) shows >99% purity of the protein. Lane 1 shows the marker proteins.

To study equilibrium binding, the initial titration experiments employed the use of the intrinsic fluorescence of Bcl-x_L. Full-length Bcl-x_L is highly fluorescent due to the content of six tryptophan residues, but cytochrome *c* does not fluoresce due to intramolecular excitation energy transfer from its lone tryptophan (W59) to the heme. Therefore, the fluorescence of Bcl-x_L can, in principle, be used to monitor its titration

with cytochrome *c*. However, the concentration of cytochrome *c* in the solution (>1.5 μM) needed to achieve a complete titration titrate was found to quench the intrinsic fluorescence of Bcl-x_L. The quenching of Bcl-x_L fluorescence due to cytochrome *c* in the bulk solution obscures the actual change in fluorescence due to the interaction of the two proteins. A control experiment where a lysozyme solution was titrated with cytochrome *c* showed exactly the same behavior, suggesting that fluorescence is not preferred to probe the Bcl-x_L-cytochrome *c* interaction.

Next, optical absorption of a fixed concentration of cytochrome *c* in the Soret heme region was measured as a function of variable concentration of Bcl-x_L. Figure 2a shows that the absorbance due to cytochrome *c* increases with increments of Bcl-x_L; for the 3 μM solution of cytochrome *c*, the change in absorbance across the complete titration is 33 milliOD. The difference spectra generated by subtracting the spectrum of cytochrome *c* alone from spectra in the presence of Bcl-x_L (Figure 2a, *inset*) show that Bcl-x_L binding causes the absorption peak to shift from 415 to 413.2 nm. These observations suggested that heme optical absorption of cytochrome *c* could be used as a reliable marker to follow its interaction with Bcl-x_L.

Figure 2b shows the plot used for binding analysis as described under Materials and Methods. The *x*-intercept of the linear fit of the data yields the association constant, $K_{ass}=8.4(\pm4)\times10^6$ M^{-1}, indicating tight affinity of cytochrome *c* for Bcl-x_L. The slope of the plot (n=0.6) indicates a 1:1 interaction. The Gibbs free energy for Bcl-x_L-cytochrome *c* interaction ($\Delta G°=-RT \ln K_{ass}$) calculated by using this value of K_{ass} is ~9.3 kcal mol^{-1} at 22°C.

Bcl-x_L-Cyt c Interaction

Cytochrome *c* is lysine-rich, and hence highly basic. It is therefore desirable to address as to how its interaction with Bcl-x_L varies with ionic strength and pH. Fig. 2c shows that K_{ass} is maximum at ~80 mM NaCl, and declines by nearly 12-fold in the presence of 600 mM NaCl, suggesting that the physiological ionic strength supports the tightest interaction between the two

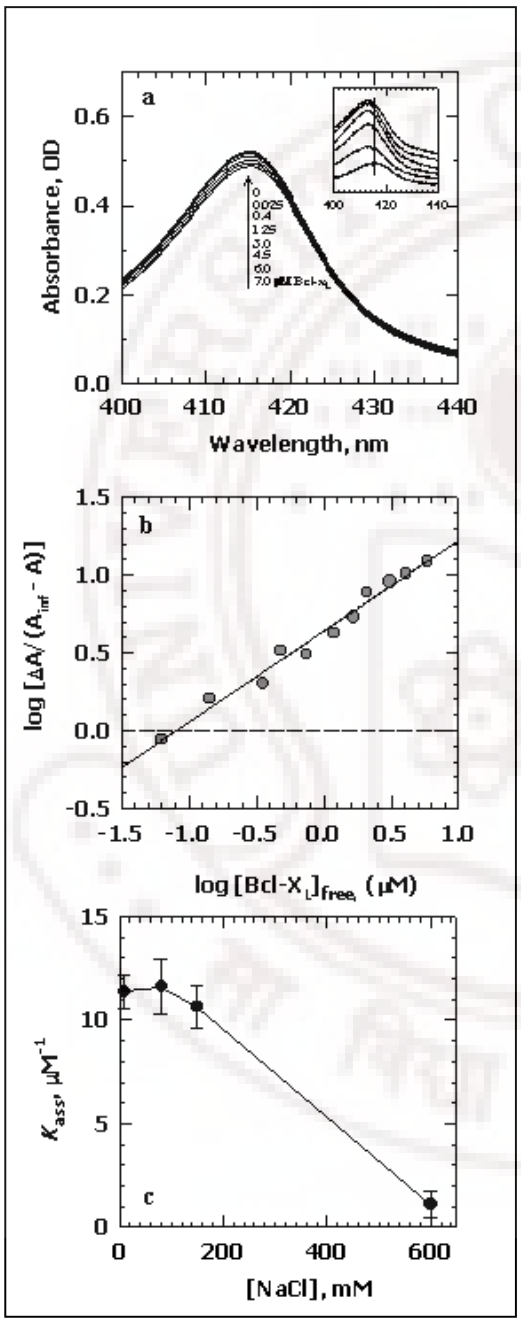

Figure 2. (a) Absorption spectra of cytochrome *c* in the presence of different concentrations of Bcl-x_L, pH 7, 22°C, 3.5 mM DTT, 100 mM NaCl. The *inset* shows difference absorption spectra obtained by subtracting the spectrum of cytochrome *c* alone from the spectra of cytochrome *c* in the presence of different concentrations of Bcl-x_L. (b) The final plot for analysis of binding data, as described under Materials and Methods (eq 1 and 2). The equilibrium association constant, K_{ass} (8.4(±4) μM^{-1}, is calculated from the *x*-intercept of the straight line (pK_{ass}). The slope of the line (*n*=0.6) indicates a 1:1 binding interaction. (c) The variation of K_{ass} as a function of NaCl concentration in 50 mM phosphate buffer, pH 7, 4 mM DTT, 22°C. Mixtures of Bcl-x_L and cytochrome *c* were incubated for 2-8 hours. Optical absorption spectra were analyzed as described under Methods.

proteins. The dependence of K_{ass} on pH could not be studied in detail due to alkaline isomerization of cytochrome *c* in basic medium (pH >8), and heme spin change in acid solutions (pH<5). In the accessible range of pH, K_{ass} was found to change little.

The kinetics of protein-protein interactions are of special significance since rates of such interactions often play important regulatory roles. To determine the rate of binding of Bcl-x_L to cytochrome *c*, we performed stopped-flow experiments where the time dependence of the change in 415-nm absorbance due to cytochrome *c* was monitored after mixing the two protein solutions. The representative traces labeled 1, 2, and 3 in Fig. 3a show the time dependence of the change in absorbance after mixing 3 μM cytochrome *c* with 6, 4, and 2 μM Bcl-x_L, respectively. The solid lines through the data are single-exponential fits, showing clearly that the rate of interaction changes with the concentration of Bcl-x_L. The dependence of the observed rate on the concentration of Bcl-x_L is shown in Fig. 3b, the slope of the linear fit of which yields the bimolecular association rate constant, $k_{bi}=0.24\times10^6$ M^{-1} s^{-1}.

Incorporation of a control experiment is necessary to show that cytochrome *c* does not interact with other proteins indiscriminately. As a negative control, the interaction of Bcl-x_L with myoglobin (the latter was chosen because it resembles cytochrome *c* in containing a heme group and a fairly sizable number of positively charged amino acids) was checked, but no binding was detected. As a positive control, the interaction of cytochrome *c* with Bad BH3 was looked into. Since the BH3 domain is involved in a number of interactions amongst the Bcl-2 family proteins and Bcl-x_L is found to interact with cytochrome *c*; one naively expects binding of the BH3 peptide to cytochrome *c*. The optical absorbance of cytochrome *c* ($\lambda_{max}\approx415$ nm) was used to assess this interaction. Advantage of the fluorescence emission of the fluorescein-labeled Bad BH3 peptide ($\lambda_{max}\approx496$ nm) was also taken to monitor the titration of 475 nM cytochrome *c* with increments of the peptide up to 7

μM. In this range of concentration of the peptide, no inner filter effect in the fluorescence of the peptide was detected. The analysis of the titration monitored by

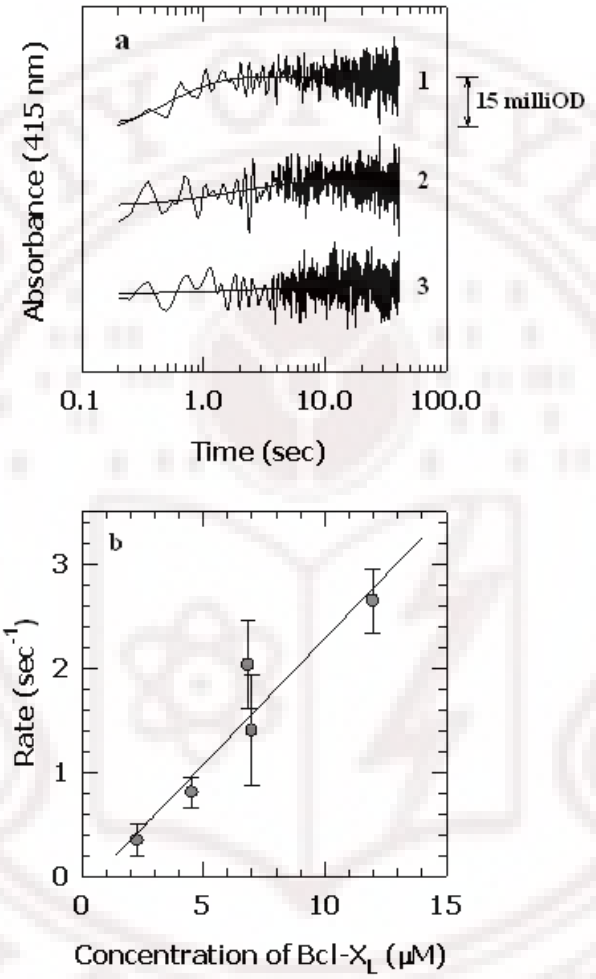

Figure 3. Kinetics of binding of Bcl-x_L to cytochrome *c* in 50 mM phosphate buffer, pH 7, 4 mM DTT, 22°C. The concentration of cytochrome *c* was held constant at 3 μM. (a) Representative kinetic traces: labels 1 to 3 correspond to 6, 4, and 2 μM Bcl-x_L, respectively. The solid lines through the data represent single-exponential fits. (b) The rate obtained is proportional to the concentration of Bcl-x_L. The slope of the linear fit through the data yields the bimolecular rate constant for binding, k_{bi}=0.24 μM^{-1} s^{-1}. The error bars represent standard deviations of the rate constants measured with different preparations of Bcl-x_L.

the absorbance of cytochrome *c* (equations 1,2) yields K_{ass}=4.1(±1)×10^6 M^{-1}, indicating rather tight affinity of the BH3 peptide for cytochrome *c* (Figure 4a), and the slope of 0.91 suggests 1:1 interaction. Values of K_{ass} and *n* extracted from the peptide fluorescence-monitored data (equation 3 and Figure 4b) are 1.2(±0.2)×10^6 M^{-1} and 1.3(±0.1), respectively, fairly consistent with the values obtained from the optical absorbance data.

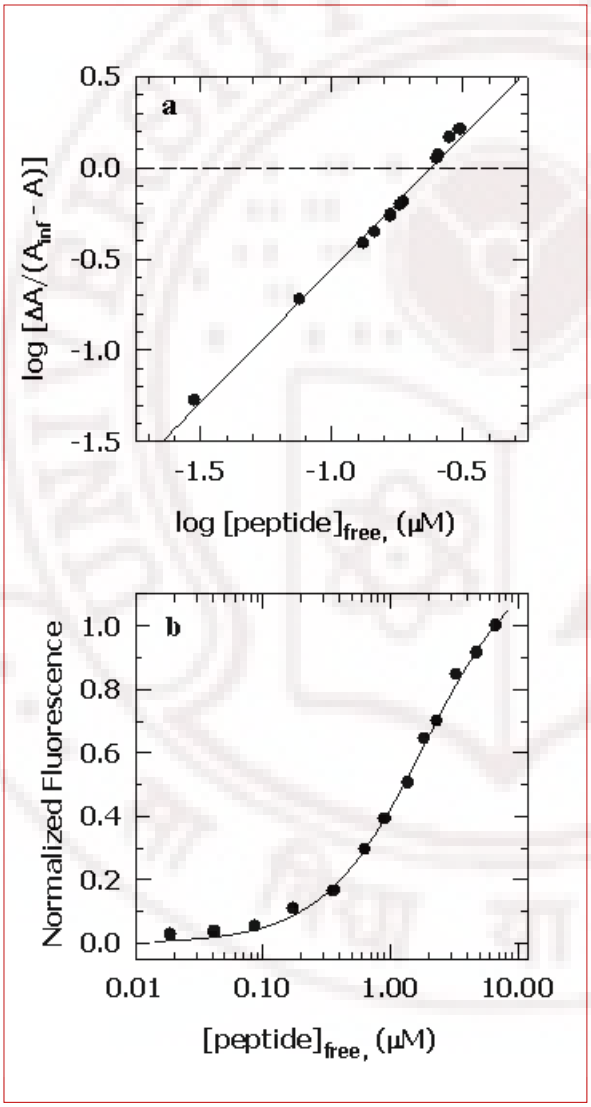

In another control experiment, the equilibrium binding of Bid with cytochrome *c* was studied. The working rationale was the same as mentioned above in the context of interaction of Bad BH3 peptide with cytochrome *c*. Since the Bid protein binds both pro- and antiapoptotic proteins,

Figure 4. (a) Analysis of horse cytochrome *c* and Bad BH3 peptide binding (equation 1,2) monitored by the optical absorbance of cytochrome *c*, pH 7, 22°C, 3.5 mM DTT, 100 mM NaCl. Values of K_{ass} and *n* are 4.1(±1) μM^{-1} and 0.91, respectively. (b) The same binding monitored by fluorescence of the fluorescein-labeled Bad BH3 peptide (equation 3). Values of K_{ass} and *n* extracted from this analysis are 1.2(±0.2) μM^{-1} and 1.3, respectively.

including Bcl-x_L, one expects its interaction with cytochrome *c* as well. Indeed, by titrating 300 nM cytochrome *c* with increments of Bid, we obtained K_{ass}=4.05(±2.25)×10^6 M^{-1} for this interaction (Table 1). These results suggest that in addition to Bcl-x_L certain pro- and antiapoptotic Bcl-2 proteins may bind to the cytosolic pool of cytochrome *c* in apoptosed cells.

4.5 Discussion

4.5.1 *Binding of Bcl-x_L to cytochrome c*

The major finding of this study is a tight 1:1 binding of Bcl-x_L and cytochrome *c*, and it is of interest as to how this affinity compares with those for known protein-protein or protein-peptide interactions involved in survival and death. The apparent binding affinities or dissociation constants (K_{diss}=1/K_{ass}) for the interaction of Bcl-x_L with other members of the Bcl-2 family have been reported in the 2-6 μM range at pH 7 (*22*). In more recent studies, the apparent K_{diss} values for the interactions of BH3 peptides from pro-apoptotic Bcl-2 family proteins with Bcl-x_L Δ*Cx* (truncated at the C-tail by *x* residues) have been found to fall in the 1-90 nM range [23], suggesting tighter binding, while the affinity of BH3 peptides from anti-apoptotic Bcl-2 family proteins with other survival or killer proteins is relatively low, into micromolar range [24]. Thus the binding of Bcl-x_L with cytochrome *c* (K_{diss}~120 nM at pH 7) is indeed tight, and is fairly comparable to its affinity for BH3 domains from the anti-survival proteins of the Bcl-2 family. Even the bimolecular/second order rate constants for the binding of Bcl-x_L to cytochrome *c* (k_{bi}=0.24 μM^{-1} s^{-1}, Figure 3b) and Bcl-x_L to other Bcl-2 family proteins (k_{bi} in the 0.27-0.34 μM^{-1} s^{-1} range [22]) are nearly identical, implying that these interprotein interactions closely match in terms of binding free energy and the activation energy barrier.

4.5.2 *Cytochrome c-Bad BH3 and cytochrome c-Bid interactions*

Another interesting finding is individual binding interactions of cytochrome *c* with Bad BH3 and Bcl-x_L. The idea that such interactions could exist emanated as a corollary of the BH3-mediated interprotein interactions amongst the Bcl-2 family of proteins, and the high-affinity binding of Bcl-x_L with cytochrome *c* observed in this study. The binding affinity (K_{diss}=1/K_{ass}) of Bad BH3 for cytochrome *c*, averaged from optical absorption and fluorescence data (Figure 4), is 538(±295) nm, which is numerically significantly higher than the value of 21.5 nm reported for the Bad BH3–Bcl-x_L interaction [25, 26]. The numerical value for the binding affinity of Bid for cytochrome *c* (373(±126) nM), on the other hand, is rather smaller than the reported value of 1.9 μM for Bcl-x_L-Bid interaction at neutral pH [22]. This suggests that while the affinity of Bad BH3 for cytochrome *c* is considerably lower, the affinity of Bid for cytochrome c is higher, both

Table 1. K_{ass} values for interactions amongst horse cytochrome *c*, human His_6-tagged Bcl-x_L, and Bad BH3 peptide

Binding interactions	K_{ass} (μM^{-1})	ref
Bcl-x_L–cytochrome *c*	8.4 (±4)	this work
Bcl-x_L–Bad BH3	46.5	31
Bad BH3–cytochrome *c*	2.65 (±1.45)	this work

compared with the affinity of cytochrome *c* for Bcl-x_L (Table 1). Nonetheless, it does appear that the cytosolic pool of cytochrome *c* is capable of interacting with both pro- and antiapoptotic proteins with varying degrees of affinity.

4.5.3 *Possible structural factors for Bcl-x_L and cytochrome c interaction*

From parametric similarity of interactions between Bcl-x_L and cytochrome *c*, and Bcl-x_L and other Bcl-2 family proteins, one may naively assume that Bcl-x_L deploys the same surface to bind cytochrome *c* as it does for binding with other Bcl-2 family members or the BH3 sequences derived from them. The availability of NMR and X-ray structures of Bcl-x_L [27, 28] augments deduction of the structural basis of these interprotein interactions. Muchmore *et al*. have proposed that an elongated hydrophobic cleft, the constituent residues of which are highly conserved in the Bcl-2 family of proteins, is the site of interaction of Bcl-x_L with death-promoting proteins [28]. Structures of BH3 peptide-bound Bcl-x_L show that the alignment of the BH3 helix along the hydrophobic cleft of Bcl-x_L is stabilized by apolar interactions at the base and polar contacts along the sides of the cleft [29]. Cytochrome *c* is a highly charged protein with 19 lysine residues most of which are surface exposed. It is likely that the polar residues along the side of the same Bcl-x_L cleft supports charged interactions with cytochrome *c*. The decrease of the binding affinity for the Bcl-x_L-cytochrome *c* interaction at high NaCl concentration (Figure 2c) lends support to this view. Strategic high-resolution surface mapping experiments are necessary to test this conjecture.

4.5.4 *How relevant is the Bcl-x_L-cytochrome c interaction for upstream regulation of apoptosis?*

From the results of this study together with earlier immunochemical results demonstrating that Bcl-x_L interacts with cytochrome *c* as a part of the cellular response to ionizing radiation and other genotoxic agents [21], it might seem that this interaction is operative *in vivo* as well. If the interaction indeed exists under cellular conditions, then a regulatory role can be established on the basis of the current understanding of upstream interprotein interactions involving cytochrome *c*. Once translocated to cytosol in response

to an apoptotic stimulus [1, 10, 15], cytochrome *c* binds Apaf-1 in the presence of dATP or dADP [10]. The binary complex in turn interacts with procaspase-9, and subsequently cleaves the CED-3-like prodomain of the zymogen form of caspase-9 [30]. The ternary cyt-Apaf-1-caspase-9 complex recruits procaspase-3 and possibly procaspase-7 in quick succession to form a functional apoptosome [2]. Thus, the initial ternary complex formed of cytochrome *c*, Apaf-1, and caspase-9 (the cyt-Apaf-1-caspase-9 complex) appears to be the hallmark of the initiation of the death cascade [31]. The quantitative and conclusive *in vitro* data presented here leads one to wonder if Bcl-x_L competes with Apaf-1 in order to block the formation of the initial Apaf-1-cytochrome *c* complex, thereby inhibiting caspase activation.

Unfortunately, there is no conclusive evidence for this regulatory response *in vivo*. If a regulatory role of Bcl-x_L–cytochrome *c* interaction is granted, the effectiveness of the regulation must be considered in the light of possible affinities of cytochrome *c* for other Bcl-2 family proteins. For example, some data here indicate variable affinity interactions of cytochrome *c* with Bid and with Bad BH3. In this perspective, the extent to which Bcl-x_L can arrest cytochrome *c* to exert a regulatory role would depend on the balance of thermodynamics of various interactions involving the pro- and antisurvival proteins, provided these interactions operate *in vivo*. Clearly, more evidence must be obtained that the Bcl-x_L–cytochrome *c* interaction is indeed relevant for regulation of apoptosis *in vivo*.

4.6 References

[1] R. M. Kluck, E. Bossy-Wetzel, D. R. Green, and D. D. Newmeyer, The release of cytochrome *c* from mitochondria: a primary site for Bcl-2 regulation of apoptosis. Science 275 (1997) 1132-1136.

[2] Y. Hu, M. A. Benedict, L. Ding, and G. Nunez, Role of cytochrome *c* and dATP/ATP hydrolysis in apaf-1-mediated caspase-9 activation and apoptosis. EMBO J. 18 (1999) 3586-3595.

[3] J. C. Goldstein, N. J. Waterhouse, P. Juin, G. I. Evan, and D. R. Green, The coordinate release of cytochrome *c* during apoptosis is rapid, complete and kinetically invariant. Nat. Cell Biol. 2 (2000) 156-162.

[4] R. Eskes, B. Antonsson, A. Osen-Sand, S. Montessuit, C. Richter, R. Sadoul, G. Mazzei, A. Nichols, and J. C. Martinou, Bax-induced cytochrome *c* release from mitochondria is independent of the permeability transition pore but highly dependent on Mg^{2+} ions. J. Cell Biol. 143 (1998) 217-224.

[5] X. Luo, I. Budihardjo, H. Zou, C. Slaugter, and X. Wang, Bid, a Bcl-2 interacting protein, mediates cytochrome *c* release from mitochondria in response to activation of cell surface death receptors. Cell 94 (1998) 481-490.

[6] M. Narita, S. Shinizu, T. Ito, T. Chittenden, R. J. Lutz, H. Matsuda, and Y. Tsujimoto, Bax interacts with the permeability transition pore to induce permeability transition and cytochrome *c* release in isolated mitochondria. Proc. Natl. Acad. Sci. USA 95(1998) 14681-14686.

[7] D. M. Finucane, E. Bossy-Wetzel, N. J. Waterhouse, T. G. Cotter, and D. R. Green, Bax-induced caspase activation and apoptosis via cytochrome *c* release from mitochondria is inhibitable by Bcl-x_L. J. Biol. Chem 274 (1999) 2225-2233.

[8] S. Desagher, A. Osen-Sand, A. Nichols, R. Eskes, S. Montessuit, S. Lauper, K. Maundrell, B. Antonsson, and J. C. Martinou, Bid-induced conformational

change of Bax is responsible for mitochondrial cytochrome *c* release during apoptosis. J. Cell. Biol. 144(1999) 891-901.

[9] G. Basanez, A. Nechushtan, O. Drozhinin, A. Chanturiya, E. Choe, S. Tutt, K. A. Wood, Y.-T. Hsu, J. Zimmerberg, and R. J. Youle, Bax, but not Bcl-x_L, decreases the lifetime of planar phopholipid bilayer membranes at subnanonmolar concentrations. Proc. Natl. Acad. Sci. USA 96 (1999) 5492-5497.

[10] X. Liu, C. N. Kim, J. Yang, R. Jemmerson, and X. Wang, Induction of apoptotic program in cell-free extracts: requirement for dATP and cytochrome *c*. Cell 86 (1996) 147-157.

[11] M. G. Vander Heiden, N. S. Chandel, E. K. Williamson, P. T. Schumacker, and C. B. Thompson, Bcl-x_L regulates the membrane potential and volume homeostasis of mitochondria. Cell 91(1997) 627-637.

[12] P. Marchetti, M. Castedo, S. A. Susin, N. Zamzami, T. Hirsch, A. Macho, A. Haeffner, F. Hirsch, M. Geuskens, and G. Kroemer, Mitochondrial permeability transition is a central coordinating event of apoptosis. J. Exp. Med. 184(1996) 1155-1160.

[13] J. C. Martinou, and D. R. Green, Breaking the mitochondrial barrier. Nat. Rev. Mol. Cell. Biol. 2(2001) 63-67.

[14] N. Zamzami, and G. Kroemer, The mitochondria in apoptosis: how Pandora's box opens. Nat. Rev. Mol. Cell. Biol. 2 (2001) 67-71.

[15] J. Yang, X. Liu, K. Bhalla, C. N. Kim, A. M. Ibrado, J. Cai, T-I. Peng, D. P. Jones, and X. Wang, Prevention of apoptosis by Bcl-2: release of cytochrome *c* from mitochondria blocked. Science 275 (1997) 1129-1132.

[16] D. G. Breckenridge, and D. Xue, Regulation of mitochondrial membrane permeabilization by Bcl-2 family proteins and caspases. Curr. Opin. Cell. Biol. 16 (2004) 647-652.

[17] M. Lutter, M. Fang, X. Luo, M. Nishijima, X. Xie, and X. Wang, Cardiolipin provides specificity for targeting of tBid to mitochondria. Nat. Cell Biol. 2 (2000) 754-761.

[18] X. Wang, J. Zhang, H. P. Kim, Y. Wang, A. M. K. Choi, and S. W. Ryter, Bcl-x_L disrupts death-inducing signal complex formation in plasma membrane induced by hypoxia/reoxygenation. FASEB J. 18 (2004) 1826-1833.

[19] G. Pan, K. O'Rourke, and V. M. Dixit, Caspase-9, Bcl-x_L, and Apaf-1 form a ternary complex. J. Biol. Chem. 273 (1998) 5841-5845.

[20] Y. Hu, M. A. Benedict, D. Wu, N. Inohara, and G. Nunez, Bcl-xL interacts with Apaf-1 and inhibits Apaf-1-dependent caspase-9 activation. Proc. Natl. Acad. Sci. USA 95(1998) 4386-4391.

[21] S. Kharbanda, P. Pandey, L. Schofield, S. Israels, R. Roncinske, K. Yoshida, A. Bharti, Z-M. Yuan, S. Saxena, T. Weishselbaum, C. Nalin, and D. Kufe, Role for Bcl-x_L as an inhibitor of cytosolic cytochrome *c* accumulation in DNA damage-induced apoptosis. Proc. Natl. Acad. Sci. USA 94 (1997) 6939-6942.

[22] X. Xie, S. Schendel, S. Matsuyama, and J. C. Reed, Acidic pH promotes dimerization of Bcl-2 family proteins. Biochemistry 37 (1998) 6410-6418.

[23] L. Chen, S. N. Willis, A. Wei, B. J. Smith, J. I. Fletcher, M. G. Hinds, P. M. Colman, C. L. Day, J. M. Adams, and D. C. S. Huang, Dfferential targeting of prosurvival Bcl-2 proteins by their BH3-only ligands allows complementary apoptotic function. Mol. Cell. 17 (2005) 393-403.

[24] A. Letai, M. C. Bassik, L. D. Walensky, M. D. Sorcinelli, S. Weiler, and S. J. Korsmeyer, Distinct BH3 domains either sensitize or activate mitochondrial apoptosis, serving as prototype cancer therapeutics. Cancer Cell 2 (2002) 183-192.

[25] H. Zhang, P. Nimmer, S. H. Rosenberg, S-C. Ng, and M. Joseph,

Development of a high-throughput fluorescence polarization assay for Bcl-x_L. Anal Biochem. 307(2002) 70-75.

[26] A. Kelekar, B. S. Chang, J. E. Harlan, S. W. Fesik, and C. B. Thompson, Bad is a BH3 domain-containing protein that forms an inactivating dimmer with Bcl-x_L. Mol. Cell. Biol. 17 (1997) 7040-7046.

[27] J. W. O'Neill, M. K. Manion, B. Maguire, and D. M. Hockenbery, Bcl-xL dimerization by three-dimensional domain swapping. J. Mol. Biol. 356 (2006) 367-381.

[28] S. W. Muchmore, M. Sattler, H. Liang, R. P. Meadows, J. E. Harlan, H. S. Yoon, D. Nettesheim, B. S. Chang, C. B. Thompson, S-L. Wong, S-C. Ng, and S. W. Fesik, X-ray and NMR structure of human Bcl-x_L, an inhibitor of programmed cell death. Nature 381(1996) 335-341.

[29] M. Sattler, H. Liang, D. Nettesheim, R. P. Meadows, J. E. Harlan, M. Eberstadt, H. S. Yoon, S. B. Shuker, B. S. Chang, A. J. Minn, C. B. Thompson, and S. W. Fesik, Structure of Bcl-x_L-Bak peptide complex: recognition between regulators of apoptosis Science 275 (1997) 983-986.

[30] P. Li, D. Nijhawen, I. Budihardjo, S. M. Srinivasula, M. Ahmad, E. S. Alnemri, and X. Wang, Cytochrome *c* and dATP-dependent formation of Apaf-1/caspase-9 complex initiates an apoptotic protease cascade. Cell 91 (1997) 479-489.

[31] Q. Bao, and Y. Shi, Apoptosome: a platform for the activation of initiator caspases. Cell Death Differ. 14 (2007) 56-65.

CHAPTER 5

Amyloid Fibrillation of Human Apaf-1 CARD

5.1 Abstract

The idea of establishing amyloid-like fibrillation tendency of pro- and anti-survival proteins of human apoptotic pathways is relevant for delineating the conditions that lead to aberrant differentiation, development, and tissue homeostasis. As the first step in this direction, we report here that the *Ca*spase *R*ecruitment *D*omain (CARD) of recombinant human *A*poptotic *P*rotease *A*ctivating *F*actor-1 (Apaf-1) can be induced to undergo amyloid-like fibrillation. The study was initiated with a set of biophysical investigations that served as the explorer of the possibility and *in vitro* conditions for fibril growth. By scanning the pH-induced conformational transitions, protein stability, and stopped-flow folding-unfolding kinetics, we have detected a molten globule (MG) transition of CARD at pH < 4. In a bid to reduce the surface-accessible hydrophobic patches in the MG state, the CARD monomer undergoes self-association to produce soluble oligomers that serve as precursor aggregates (PA) for protofibril formation. The monomer-to-oligomer self-association process is akin to the well known homophilic CARD/CARD interaction by which CARD of the same or different apoptotic proteins associate in order to transduce and regulate the apoptotic signal. The fibrillation reaction of Apaf-1 CARD was carried out at pH 2.1 and 60°C, because reduction of exposed hydrophobic surfaces in the MG state is more favored at the moderated solution condition. The Gaussian distributions of diameters of fibril population suggest values of 2.1 and 2.7 nm for the mean diameter of PA and protofibrils or elongated fibrils, respectively. We discuss the consequences of fibrillation supposing a finite probability of the process occurring under cellular conditions.

5.2 Introduction

The supramolecular assembly of a sizable number of diverse proteins and polypeptides into amyloid and amyloid-like fibrils has attracted attention of many for a number of reasons. First, the pathogenesis of a number of human conditions, including Alzheimer's disease, Parkinson's disease, spongiform encephalopathy, Huntington's disease, senile amyloidosis, and type II diabetes [1-7] is fundamentally associated with amyloids. A detailed understanding of the processes leading to extracellular amyloid deposition, intracellular neurofibrillary tangles, and the development of amyloid toxicity is necessary to devise strategies for therapeutic intervention and management of these diseases. Such β-sheet-based structural assemblies are also promising for industrial application, and in material science and biotechnology [21-26]. Second, the observation that a wide variety of non-disease-related proteins and polypeptides that presumably do not undergo amyloid-like transitions *in vivo*, but can be induced to do so in test tubes by changing the solution conditions [5, 8-13], has added newer dimensions to the multifarious response of proteins to solvent conditions. Given the number and variety of proteins from which amyloids have been formed, it is now generally accepted that amyloid aggregates are a generic structure for all proteins.

Since the amino acid composition, sequence, and the native-state structure are not determinants of amyloidogenecity [2, 14], amyloid fibrillation could originate from anywhere in the conformational landscape, entropically as low as the native or native-like states to as high as unfolded states in a protein specific manner [2, 15, 16], implying that some combination of the initial structure, number of intramolecular contacts, chain dynamics, and surface dielectric may be required to promote fibrillation, and that these factors may also be related to kinetic mechanism of the composite fibrillation reaction. Understanding of such issues needs to be augmented.

Amyloid fibrillation of CARD

Atomic models of amyloid fibril structure based on a variety of evidences, each limited by the extent amenable to the experiment, have been discussed [17-20]. Although there is a consensus that amyloid and amyloid-like fibrils contain β-sheet conformations, achieving atom-level resolution of arrangements of β-sheet structures has been seriously hindered by the difficulties of handling fibrous supramolecular forms that are often insoluble, especially at concentrations required for structural work. Thus, the specific structural and chemical features of proteins and the solvent-dependent reactivity that promote amyloidogenesis are at the focus of current research.

Concerning the etiology of amyloid cytotoxicity at the molecular level, fewer studies conducted to date have indicated that the fibrils and the precursor β oligomers trigger apoptosis in cells [27-35]. These *in vitro* studies confined to cultured neurons have relied principally on the observation of cell morphology and biochemical characteristics of apoptosis in response to treatment with soluble fibrils and PA. The evidences provided are compelling that amyloid-induced activation of an apoptotic pathway is one of the reasons for neural cell death in neurodegenerative diseases.

We were contemplating on the general possibility of amyloid-like transition of the pro- and anti-survival proteins of mammalian apoptotic pathways, even though at present there is no known amyloidosis that results from aggregation of any of these proteins, wildtype or otherwise. Should any of these proteins undergo amyloid fibrillation, the normal development, tissue differentiation, and homeostasis will be critically affected. In this study, we report on the *in vitro* transformation of the recombinant CARD domain of human Apaf-1 (Figure 1) into amyloid protofibrils. Apaf-1, a large anti-survival protein (~ 130 kDa), is the key molecule for activation of procaspase-9 in mitochondrial pathway of apoptosis in neuronal and somatic cells alike [36, 37]. Structurally, the Apaf-1 CARD domain consists of six tightly packed

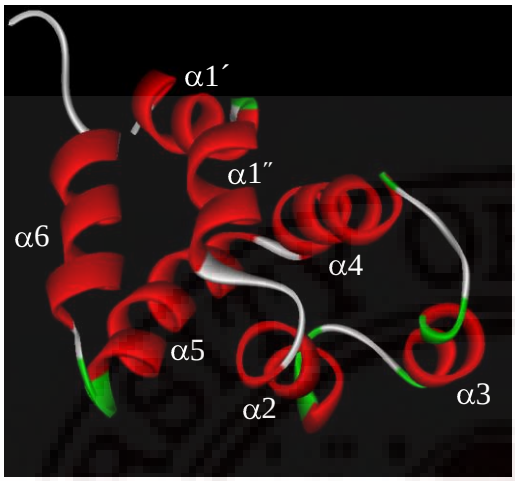

Figure. 1. Ribbon diagram of Apaf-1 CARD (pdb file: 1C15) with helices.

amphipathic α-helices (Figure 1, ref 38). The rationale for using the CARD domain is the fact that this domain is present as the N-terminal prodomain in a sizable set of apoptotic proteins, including some caspases, and CARD domains are known to mediate apoptotic signaling through homophilic CARD/CARD interactions [38-42]. To arrive at the *in vitro* conditions for transformation of the CARD protein to fibrils, we carried out a series of biophysical experiments as the prelude. The results of pH dependent conformational transitions, protein stability, and folding-unfolding kinetics showed that Apaf-1 CARD undergoes a molten globule-like transition under acidic conditions. This low pH-denatured form of CARD then undergoes further conformational transitions to produce soluble precursor aggregates (PA) of amyloid-like protofibrils. The consequences of CARD fibrillation and possible implications for cell survival are discussed.

5.3 Material and methods

5.3.1 *Cloning and generation of the CARD expression construct*

Total RNA isolated from HeLa cells was used for the cDNA amplification of the 300 bp gene fragment of Apaf-1. The 300 bp region of CARD domain of Apaf-1 was amplified by standard PCR reaction using the, forward and reverse primers designed with pGEX4T-1 compatible restriction sites at their 5' ends. The forward primer has a *Bam*H1 site, and the reverse a *Xho*1 site.

CARD-F: 5′ CGGGATCCATGGATGCAAAAGCTCGAA 3′ T_m = 56 °C

BamH1

CARD-R: 5′ CCCTCGAGCTAAGAAGAGACAACAGGAATG 3′ T_m = 56 °C

Xho1

cDNA was synthesized by reverse transcriptase, and the 300 bp CARD fragment was amplified by Taq DNA polymerase. Both steps were achieved by the use of the 'one-step RT-PCR kit' from ABGene Technologies. The PCR-amplified fragment was isolated by Qiagen Gel extraction kit, ligated into TA cloning vector pTZ57 R/T (MBI-Fermentas), and transformed into competent DH5α *E. coli* $CaCl_2$ treatment. The transformed cells were plated onto LB agar plates with 100 μg/mL ampicillin and 1mM IPTG and X-gal. The positive clones were selected by blue-white screening and colony PCR. The positively-screened colonies were used for isolation of plasmid DNA by standard protocols. The PCR fragment cloned into the TA cloning vector was restricted using *Bam*H1 and *Xho*1, and analyzed on 1% agarose gel. The expression vector pGEX4T-1 was also restricted in the same manner. The CARD gene fragment was then ligated into the digested pGEX4T-1 by using T4 DNA ligase, and transformed into DH5α cells. Cell colonies positive with the recombinant plasmid were screened by colony PCR. That the recombinant plasmids contained the expression vector carrying the insert was once again checked by restriction digestion. The sequence and orientation of CARD fragment was confirmed by sequencing. The restriction-positive plasmids were transformed into *E. coli* BL21 cells for expression of the CARD protein.

5.3.2 *Protein expression and purification*

500 ml LB broth with 100 μg ml^{-1} ampicillin was inoculated with 25 ml of overnight- grown culture (1:20 ratio) that contained the recombinant positive clone.

The protein expression was induced at OD_{600}=0.5 with 1 mM IPTG. Cells were grown for 5 hrs at 30 °C. Cells were pelleted and resuspended in 20 ml PBS and lysed by sonication for 3 min with repetitive 30 sec on and off cycles. The lysate was centrifuged at 3000 g for 30 min at 4 °C. The supernatant was collected and DTT was added to a final concentration 1 mM. This was loaded onto 1 mL GSH Sepharose 4B column that was preequilibrated with 10 volumes of PBS. The column was washed with 20 volumes of PBS. The GST-CARD protein that was bound to the column was eluted with 10 volumes of elution buffer (50 mM Tris-HCl, 10 mM reduced glutathione, pH 8). The purified GST-CARD protein was dialyzed against 1X PBS to remove the glutathione, and digested with recombinant thrombin (Amersham Biosciences) by standard protocols. Following digestion, thrombin was removed by Benzamidine Sepharose, and the protein mixture was loaded on a GSH-Sephrose 4B column. The 10 kDa CARD protein was eluted in the flow through. The eluted fractions were pooled and loaded on to a 1.6 X 100 cm (diameter and height, respectively) Sephadex G75 column preequilibrated with 50 mM Tris.Hcl, pH 7.5. Fractions each of 1.0 ml size were collected at a flow rate of 20 ml/h. The fractions were pooled and concentrated by ultrafiltration.

For western blot analysis of expressed CARD protein, the thrombin digested GST-CARD was transferred onto a PVDF membrane. The membrane was probed with anti-Apaf-1 rabbit polyclonal IgG and then with ALP conjugated anti-rabbit 2° antibody. The blot was developed with BCIP-NBT solution.

5.3.3 *Equilibrium measurement of CARD stability towards pH, NaCl, and GdnHCl*

For these titrations, separate samples of identical protein concentration (5-7 μM) were employed. Protein solutions held at different values of pH or NaCl concentration were incubated for ~6 hours before taking fluorescence spectra. For

GdnHCl unfolding, samples containing different concentrations of the denaturant were prepared by mixing two stock protein solutions, one containing 4 M GdnHCl and the other without. Buffers for various pH ranges were: 50 mM glycine (pH <3), 50 mM sodium acetate (pH 3-5), 17 mM each of HEPES-PIPES-Tris (pH 6-9), and 25 mM each of Glycine-CAPS (pH 9-11). All experiments were done at 22 °C using a Fluoromax-4 (Horiba Jobin Yvon) instrument.

5.3.4 *Stopped-flow kinetics of CARD folding and unfolding*

These experiments involved two-syringe mixing, and invariably employed 8-fold dilution of a 10 μM protein solution with the relevant buffer. For refolding, the protein initially unfolded in 5.4 M GdnHCl and equilibrated for ~1 hour was mixed with the refolding buffer containing variable amount of GdnHCl. Unfolding was initiated by diluting the native protein solution with the unfolding buffer containing desired concentrations of GdnHCl. The buffer systems were same as given above. Kinetics were recorded at 22 °C in a Bio-Logic SFM4 mixing module using a 0.8 mm square flow cell (mixing dead time, ~ 2 ms). Typically, 8-10 shots were averaged for noise reduction.

5.3.5 *Fibrillation kinetics*

CARD solutions (~15 μM) containing ~50 μM thioflavin (4-(3,6-dimethylbenzothiazol-2-yl)-N,N-dimethyl-aniline, ThT) were prepared in 50 mM glycine-HCl buffer, pH 2.1, and incubated at 60 °C in a heating block. Samples incubated up to different time extent were cooled and analyzed by 482-nm ThT fluorescence, excited at 432 nm.

5.3.6 *Atomic force microscopy*

For microscopy, fibrillation was allowed in the absence of thioflavin. Films of samples incubated up to variable extent of time were deposited on freshly cleaved mica plates, and allowed to dry under nitrogen for ~15 minutes. Films were then washed thoroughly by gently flowing deionized water over the mica plate, and dried under nitrogen for ~1 hr. Imaging in the semi-contact mode was performed in a NT-MDT Solver microscope using a 3-micron scanner head. Images were processed using the NOVA software supplied by the microscope manufacturer.

5.4 Results

5.4.1 *The Apaf-1 CARD expression system and the recombinant protein*

Initially we generated two gene constructs for *E. coli* expression of human Apaf-1 CARD, one with a N-terminal His_6 tag (pET28a vector) and the other with GST fused at the N-terminus (pGEX4T-1 vector), but the latter was chosen for the production of the recombinant protein because of the ease and convenience of purifying GST-fused small proteins.

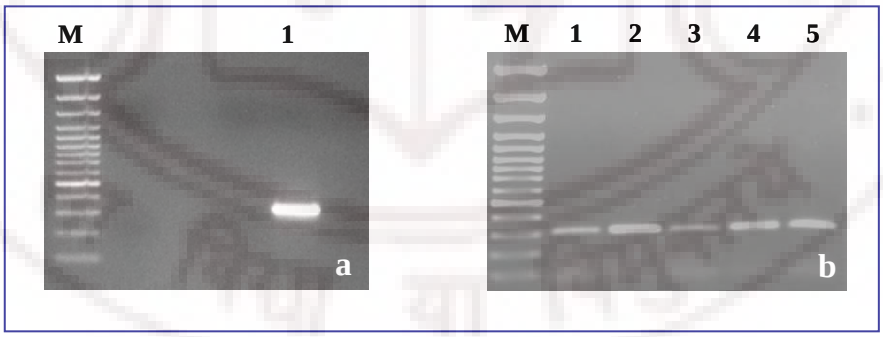

Figure 2. (a) Agarose gel electrophoresis showing one step RT –PCR amplification of 300bp Apaf-1 CARD from HeLa cells total RNA. Lane labels are: M, 100 bp DNA ladder; 1, amplified 300 bp CARD fragment. (b) Colony PCR analysis for recombinant pGEX4T-1 CARD. Lane labels are: M,100 bp DNA ladder; Lanes 1-5 300 bp amplification CARD in positive clones.

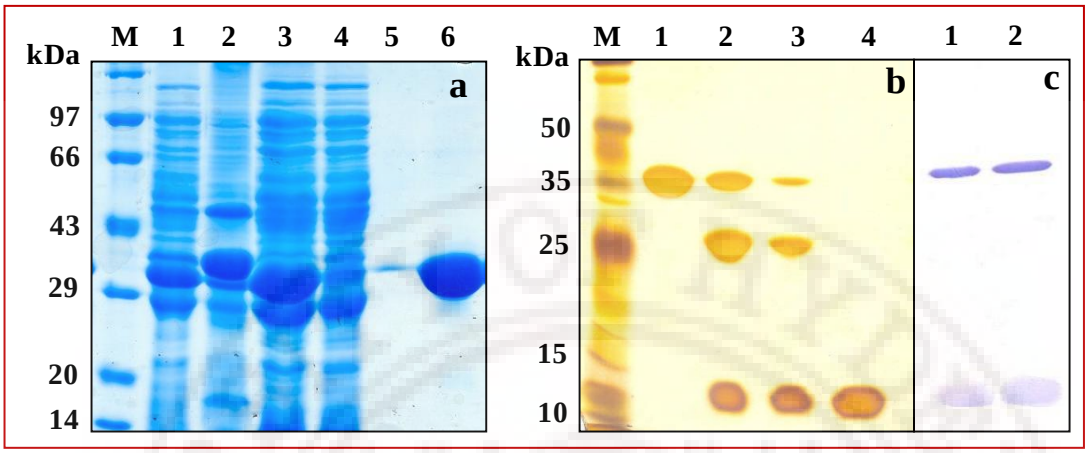

Figure 3. (a) SDS-PAGE analysis of Affinity purification of Apaf-1 CARD by GSH-Sepharose 4B column. Lane labels are: M, molecular weight markers; 1, whole cell lysate; 2, insoluble pellet fraction; 3, Cleared lysate loaded onto the column; 4, column flow through fraction; 5, wash fraction; 6, eluted GST-CARD. (b) SDS-PAGE analysis of thrombin digestion and purification of Apaf-1 CARD. Lane labels are: M, molecular weight markers; 1, GST-CARD purified from GSH Sepharose 4 B column; 2, the thrombin-digested GST-CARD mixture; 3, the digest after removal of thrombin by Benzamidine Sepharose; 4, homogeneous and pure CARD obtained after passing the thrombin-stripped digest through a GSH-Sepharose 4B column. The CARD protein elutes in the flow through fractions. (c) Western blot analysis of thrombin digested GST-CARD. The upper ~35 kDa band is undigested GST-CARD and lower 10 kDa band is Apaf-1CARD.

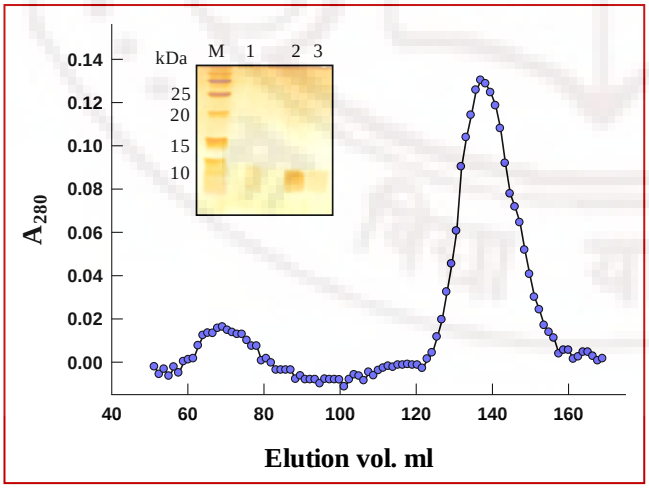

Fig.4. Sephadex G-75 purification of Apaf-1 CARD. The single peak in chromatogram corresponds to the monomeric CARD. The Lanes 1-3 in the inset SDS-PAGE picture are the purified CARD protein.

This expression vector was used in earlier studies of NMR solution structure of Apaf-1 CARD [38], although mutagenesis-based cloning and expression in pET-3d vector has also been reported [43]. As Figure 3 shows, the recovered CARD (~6 mg per liter of *E. coli* culture) is homogeneous and highly pure. The purified CARD was monomeric which was confirmed by Sephadex G-75 gel filtration chromatography (Figure 4). The western blot of thrombin digested GST-CARD shows the detected 10 kDa CARD protein by the polyclonal anti-Apaf-1 rabbit IgG.

5.4.2 *Different pH forms of CARD*

The rationale for examining CARD conformational changes as a function of pH was that partly denatured proteins at acidic and alkaline pH can often reveal structural and functional regulation of proteins. A contextual example is low-pH dimerization of apoptotic Bcl-2 family of proteins which possibly leads to ion channel formation in synthetic membranes [44]. For Apaf-1 CARD, Figure 5a shows the general trend of fluorescence decrease with increasing pH. The primary structure of CARD has no tryptophan and the observed fluorescence with the λ_{max} of 309 nm, due likely to tyrosine, is weak. The absence of any shift in the fluorescence maximum across the pH range may be due to very similar polarity of the environment of tyrosines under native and denaturing conditions. Absence of fluorescence band shift across the folding-unfolding transition is seen for cytochrome *c* also. A closer examination of the pH dependence of the 309-nm fluorescence (figure 5b) shows a pronounced dip at ~pH 4 on either side of which the fluorescence signal increases. In the 5-8 range of pH, the fluorescence remains unchanged, but decreases gradually for pH>8. The data thus indicate three pH transitions: an alkaline transition with a pH midpoint near 10 attributable to tyrosyl side-chain ionization, a weakly acidic transition with a midpoint around pH 4.5 due likely to ionization of Glu or Asp side-

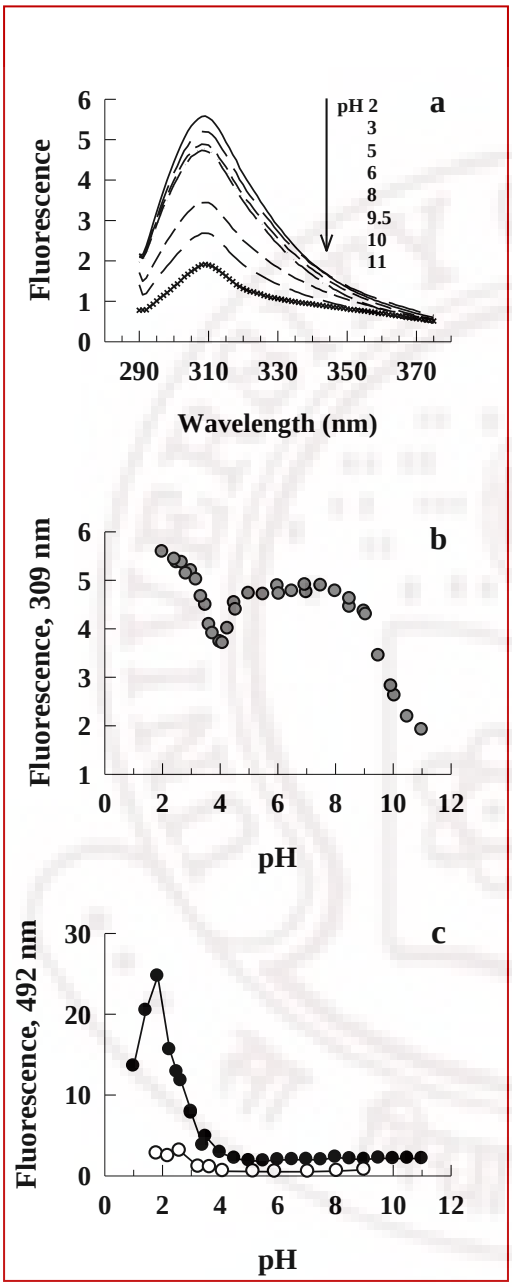

Figure 5. Fluorescence monitored pH depen--dence of CARD conformational transitions. For all these experiments, the protein concentration was ~6 μM.

(a) Fluorescence spectra as a function of pH generally conveys increased quenching with pH increments. (b) The plot of 309-nm fluorescence with pH, however, shows three prominent transitions: an alkaline transition, a weekly acidic transition, and a more acidic transition. The interpretations and assignment of each of the transitions to specific conformational changes of CARD are described in the text. Due to the complexity of analysis of the three linked transitions, the data have not been fitted to a function. (c) pH effects on ANS binding to CARD. The protein and ANS concentrations in the solution at different pH were 7 and 15 μM, respectively. The open circles show the 492-nm fluorescence of control samples from which the protein was excluded.

chain -COOH, and a molten globule-like transition when strongly acidic conditions are approached. While the molten globule-like transition involves a global denaturation transition of CARD, the other two transitions could simply be associated with side-chain ionization-linked conformational perturbation. As a simple test for the extent of structure perturbation

in each of these transitions, we measured the ANS fluorescence of CARD solutions containing ANS (6 μM protein and 12 μM ANS) as a function of pH. As Figure 5c shows, ANS is fluorescence-silent at pH>4, but is very highly fluorescent at pH values less than 4. The ANS fluorescence indicates a major transition in the 2-4 range of pH, closely reproducing the molten globule-like transition considered above (Figure 5b). Indeed, ANS binds to solvent exposed clusters of hydrophobic groups, and its strong binding is a particularly convenient test for the molten globule state [45]. But then, the ANS fluorescence decreases when the pH value falls below 2 (Figure 5c), indicating self-association or oligomerization of acid-denatured CARD in a manner that conceals the exposed hydrophobic surfaces. The CARD monomers possibly oligomerize by hydrophobic interactions.

To understand the CARD conformational changes further, we extended the pH dependent fluorescence experiment by including NaCl concentration as another variable (Figure 6a). Clearly, all three transitions seen in Figure 5b the alkaline, the acidic, and the molten globule-like transition are reproduced in the presence of any concentration of NaCl used in the 0-1 M range (Figure 6a). Further, NaCl sets the fluorescence in a pH dependent manner (Figure 6b). At intermediate pH values, the fluorescence increases with NaCl, but decreases relatively more at acidic and alkaline values most likely due to electrostatic screening of protein charges by Cl^- and Na^+ ions, respectively. Thus, at pH near 2, the acid-denatured state is transformed to a molten globule state. To summarize this section, CARD at acid pH (<4) undergoes a major denaturational transition accompanied by a substantial exposure of otherwise buried hydrophobic surfaces. Under strongly acidic conditions (<pH 2), the denatured monomers interact with each other possibly by hydrophobic interactions to produce soluble oligomers or aggregates. We have called them precursors aggregates (PA).

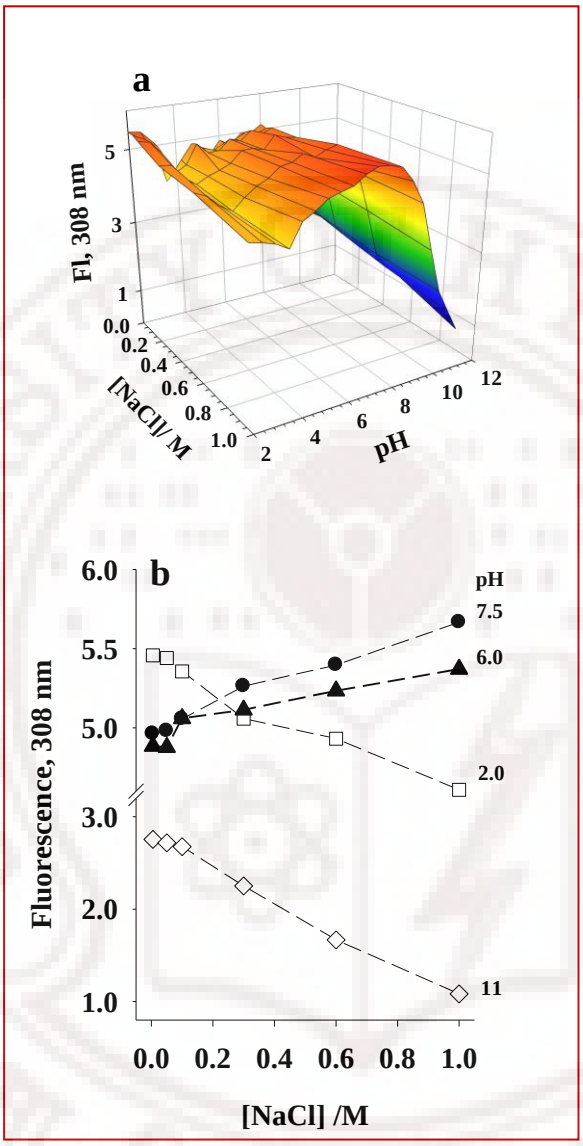

Figure 6. CARD fluorescence as a function of pH at different concentrations of NaCl. (a) All three pH-induced conformational transitions of CARD are seen in NaCl independent manner, although some details of the transitions, including the sharpness and fluorescence amplitudes, are affected (see Results). (b) The effect of NaCl on the fluorescence amplitude depends on the pH of the medium. The substantial decrease of fluorescence at acidic and alkaline pH is likely due to electrostatic screening of protein charges by Cl^- and Na^+ ions, respectively.

5.4.3 *Equilibrium and kinetic aspects of folding of Apaf-1 CARD at acid and neutral pH*

To learn more about the influence of pH on the stability and structure, we examined the GdnHCl-induced folding behavior of the protein by equilibrium and stopped-flow kinetic methods. Figure 7a shows the equilibrium unfolding transition at pH values 6 and 3.1. At pH 6, the initial increase of fluorescence in the pretransition region is followed by a relatively sharp drop in the unfolding transition region. The structural details associated with these changes is subject to scrutiny. For the present though, a fit of the data to the two-state N $\rightleftharpoons$ U model [46], where N and U are native and unfolded states, respectively, by assuming a second-order polynomial dependence of the pretransition fluorescence with GdnHCl yields the protein stability, $\Delta G°$=12.5±0.5 kcal mol^{-1}, and the transition midpoint, C_m≈2.4±0.1 M. In an earlier study of CARD unfolding in the presence of urea, ~6 kcal mol^{-1} was reported for the value of $\Delta G°$ [47]. Generally, the $\Delta G°$ value determined by urea unfolding is lower than that extracted from GdnHCl unfolding. Part of the discrepancy also arises from the large increase in the fluorescence in the pretransition baseline (Figure 7a) which the earlier authors did not notice in their study by the use of urea [47]. At pH 3.1, a clear unfolding transition of CARD is not detected. The change in the fluorescence stretches out for GdnHCl>1.5 M, indicating lack of compactness and well defined structural elements typical of an acid-denatured state in the absence of added anions [45]. The monotony in fluorescence change might simply reflect expansion of the chain. To show that the unfolded state in the presence of 4 M GdnHCl does not contain any considerable structure, the protein was titrated in the 1-7.5 range of pH holding the denaturant concentration constant at 4 M (Figure 7b).Within the error limit, the fluorescence hardly changes in the pH range 2-7.5, suggesting that unfolding is complete at 4 M GdnHCl.

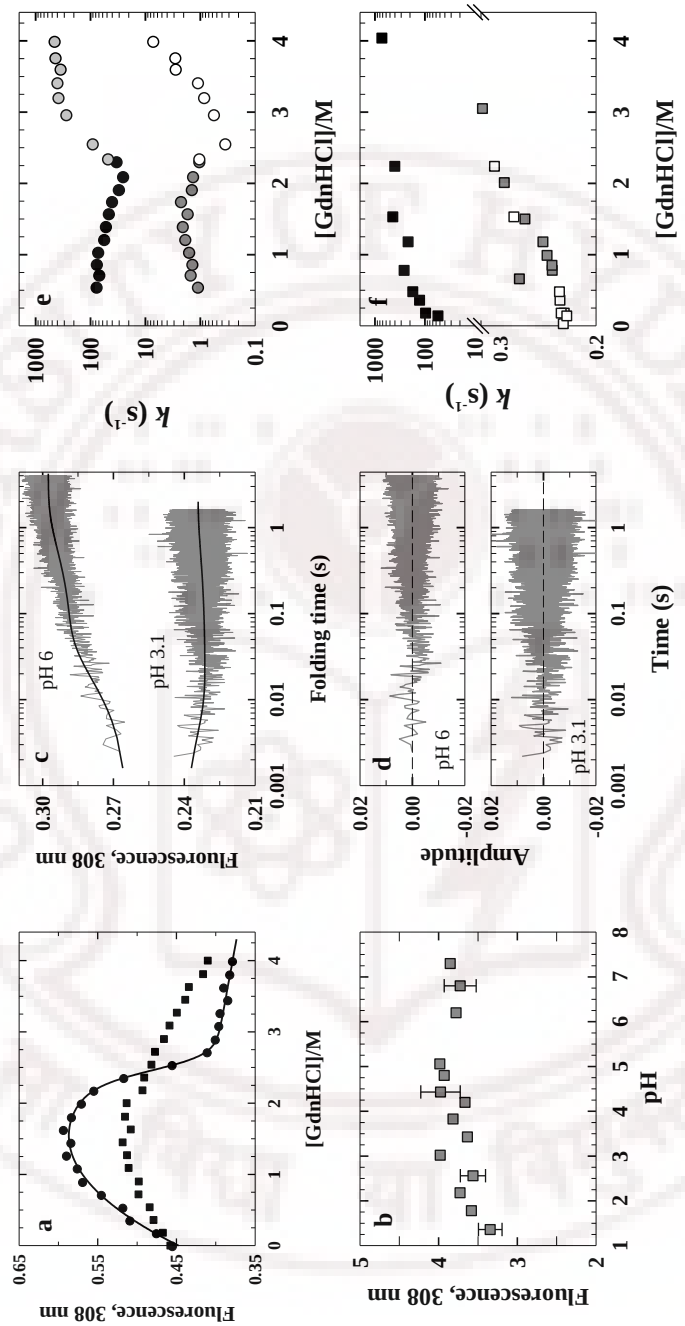
a
b
c
d
e
f
Fluorescence, 308 nm
[GdnHCl]/M
pH
Amplitude
Time (s)
Folding time (s)
k (s-1)
pH 6
pH 3.1

Figure 7. pH-dependent stability and folding kinetics of Apaf-1 CARD. (a) GdnHCl-induced equilibrium unfolding at pH 6 (●) and pH 3.1 (■).At pH 6, the global unfolding transition is preceded by a pretransition zone characterized by a substantial increase in fluorescence. Since the details of CARD structural changes occurring in the pretransition region is unclear at the moment, the data were modeled with a two-state **N⇔U** tansition by assuming that the pretransition changes are due to solvent dependent baseline effect having a second-order polynomial dependence for fluorescence changes with GdnHCl. The fit of the data yields $\Delta G°$=12.5±0.5 kcal mol^{-1} and C_m≈2.4±0.1 M (see text). At pH 3.1, no pronounced global transition is apparent, suggesting the absence of well-defined tertiary structure. (b) pH titration of the 4 M GdnHCl-unfolded protein. (c) Representative kinetic traces for refolding of CARD in the presence of 1 M GdnHCl (pH 6) or 0.7 M GdnHCl (pH 3.1). For both experiments the protein was initially unfolded in 5.4 M GdnHCl at the respective pH. The refolding at pH 6 is described by two rising exponentials, k_{fast}=60 s^{-1} and k_{slow}=1.8 s^{-1} with fractional observed amplitudes of 0.7 and 0.3, respectively. At pH 3.1, there is a fast decaying phase (k_{fast}=262 s^{-1}) followed by a slow rising phase (k_{slow}=2 s^{-1}), suggesting the possible formation of an aggregate or misfolded intermediate at early times of refolding. (d) Residuals of the 2-exponential fits. (e) GdnHCl dependence of the apparent rates for the major (upper chevron) and the minor phase (lower chevron) at pH 6. In each chevron, the data forming the left (darker symbols) and right (lighter symbols) arms

Figure 7c shows two representative kinetic traces for refolding of CARD, one at pH 6 and the other at pH 3.1, both initially unfolded in 5.4 M GdnHCl at the respective pH and refolded in the presence of 1 M GdnHCl for pH 6, and 0.7 M GdnHCl for pH 3.1. Both traces are best fit by two exponentials, and the residuals are shown in Figure 7d. At pH 6, the two kinetic phases have the same sign for amplitudes and are associated with refolding. At pH 3.1, only the slow rising phase is

indicative of refolding. The initial phase which is faster than the slow phase by at least two orders of magnitude and during which the fluorescence decay is associated with an unfolding event (Figure 7c). The GdnHCl distributions of the apparent rate constants (k_{obs}) for both kinetic phases of refolding and unfolding at pH 6 are shown in Figure 7e. Except for the unfolding by the slow kinetic phase, the rates clearly roll over as strongly native-like or strongly unfolding conditions are approached. Classically, multiple chevrons indicate existence of interconverting ensembles of unfolded conformations with ensemble-specific refolding rates producing parallel folding routes, and chevron rollover is thought to arise from accumulation of kinetic intermediates [48]. For Apaf-1 CARD, the two distinct chevrons with limb rollovers then suggest the occurrence of two ensembles of unfolded conformations, one folds faster than the other. The folding routes for both fast-folding (U_F) and slow-folding (U_S) ensembles involve kinetic intermediates; but how many intermediates are involved in the folding of U_F and U_S cannot be determined with the data at hand. Available results allow the description of Apaf-1 CARD folding by the following basic model

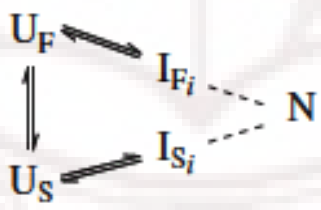

where I_{Fi} and I_{Si} represent intermediates. But for the kinetic intermediates invoked here, this model is consistent with the one proposed earlier based on the kinetic study of Apaf-1 CARD folding [47]. That work employed urea as the denaturant unlike

GdnHCl used here, and observed only one chevron with no rate rollover in the limbs. Part of the discrepancy in the results may arise from the use of two different chemical denaturants. The present study provides a direct evidence for distinct unfolded state ensembles based on the finding of two distinct chevrons.

Figure 7f shows the rate-denaturant distribution for CARD folding-unfolding at pH 3.1. At all concentrations of GdnHCl, the observable fast phase in the stopped-flow kinetics is due to unfolding. So is the case with the slow phase when the GdnHCl concentration is higher than ~0.3 M. Importantly, the GdnHCl dependences of both rates are associated with considerable positive slope or kinetic *m*-value (given by $m_u^{\ddagger}=2.3RT\,\partial\log k_u/\partial[\text{GdnHCl}]$, where k_u is the apparent rate constant of unfolding), indicating that CARD at pH 3.1 is still substantially structured with a defined core. Also, as it happens at pH 6, the unfolding rates at pH 3.1 roll over under strongly unfolding conditions, suggesting the occurrence of two ensembles of unfolded conformations and an unknown number of kinetic intermediates as depicted in folding model given above. It thus appears that the structure and topology of CARD at pH 3.1 resemble that of the pre-molten globule state characterized by fluctuating structural elements [45].

5.4.4 *Kinetics of protofibril formation for Apaf-1 CARD*

The indication provided by ANS fluorescence results (Figure 5c) that acid-denatured and molten globule-like CARD can form soluble oligomers or PA at pH near 2 led us to examine whether the precursors have the propensity to grow into protofibrils. Since the dye ThT is specifically used to probe amyloid fibrils [49, 50], we incubated a 15 μM CARD solution containing 50 μM ThT at 60°C held at pH 2.1 in Gly-HCl buffer, and periodically measured the time dependence of the dye

fluorescence up to 100 hours. As Figure 8 shows, following a lag time of ~9 hours, the fluorescence increases in a single-exponential phase with an apparent rate constant of 0.04 per hour, suggesting the formation of amyloid fibrils [51]. Generally, the presence of the lag phase and the fibrillation rate both depend on the protein concentration as well as the incubation temperature and buffer conditions used. This should hold for the formation of CARD fibrils also, although we have not explored conditions that would reduce the lag time or increase the rate of fibril formation.

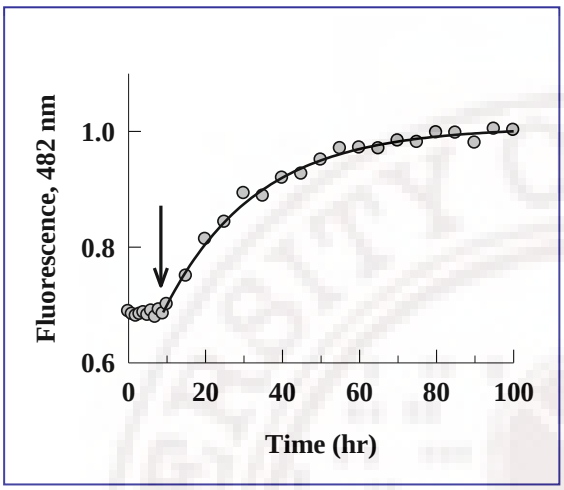

Figure 8. Fibrillation kinetics monitored by ThT fluorescence. The sample contained 15 μM CARD and 50 μM ThT was held at pH 2.1 and 60°C. The arrow indicates the end of the lag phase (~9 hours). The fit of the data after the lag phase yields k=0.04 hr^{-1}.

5.4.5 *Images and dimensions of Apaf-1 CARD fibrils*

The formation of fibrils was confirmed by direct images of CARD samples held at pH 2.1 and incubated at 60°C for varying length of time (Figure 9). By using ~10 μM protein, we see signs of elementary combination of PA within ~15 minutes (Figure 9a, panel 1). The growth into protofibrils requires several hours shown here at the end of 8 hours (panel 2), and longer fibrillar structures begin to appear by ~14 hours of incubation (panel 3). At ~100 μM protein, the fibrillation kinetics was very rapid (Figure 9b). The rich lattice of amyloid fibrils observed after 1 hour of incubation (panel 1) becomes denser after ~3 hours (panel 2), but appears diffused

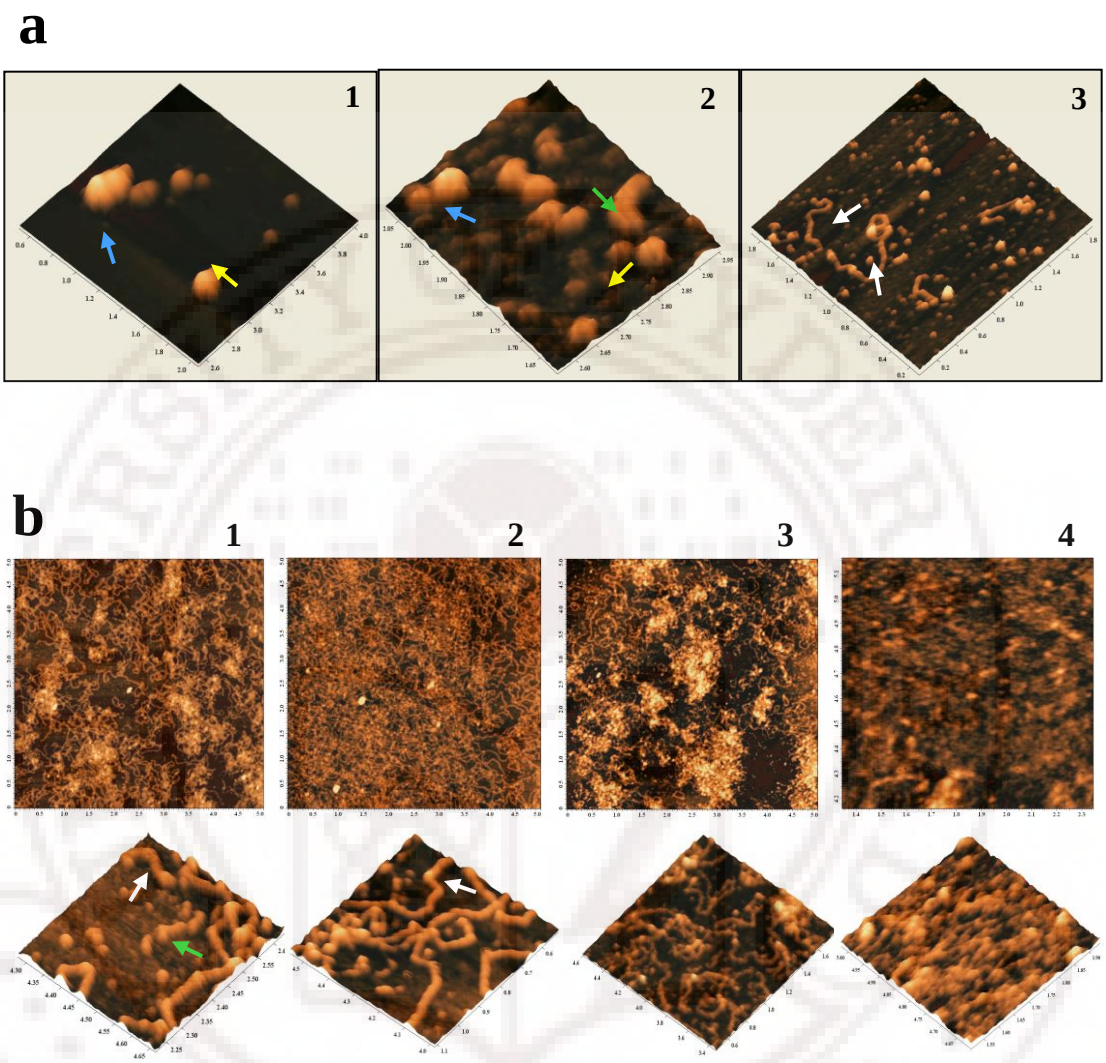

Figure 9. AFM images of Apaf-1 CARD aggregates. (a) A 10 μM protein solution incubated at 60°C, pH 2.1, shows first signs of combination of the PA within ~15 min (panel 1). The growth and elongation of protofibrils are shown in panels 2 and 3 imaged at the end of 8 and 14 hours, respectively, of incubation. Yellow, blue, green, and white arrows indicate PA, nascent protofibrils, and elongated protofibrils, respectively. (b) At ~100 μM protein concentration, fast and rich growth of fibrils is observed. Imgaes shown in panels 1, 2, 3, and 4 were recorded with samples incubated for 1

To achieve a dimensional distinction of PA, protofibrils, and large fibrils, we determined the Gaussian distribution of diameter *d* for each population. The diameters respectively, were arranged into groups of 0.25 nm increments, and the % population falling in each diameter group was determined (Figure 10). The solid lines through the data are 3-parameter Gaussian fits according to

$$P(d) = P(d_o) exp\left[-0.5\left(\frac{d-d_o}{b}\right)^2\right]$$

where, $P(d_o)$ is the amplitude corresponding to the mean diameter d_o, and b is the Full Width at Half Maximum (FWHM). The value of d_o for PA is 2.1 nm as against 2.7 and 2.63 nm for protofibril and elongated protofibrils, respectively. This dimensional difference between the initial PA and the fibrils should arise from differences in the content of presumably β-sheet. The FWHM values (1.5, 1.6, and 1.25 nm for the distributions corresponding to PA, protofibrils, and elongated protofibrils, respectively) indicate the population inhomogeneity, being largest for protofibrils and smallest for large fibrils.

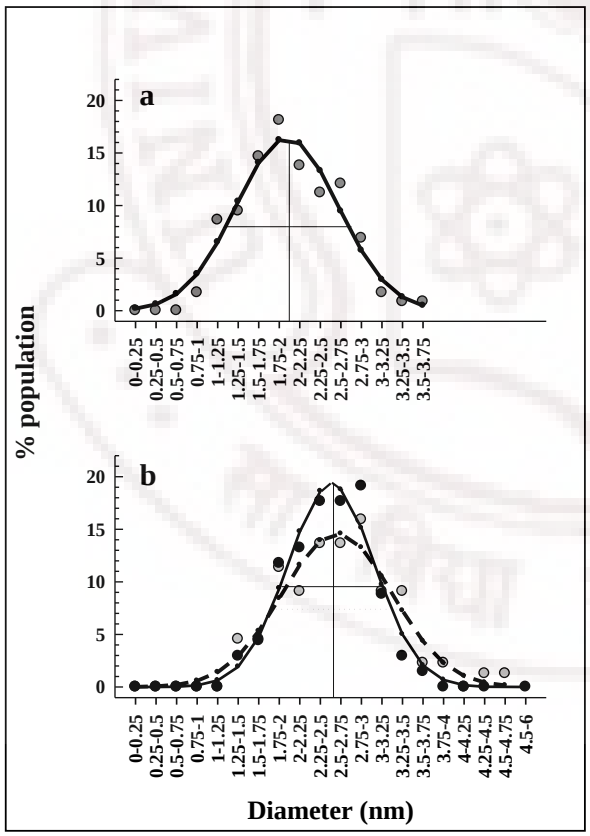

Figure 10. Distribution of population diameters. The solid lines are three-parameter Gaussian fits to the measured data according to equation 1. (a) PA with a mean diameter, d_o= 2.1 nm. (b) The protofibrils and elongated protofibrils d_o values of 2.7 and 2.63 nm, respectively.

The differences in the inhomogeneity may partly arise from the fact that structurally PA and fully grown fibrils are characterized by α-helical and β-sheet content, whereas the protofibrils at the initial formation stages contain both in proportion different from one set of population to another (large FWHM).

5.5 Discussion

Examinations of the pH-induced conformational transitions and folding stability of recombinant human Apaf-1 CARD have shown that the acid-denatured protein self-associates to form soluble precursor aggregates which can combine and undergo structural transitions to form amyloid protofibrils.

.

5.5.1 *Soluble oligomers and protofibrils of Apaf-1 CARD.*

Many pro- and anti-survival proteins of the apoptotic machinery are known to homodimerize, heterodimerize, and even homo-oligomerize to exert their survival and death effects [52-60]. Some are constitutively oligomeric due to ready accessibility of the interacting surfaces, and others are prevented from oligomerization by sequestration of the interacting surfaces until functional activation occurs. The former class is exemplified by the pro-survival protein Bcl-x_L, for which a large fraction of the cellular population homodimerizes by homophilic interaction of the C-terminal hydrophobic tails [44, 60-62], and the latter is represented by quiescent Apaf-1 known to exist in the monomeric form [36, 63]. It appears that the structural surface of CARD of Apaf-1 required for homophilic interaction with the CARD of procaspase-9 [38] is partially buried in the inactive state of Apaf-1 due to intramolecular interactions, an observation based on the crystal structure of the WD40-deleted Apaf-1 [64]. When activated by binding with cytochrome *c* and dATP [63], Apaf-1 forms a wheel-shaped homoheptamer complex or apoptosome having a seven-fold symmetry

[65, 66]. Although atomic details and packing interactions in the apoptosome are not known, the CARD can now interact with the CARD of procaspase-9. Thus, homo-heptameization of Apaf-1 seems to be crucial for sensitizing the CARD for binding interactions.

But, Apaf-1 CARD alone in neutral-pH solutions exists in the monomeric state (Figures 5-7), consistent with the earlier report that no dimerization occurs even at concentrations as high as 1 mM [38]. On the other hand, isolated Apaf-1 CARD forms a complex with isolated caspase-9 CARD in which the former deploys sets of acidic and hydrophobic residues in a manner that creates a contiguous binding surface, suggesting that intermolecular associations of Apaf-1 CARD require both electrostatic and hydrophobic interactions [38]. Should Apaf-1 CARD alone undergo homo-oligomerization, the operative forces of interaction must be hydrophobic in nature, because the surface charge complementarity is not available. The existence of Apaf-1 CARD in the monomeric form in the neutral-pH region then suggests that the hydrophobic interactions afforded by the native protein surface are insufficient for dimerization to occur. The situation is quite interesting under acidic conditions (~pH 3-4) where CARD undergoes a MG-like transition. Relative to the native state, the molecular surface in the MG state is more hydrophobic as evidenced by binding of small nonpolar molecules like ANS (Figure 5b, c). The increased surface hydrophobicity should favor CARD-CARD self association, but electrostatic repulsion due to excess positive charge and large-scale fluctuations of the structural elements in the MG-like state [45] are the principal opposing forces. A dramatic increase in surface hydrophobicity can occur under strongly acidic conditions (<pH 2.5) where the already weakened structural elements of the CARD MG break down causing exposure of buried nonpolar residues. We believe, the preponderance of hydrophobic surfaces in the acid-denatured proteins is now so overwhelmingly favorable toward CARD oligomerization that electrostatic repulsions are subdued, and

a monomer $\rightleftharpoons$ oligomer equilibrium is readily established. The oligomerization event can be thought of as a transition to an alternative non-native global free-energy minimum [67]. We should also note that protein oligomerization by hydrophobic interactions at low pH very likely buries some positive charges in the protein-protein apolar interface, and because charge burial in the low dielectric apolar environment is energetically expensive, the CARD oligomers are unlikely to be very highly stable.

These soluble oligomers are precursor aggregates (PA) which grow in size to form elongated protofibrils (PA$\rightarrow$protofibril). We have not investigated the mechanism and the events associated with the PA$\rightarrow$protofibril condensation in this work, but the CARD fibrillation pathway may be depicted as: MG $\rightleftharpoons$ PA $\rightarrow$ protofibril $\rightarrow$ elongated protofibril. The inference that the MG-like conformation facilitates PA formation is consistent with the survey-based observation that the amyloidogenic conformation shares many structural and dynamical properties with the pre-molten globule state [2].

5.5.2 *Relevance to in vivo fibrillation of Apaf-1*

Although we obtained amyloid fibrils from acid-denatured CARD at an elevated temperature, the question is: what relevance this has for *in vivo* situations, given that none of the pro- and anti-survival proteins is known to undergo fibrillation? This study rests on a limited empirical search for a *in vitro* condition that facilitate fibrillation. The low pH and high temperature encourage, respectively, higher surface hydrophobicity for the monomers and stronger hydrophobic interactions between them. Such conditions are certainly not physiological, but one cannot exclude yet unknown intrinsic cellular factors, accidental biochemical insults, or pathological conditions that could promote formation of soluble oligomers of Apaf-1 required for protofibril growth. As mentioned earlier, fibril growth may require some combination

of the initial molecular structure, packing density, bonding, intramolecular dynamics, and surface dielectric. Since the underlying physico-chemical principles for fibril growth are not fully understood, the conditions that might promote fibrillation *in vivo* need to be empirically found. Facing the two counteracting scenarios −the absence of specific evidence for amyloidosis of apoptotic proteins on one hand, and the finding that CARD could undergo fibrillation, albeit under nonphysiological conditions, on the other− one could at the most say that there is a very low or a restricted likelihood of Apaf-1 fibrillation *in vivo*. Even this likelihood could narrow down for a protein the size of Apaf-1 given that amyloidogenic proteins and peptides are generally smaller in size. The CARD is a small domain of Apaf-1, and it independently might not form fibrillar aggregates under physiological conditions. Nonetheless, a discounted possibility of Apaf-1 fibrillation still exists.

It is often hard to foresee the cellular or physiological relevance of a phenomenon tested under non-physiological conditions. For example, the MG states are best stabilized under extreme pH conditions in the presence of counter ions [45], and indeed the significance of the MG state was elusive in the seminal days, except for the recognition that it represented the third thermodynamic state of proteins [45]. It is now clear that a class of intrinsically disordered proteins that resemble MG and lack tertiary folds [68] are involved in cell signaling and regulatory function by protein–DNA and protein–protein interactions [69, 70].

In the same spirit, fibrillation of apoptotic proteins might find relevance to cell survival. In the absence of specific evidence at the moment, we simply say that there is a finite likelihood of Apaf-1 fibrillation *in vivo*.

5.5.3 *Amyloid fibrils and cell survival*

Although cytotoxicity of amyloid fibrils and progression of degenerative disorders such as Alzheimer’s and Creutzfeldt-Jacob diseases, due to insoluble fibrils

of amyloid-β protein (Aβ) and prion protein (PrP), respectively [31-35, 71, 72], is well established, the molecular mechanism by which the amyloid fibrils and their precursors kill cells is less understood. It is however recognized that activation of an apoptotic pathway is one of the major causes of amyloid fibril-induced cell death [27-30]. Credible evidences for this recognition are provided by observation of morphological and biochemical characteristics of apoptosis in healthy neurons and cultured cells treated with fibrils of Aβ [27, 29], and with fibrils produced differentially from PrP [30-35]. But whether it is the extent of fibrillation or the fibril dimension or the inherent property of the precursor amyloid protein that forces cells to undergo apoptosis is unsettled. For example, insulin fibrils are non-toxic to neurons [30], but precursor oligomers of hen lysozyme fibrils decrease the viability of neuroblastoma SH-SY5Y cells by presumably apoptotic activation of caspases [73].

But the issue of cytotoxicity of prefibrillar aggregates of pro- and anti-survival apoptotic proteins, assuming that one or more of them could possibly undergo *in vivo* fibrillation, is redundant. Cytotoxicity is irrelevant here because prefibrillar aggregates of any of these proteins as such would be very detrimental to cell survival. Since Apaf-1 is the key anti-survival protein of the mitochondrial pathway of apoptosis in neuronal and non-neuronal cells alike, amyloid fibrillation of this protein will arrest normal development of organs in adults and lack of embryonic differentiation leading to death, just the way Apaf-1-null mice die due to a pronounced enlargement of the periventricular proliferative zone during late embryonic development [74]. To find out if this is one of the manners by which cell survival could be challenged, the *in vivo* fibrillation tendency of apoptotic proteins needs to be determined.

5.6 References

[1] J. Hardy, and D. J. Selkoe, The amyloid hypothesis of Alzheimer's disease: progress and problems on the road to therapeutics. Science 297 (2002) 353-356.

[2] V. N. Uversky, and A. L. Fink, Conformational constraints for amyloid fibrillation: the importance of being unfolded, Biochim. Biophys. Acta 1698 (2004) 131-153.

[3] G. Perry, P. Cras, S. L. Siedlak, M. Tabaton, and M. Kawai, Beta protein immuno reactivity is found in the majority of neurofibrillary tangles of Alzheimer's disease. Am. J. Pathol. 140 (1992) 283-290.

[4] D. J. Selkoe, The molecular pathology of Alzheimer's disease. Neuron 6 (1991) 487-498.

[5] F. Chiti, and C. M. Dobson, Protein misfolding, functional amyloid, and human disease. Annu. Rev. Biochem. 75 (2006) 333-366.

[6] D. Selkoe, Folding proteins in fatal ways. Nature 426 (2003) 900-904.

[7] C. Soto, L. Estrada, and J. Castilla, Amyloids, prions and the inherent infectious nature of misfolded protein aggregates. Trends Biochem. Sci. 31 (2006) 150-155.

[8] M. Stefani, and C. M. Dobson, Protein aggregation, and aggregate toxicity: new insights into protein folding, misfolding diseases and biological evolution. J. Mol. Med. 81 (2003) 678-699.

[9] O. S. Makin, E. Atkins, P. Sikorski, J. Johansson, and L. C. Serpell, Molecular basis for amyloid fibril formation and stability. Proc. Natl. Acad. Sci. USA 102 (2005) 315-320.

[10] C. M. Dobson, Protein folding and misfolding. Nature 426 (2003) 884-890.

[11] Y-H. Lee, E. Chatani, K. Sasahara, H. Naiki, and Y. Goto, A comprehensive model for packing and hydration for amyloid fibrils of β_2-microglobulin. J. Biol. Chem. 284 (2009) 2169-2175.

[12] M. Bucciantini, E. Giannoni, F. Chiti, F. Baroni, L. Formigli, J. Zurdo, N. Taddei, G. Ramponi, C. M. Dobson, and M. Stefani, Inherent toxicity of aggregates implies a common mechanism for protein misfolding diseases. Nature 416 (2002) 507-511.

[13] P. Mishra, and V. Bhakuni, Self-assembly of bacteriophage-associated hyaluronate lyase (HYLP2) into an enzymatically active fibrillar film. J. Biol. Chem. 284 (2009) 5240-5249.

[14] M. Vendruscolo, J. Zurdo, C. E. MacPhee, and C. M. Dobson, Protein folding and misfolding: a paradigm of self-assembly and regulation in complex biological systems. Phil Trans. R. Soc. Ser. A 361 (2003) 1205-1222.

[15] M. V. Fändrich, V. Forge, K. Buder, M. Kittler, C. M. Dobson, and S. Diekmann, Myoglobin forms amyloid fibrils by association of unfolded polypeptide segments. Proc. Natl. Acad. Sci. USA 100 (2003) 15463-15468.

[16] J. Juarez, P. Taboada, and V. Mosquera, Existence of different structural intermediates on the fibrillation pathway of human serum albumin. Biophys. J. 96 (2009) 2353-2370.

[17] O. S. Makin, and L. C. Serpell, Structures for amyloid fibrils. FEBS J. 272 (2005) 5950-5961.

[18] R. Nelson, and D. Eisenberg, Structural models of amyloid-like fibrils. Adv. Protein Chem. 73 (2006) 235-282.

[19] R. Nelson, and D. Eisenberg, Recent atomic models of amyloid fibril structure. Curr. Opin. Struct. Biol. 16 (2006) 260-265.

[20] P. Walsh, K. Simonetti, and S. Sharpe, Core structure of amyloid fibrils formed by residues 106-126 of the human prion protein. Structure 17 (2009) 417-426.

[21] S. Zhang, Fabrication of novel biomaterials through molecular self-assembly. Nat. Biotechnol. 21 (2003) 1171-1178.

[22] M. G. Ryadnov, and D. M. Woolfson, Engineering the morphology of a self-assembling protein fibre. Nat. Mater. 2 (2003)329-332.

[23] M. Reches, and, E. Gazit, Casting metal nanowires within discrete self-assembled peptide nanotubes. Science 300 (2003) 625-627.

[24] K. Rajagopal, and J. P. Schneider, Self-assembling peptides and proteins for nanotechnological applications. Curr. Opin. Struct. Biol. 14 (2004) 480-486.

[25] E. Gazit, Use of biomolecular templates for the fabrication of metal nanowires. FEBS J. 274 (2007) 317-322.

[26] I. W. Hamley, Peptide fibrillization. Angew. Chem. Int. Ed. Engl. 46 (2007) 8128-8147.

[27] D. T. Loo, A. Copani, C. J. Pike, E. R. Whittemore, A. J. Walencewicz, and C. W. Cotman, Apoptosis is induced by β-amyloid in cultured central nervous system neurons. Proc. Natl. Acad. Sci. USA 90 (1993) 7951-7955.

[28] J. Yuan, and B. A. Yankner, Apoptosis in the nervous system. Nature 407 (2000) 802-809.

[29] Y. Zhang, R. McLaughlin, C. Goodyer, and A. LeBlanc, Selective cytotoxicity of intracellular amyloid β peptide$_{1-42}$ through p53 and Bax in cultured primary human neuron. J. Cell. Biol. 156 (2002) 519-529.

[30] V. Novitskaya, O. V. Bocharova, I. Bronstein, and I. V. Baskakov, Amyloid fibrils of mammalian prion protein are highly toxic to cultured cells and primary neurons. J. Biol. Chem. 281 (2006) 13828-13836.

[31] G. Forloni, N. Angeretti, R. Chiesa, E. Monzani, M. Salmona, O. Bugiani, and F. Tagliavini, Neurotoxicity of a prion protein fragment. Nature 362 (1993) 543-536.

[32] A. Giese, D. R. Brown, M. H. Groschup, C. Feldmann, I. Haist, and H. A. Kretzschmar, Role of microglia in neuronal cell death in prion disease. Brain Pathol. 8 (1998) 449-457.

[33] D. R. Brown, B. Schmidt, and H. A. Kretzschmar, Role of microglia and host prion protein in neurotoxicity of a prion protein fragment. Nature 380 (1996) 345-347.

[34] C. Hetz, M. Russelakis-Carneiro, K. Maundrell, J. Castilla, and C. Soto, Caspase-12 and endoplasmic reticulum stress mediate neurotoxicity of pathological prion protein. EMBO J. 22 (2003) 5435-5445.

[35] Y.Gu, H. Fujioka, R. S. Mishra, R. Li, and N. Singh, Prion Peptide 106-126 Modulates the Aggregation of Cellular Prion Protein and Induces the Synthesis of Potentially Neurotoxic Transmembrane PrP. J. Biol. Chem. 277 (2002) 2275-2286.

[36] H. Zou, Y. Li, X. Liu, and X. Wang, An Apaf-1·cytochrome *c* multimeric complex is a functional apoptosome that activates procaspase-9. J. Biol. Chem. 274 (1999) 11549-11556.

[37] Y. Hu, M. A. Benedict, L. Ding, and G. Núñez, Role of cytochrome *c* and dATP/ATP hydrolysis in Apaf-1-mediated caspase-9 activation and apoptosis. EMBO J. 18 (1999) 3586-3595.

[38] P. Zhou, J. Chou, R. S. Olea, J. Yuan, and G. Wagner, Solution structure of Apaf-1 CARD and its interaction with caspase-9 CARD: a structural basis for specific adaptor/caspase interaction. Proc. Natl. Acad. Sci. USA 96 (1999) 11265-11270.

[39] N. Yan, and Y. Shi, Mechanisms of apoptosis through structural biology. Annu. Rev. Cell. Dev. Biol. 21 (2005) 35-56.

[40] J. J. Chou, H. Matsuo, H. Duan, G. Wagner, Solution structure of the RAIDD CARD and model for CARD/CARD interaction in caspase-2 and caspase-9 recruitment. Cell 94 (1998) 171-180.

[41] H. Liang, and S. W. Fesik, Three-dimensional structures of proteins involved in programmed cell death. J. Mol. Biol. 274 (1997) 291-302.

[42] S. Nagato, Apoptosis by death factor. Cell 88 (1997) 355-365.

[43] H. Qin, S. M. Srinivasula, G. Wu, T. Fernandes-Alnemri, E. S. Alnemri, and Y. Shi, Structural basis of procaspase-9 recruitment by the apoptotic protease-activating factor 1. Nature 399 (1999) 549-557.

[44] Z. Xie, S. Schendel, S. Matsuyama, and J. C. Reed, Acidic pH promotes dimerization of Bcl-2 family proteins. Biochemistry 37 (1998) 6410-6418.

[45] O. B. Ptitsyn, Molten globule and protein folding. Adv. Protein Chem. 47 (1995) 83-229.

[46] M. M. Santoro, and D. W. Bolen, Unfolding free energy changes determined by the linear extrapolation method. 1. Unfolding of phenylmethanesulfonyl alpha-chymotrypsin using different denaturants. Biochemistry 27 (1988) 8063-8068.

[47] S. L. Milam, N. I. Nicely, B. Feeney, C. Mattos, and A. C. Clark, Rapid folding and unfolding of Apaf-1 CARD. J. Mol. Biol. 369 (2007) 290-304.

[48] A. Matouschek, J. T. Kellis, L. Serrano, M. Bycroft, and A. R. Fersht, Transient folding intermediates characterized by protein engineering. Nature 346 (1990) 440-445.

[49] H. LeVine, Thioflavin T interaction with amyloid β-sheets structure. Amyloid 2 (1995) 1-6.

[50] H. Naiki, K. Higuchi, M. Hosokawa, T. Takeda, Fluorometric determination of amyloid fibrils in vitro using the fluorescent dye, Thioflavin T. Anal. Biochem. 177 (1989) 244-249.

[51] L. A. Munishkina, and A. L. Fink, Fluorescence as a method to reveal structures and membrane-interactions of amyloidogenic proteins. Biochim. Biophys. Acta 1768 (2007) 1862-1885.

[52] J. W. O'Neill, M. K. Manion, B. Maguire, and D. M. Hockenbery, Bcl-xL dimerization by three-dimensional domain swapping. J. Mol. Biol. 356 (2006) 367-381.

[53] J. C. Reed, Bcl-2 and the regulation of programmed cell death, J. Cell Biol 124 (1994) 1-6.

[54] M. C. Wei, W. Z. Zong, E. H. Y. Cheng, T. Lindsten, V. Panoutsakapoulou, A. J. Ross, K. A. Roth, G. R. MacGregor, C. B. Thompson,and S. J. Korsmeyer, Proapoptotic Bax and Bak: a requisite gateway to mitochondrial dysfunction and death. Science 292 (2001) 727-730.

[55] A. Kelekar, B. S. Chang, J. E. Harlan, S. W. Fesik, and C. B. Thompson, Bad is a BH3 domain-containing protein that forms an inactivating dimer with Bcl-x_L. Mol. Cell. Biol. 17(1997) 7040-7046.

[56] R. Eskes, S. Desagher, B. Antonsson, and J. C. Martinou, Bid induces the oligomerization and insertion of Bax into the outer mitochondrial membrane. Mol. Cell. Biol. 20 (2000) 929-935.

[57] M. C. Wei, T. Lindsten, V. K. Mootha, S. Weiler, A. Gross, M. Ashiya, C. B. Thompson, and S. J. Korsmeyer, tBid, a membrane targeted death ligand, oligomerizes Bak to release cytochrome *c*. Genes Dev. 14 (2000) 2060-2071.

[58] E. H. Cheng, M. C. Wei, S. Weiler, R. A. Flavell, T. W. Mak, T. Lindsten, S. J. Korsmeyer, Bcl-x_L sequester BH3 domain-only molecules preventing Bax- and Bak mediated mitochondrial apoptosis. Mol. Cell. 8 (2001) 705-711.

[59] S. C. Ruffolo, and G. C. Shore, Bcl-2 selectively interacts with the Bid-induced open conformer of Bak, inhibiting Bak auto-oligomerization. J. Biol. Chem. 278 (2003) 25039-25045.

[60] M. Yadaiah, P. Nageswara Rao, P. Harish, and A. K. Bhuyan, High affinity binding of Bcl-x_L to cytochrome c: implication for a possible interception of translocated cytochrome *c* in apoptosis. Biochim. Biophys. Acta 1774 (2007) 1370-1379.

[61] B. Antonsson, S. Montessuit, B. Sanchez, and J. C. Martinou, Bax is present as a high molecular weight oligomer/complex in the mitochondrial membrane of apoptotic cells. J. Biol. Chem. 276 (2001) 11615-11623.

[62] G. Basanez, J. Zhang, B. N. Chau, G. I. Maksaev, V. A. Frolov, T. A. Brandt, J. Burch, J. M. Hardwick, and J. Zimmerberg, Pro-apoptotic cleavage products of Bcl-x_L form cytochrome *c*-conducting pores in pure lipid membranes. J. Biol. Chem. 276 (2004) 31083-31091.

[63] P. Li, D. Nijhawan, I. Budihardjo, S. M. Srinivasula, M. Ahmad, E. S. Alnemri, and X. Wang, Cytochrome c and dATP-dependent formation of Apaf-1/caspase-9 complex initiates an apoptotic protease cascade. Cell 91 (1997) 479-489.

[64] S. J. Riedl, W. Li, R. Schwarzenbacher, and Y. Shi, Structure of the apoptotic protease-activating factor 1 bound to ADP. Nature 434 (2005) 926-933.

[65] D. Acehan, X. Jiang, D. G. Morgan, J. E. Heuser, X. Wang, and C. W. Akey, Three dimensional structure of the apoptosome: implications for assembly, procaspase-9 binding and activation. Mol. Cell 9 (2002) 423-432.

[66] X. Yu. D. Acehan, J. Ménétret, C. R. Booth, S. J. Ludtke, S. J. Riedl, Y. Shi, X. Wang, C. W. Akey, A structure of the human apoptosome at 12.8Å resolution provides insights into this cell death platform. Structure 13 (2005) 1725-1735.

[67] E. Gazit, The "correctly folded" state of proteins: is it a metastable state? Angew. Chem. Int. Ed. Engl. 41(1995) 257-259.

[68] A. L. Fink, Natively unfolded proteins. Curr. Opin. Struct. Biol. 15 (2005) 35-41.

[69] A. K. Dunker, I. Silman, V. N. Uversky, and J. L. Sussman, Function and structure of inherently disordered proteins. Curr. Opin. Struct. Biol. 18 (2008) 756-64.

[70] P. Tompa, M. Fuxreiter, C. J. Oldfield, I. Simon, A. K. Dunker, and V. N. Uversky, Close encounters of the third kind: disordered domains and the interactions of proteins. Bioessays 31 (2009) 328-335.

[71] B. A. Yankner, Mechanisms of neuronal degeneration in Alzheimer's disease. Neuron 16 (1996) 921-932.

[72] C. Guela, C-K. Wu, D. Saroff, A. Lorenzo, M. Yuan, and B. A. Yankner, Aging renders the brain vulnerable to amyloid -protein neurotoxicity. Nat. Med. 4 (1998) 827-831.

[73] A. L. Gharibyan, V. Zamotin, K. Yanamandra, O. S. Moskaleva, B. A. Margulis, I. A. Kostanyan, and L. A. Morozova-Roche, Lysozyme amyloid oligomers and fibrils induce cellular death via different apoptotic/necrotic pathways. J. Mol. Biol. 365 (2007) 1337-1349.

[74] F. Cecconi, G. Alvarez-Bolado, B. I. Meyer, K. A. Roth, and P. Gruss, Apaf-1 (CED-4 homolog) regulates programmed cell death in mammalian development. Cell 94 (1998) 727-737.

Publications

[1] **P. Nageswara Rao**, M. Yadaiah, R. Ram Mohan Roy, P. Harish, and Abani K. Bhuyan, Cloning, bacterial expression, refolding, and ATP-binding properties of a WD40-deleted Apaf- 1 isoform. ***Protein Expression and Purification*** 56 (2007) 200-228.

[2] M. Yadaiah, **P. Nageswara Rao**, P. Harish, and Abani K. Bhuyan, High Affinity Binding of Bcl- XL to Cytochrome *c*: Implication for a Possible Interception of Translocated Cyt *c* in Apoptosis. ***Biochimica et Biophysica Acta (BBA)-Proteins& Proteomics*** 774(2007) 1370-1379.

[3] **P. Nageswara Rao**, Damodar Gullipalli, Abani K. Bhuyan, Bacterially expressed recombinant WD40 domain of human Apaf-1. ***Protein Expression and Purification*** 67(2009) 53-60.

[4] **P. Nageswara Rao**, Sony reddy, Abani K Bhuyan, Amyloid fibrils of the CARD domain of Apaf-1. ***Biochemistry*** (2009) (In Revision).

[5] M.Yadaiah, **P. Nageswara Rao**, S.G. Hussain, K.V.A. Ramaiah & Abani K Bhuyan, The S_4 protein of wheat ribosome is a cystein protease that blocks protein synthesis in the actively Translating lysate. ***Plant Cell*** (2009) (In Revision).

[6] **P. Nageswara Rao**, Abani K Bhuyan, Protein Folding – Where Empirical Patterns are inconsistent with Theory based ideas. Published in 93rd Indian Science Congress souvenir (Jan, 2006).